Ministry of Higher Education

and Scientific Research

University of Babylon

College of Education for Pure Sciences

Department of Physics

Fabrication and Characterization of CdTe Nano films Prepared by Thermal Evaporation Technique

A Thesis

Submitted to the Council of the College of Education for Pure Sciences of University of Babylon in Partial Fulfillment of the Requirements for the Degree of Master in Education / Physics

By

Hanan Salim Hadi Salih

B. E. Sc. in Physics

University of Babylon (2016)

Supervised by:

Prof. Dr. Khalid Haneen Abass

2023 A.D **1445 A.H**

بِسْمِ ٱللَّهِ ٱلرَّحْمَٰنِ ٱلرَّحِيمِ

" قَالُواْ سُبْحَٰنَكَ لَا عِلْمَ لَنَآ
إِلَّا مَا عَلَّمْتَنَآ ۖ إِنَّكَ أَنتَ ٱلْعَلِيمُ
ٱلْحَكِيمُ "

صدق ٱللَّه ٱلعظيم

سورة البقرة آية (٣٢)

Dedication

In the beginning, all thanks and appreciation to Allah for his unlimited blessings and for giving me the strength to complete this dissertation. I wish to express my profound gratitude to ***Prof. Dr. Khalid Haneen Abass*** *for his continued guidance, supervision, and comments throughout this research. There has been an ever-present force in helping me to mature as a student and as a researcher.*

I wish to express my sincere thanks to my wonderful parents, my husband, my brothers, and my sister, who have supported me during my life, and pray to ALLAH to protect them. All thanks to someone who helped me during the preparation of this thesis.

Hanan

ACKNOWLEDGMENTS

First of all, all thanks and appreciation to Allah for his unlimited blessings and for giving me the strength to complete this dissertation. I wish to express my profound gratitude to Prof. Dr. Khalid Haneen Abbas for his continued guidance, supervision, and comments throughout this research. There has been an ever-present force in helping me to mature as a student and as a researcher. Their dedication to helping succeed is deeply appreciated. the teaching, and administrative for their kind support.

Hanan

Supervisor's Certification

I certify that this thesis entitled " **Fabrication and Characterization of CdTe Nano film Prepared by Thermal Evaporation Technique**" was prepared by the student **(Hanan Salim Hadi Salih)** under my supervision at the College of Education for Pure Sciences of University of Babylon in Partial Fulfillment of the Requirements for the Degree of Master in Education/ Physics.

Signature:

Name: *Dr. Khalid Haneen Abass*

Title: Professor

(Supervisor)

Date: / / 2023

Head of the Department Certificate

In view of the available recommendations, I forward this thesis for debate by the examining committee.

Signature:

Name: **Dr. Khalid Haneen Abass**

Title: Professor

(Head of Physics Department)

Date: / / 2023

Summary

There are numerous optoelectronic uses for semiconductor thin films II-VI. One such substance that has proven effective in creating solar cells, photodetectors, and other optical device applications is cadmium telluride (CdTe).

In the current study, CdTe thin films were prepared by thermal evaporation of the material under a high vacuum and depositing them on glass substrates with different thicknesses (65, 72, 80, 88, 100, 110, 124, and 140) nm.

The effect of film thickness on structural, morphological, and optical properties was investigated. The thermal evaporated CdTe films were found a cubic structure from the X-ray diffraction (XRD) test.

The Scanning Electron Microscopy (SEM) micrographs of thin films show an improvement in the crystallite size of CdTe. The grain size of CdTe films becomes larger.

The morphology of the film is examined by an atomic force microscope (AFM) confirming that the films grown had a good homogeneous surface. The roughness, root mean square value, and average diameter increased with the increasing thickness (100-140) nm, and from the thickness (65 - 88) nm the morphology of the film was unstable.

The optical measurements of the films are studied by a UV-Visible spectrophotometer in the wavelength range (200- 1100) nm, When the thickness increased, the absorbance increased while the transmittance decreased. The direct energy gap decreased from (3.60 to 3.42) eV with increasing thickness.

The surface energy loss function (SELF) and volume energy loss function (VELF) it was found to increase with increasing thickness. The dispersion parameters of the films were also evaluated using Wemple– DiDomenico (WDD) single oscillator model. The dispersion energy (E_d) and oscillator energy

(E_o) of the films were evaluated and varied in the range of (2.18-10.20) eV and (5.02-7.65) eV respectively, the optical dispersion moments (M_{-1} and M_{-3}) were also calculated that varied from (0.43-1.333) and from (0.0171-0.0227) respectively.

List of Contents

List of Figures

List of Tables

List of Symbols and Abbreviations

Symbols	Definition
A	Absorbance
a	Lattice Constant
AFM	Atomic Force Microscopy
ALE	Atomic Layer Epitaxy
c	Speed of light
C.B	Conduction Band
Cd	Cadmium
CdTe	Cadmium Telluride
CSVT	Close Space Vapor Transport
D	Average Grain Size
E_d	energy parameter
E_g	Energy Gap
E_0	Single oscillator energy
E_p	Energy of Absorbed
eV	Electron Volt
ε_i	Imaginary Dielectric Constant
ε_r	Real Dielectric Constant
SEM	Scanning Electron Microscopy
FWHM	Full Width at Half Maximum
I_A	absorbed light intensity by material
I_o	the incident intensity of light.
I_T	The intensity of the Beam From The Membrane
K	Wave vector of electron
PLD	Pulsed Laser Deposition
R.T	Room Temperature
SELF	Surface energy loss function
STM	Scanning tunneling microscope
T	Transmittance
t	Thickness
Te	Telluride
UV	Ultra Violet Spectrum
V.B	Valence Band
VELF	Volume energy loss function
WDD	Wemple–DiDomenico

XRD	**X-Ray Diffraction**
α	**Absorption coefficient**
β	**the full width**
θ	**Bragg angle**
ν	**frequency**
hν	**Photon energy**
n	**Refractive index**
λ	**Wavelength**
$k_{\circ}$	**Extinction coefficient**
D	**Crystallite size**
R	**Reflectance**
M_{-1} and M_{-3}	**Moments of the optical spectra**
PVD	**Physical Vipar Disposition**
ρ	**Density**

CHAPTER ONE

INTRODUCTION

and

Literature review

1.1 Introduction :

Thin films, ubiquitous in today's world, have a documented history of more than 5000 years [1]. The expression of "Thin Films" is used to describe a layer or several layers of atoms for a certain substance whose thickness less than (1 μm) [2]. Many different types of applications, such as semiconductor devices, optical lenses and filters, sensors, and display technologies. By depositing materials onto a substrate using a variety of methods, including thermal evaporation, chemical vapor deposition, and sputtering, thin films can be created. Thin film technology has also developed to incorporate new types of methods that enable exact control of thickness and composition, making them a crucial component in many industries like electronics, biology, and optics [3].

Thin films are uniformly thin layers of material that have been deposited in a controlled manner onto a substrate. Based on their atomic structure, thin films can be categorized as amorphous, crystalline, polycrystalline, nanocrystalline, nanostructured, nanocomposite, multilayer, or monolayer [4].

Thin films are widely used nowadays in practically every industry as a means of improving materials' physical and chemical qualities [5].

The thickness of a thin film is a crucial measurement since it determines many of the film's characteristics. Many factors influence the structure of thin-film materials, which in turn determines their mechanical, optical, magnetic, electrical, etc. characteristics. Thin-film materials of varying thicknesses have been the subject of a number of published investigations [6]. Physical vapor deposition (PVD) and chemical vapor deposition (CVD) are the two most prevalent deposition methods used for thin film fabrication [7]. There are two main categories of techniques used for thin-layer deposition: physical and chemical. Fig. (1.1) Different Physical and Chemical Thin Film Deposition Processes [8].

A thin film is a thin layer of material, typically between a few nanometers and a few micrometers in thickness [9]. Thin films can be made from various

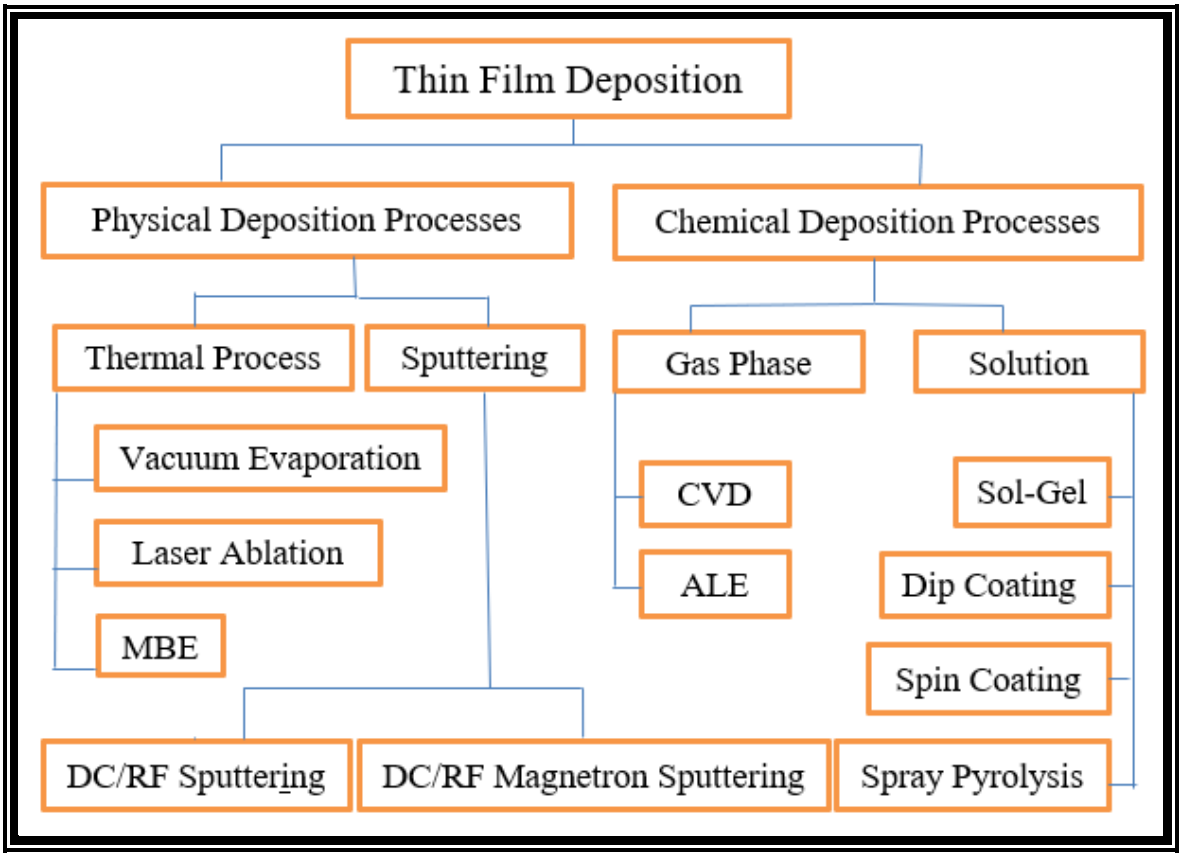

Fig. (1.1): Different Physical and Chemical Thin Film Deposition Processes [8].

materials, including metals, semiconductors, and insulators [10]. There are Three steps process creation, transportation, and condensation of atoms, ions, and molecules involved in deciding the thin film structures Fig. (1.2) shows the processes [11,12]. Thin films are often preferred over thick films due to their unique properties, such as the high surface area to volume ratio, sensitivity to external stimuli, and the ability to manipulate their optical, electrical, and mechanical properties, all of which depend on the deposition method, the material used, and the thickness of the thin film [13,14].

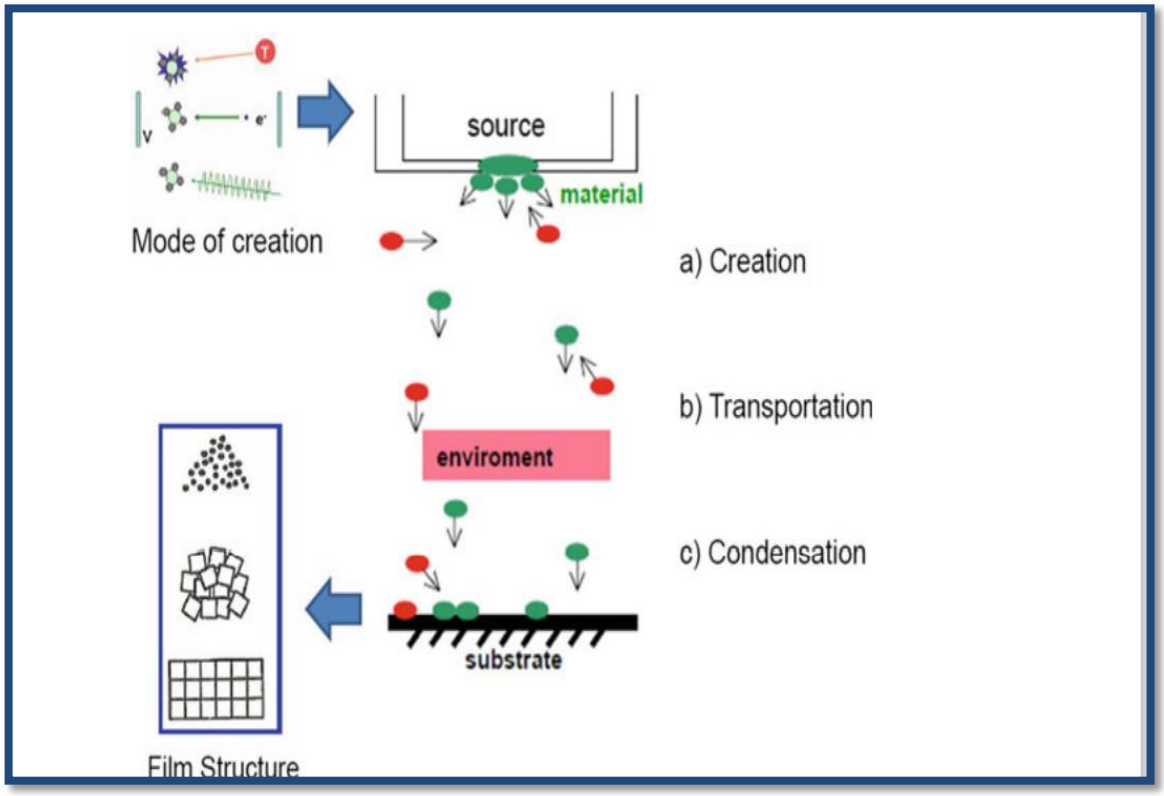

Fig. (1.2): Three steps process (a) creation, (b) transportation, and (c) condensation of atoms, ions, and molecules. involved in deciding the thin film structures [11].

1.2 Nanomaterials

Nanotechnology, or the manipulation of materials at atomic or molecular size, is the art of building structures and devices at the nanometer scale. Designing, characterizing, synthesizing, and applying materials, structures, devices, and systems whose form and size are controlled on the nanoscale scale is a busy area of research with rapid growth [15]. The study of nanomaterials takes a materials science approach to nanotechnology, building on the progress made in materials synthesis and characterization through microfabrication studies. Nanostructured materials typically exhibit good optical, electrical, thermophysical, or mechanical characteristics due to their small size [16]. Nanomaterial in principle, is materials of which a single unit small sized (in at least one dimension) between (1 – 100) nm the usual definition of nanoscale and nanoscale defined as the length range approximately from (1 nm to 100) nm [17].

There is a wide variety of nanostructured materials with different dimensions which range from zero-dimensional (0-D) nanoparticles, one-dimensional (1-D) Nanorods and nanowires, two-dimensional (2-D) Nanosheets and films, three-dimensional (3-D) polycrystals and ultra porous nanostructures, and Nano scaffolds [18]. Generally, the fabrication of nanostructured materials is considered to proceed via two main strategies which include the "bottom-up" and "top-down" approaches [19]. The difference between these two general strategies is based on the processes involved in the construction of the nanostructures [20]. In the bottom-up approach, a structure is normally built up of small units while in the top-down approach, a larger unit is reduced in size to a finished structure as shown in Fig. (1.3) [21].

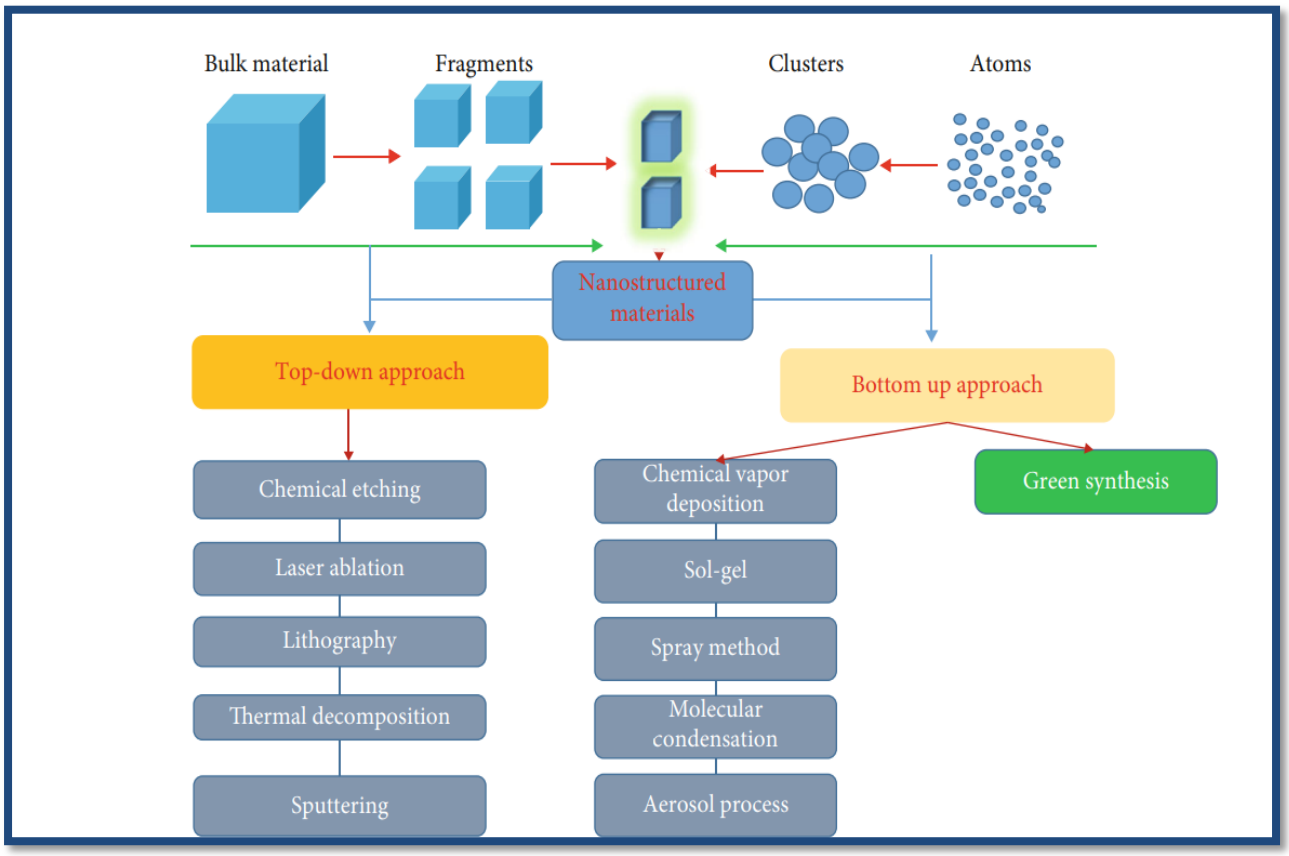

Fig. (1.3): A schematic representation of the top-down and bottom-up approaches for the fabrication of nanostructures [22].

In recent years, these materials have been the focus of much study and investigation because of the novel features they exhibit that cannot be seen in

the bulk form of the same substance. Quantum dots, nanotubes, nanofibers, nanowires, and nanoparticles are among the most well-known examples of nanomaterials [23,24]. These materials have received significant attention due to their potential applications in various fields, including biomedical engineering, electronics, and energy production [25]. The properties of nanomaterials, such as mechanical, optical, and chemical properties, depend strongly on their size and geometric structures. Nanomaterials have a large surface area to volume ratio which makes them highly reactive, and they can exhibit unique optical, electronic, and magnetic properties [26].

1.3 Cadmium Telluride (CdTe) Properties:

Cadmium telluride (CdTe) is a semiconductor commonly used in the production of thin film solar cells, x-ray detectors, and radiation sensors, table (1.1) explains some important properties of CdTe [27]. CdTe contains toxic elements (cadmium and telluriud), which can be hazardous if released into the environment or handled improperly [28]. Electrical conductivity CdTe is a semiconductor material, meaning it has intermediate electrical conductivity between that of conductors and insulators [29]. It exhibits excellent optical absorption properties in the near-infrared to ultraviolet regions [29, 30].

Table (1.1): Some important properties of CdTe [28,29].

Property	Value
Symbol	CdTe
Color	black or dark brown
Crystal structure	It has a crystalline structure, typically with hexagonal or cubic symmetry
Energy gap	1.45 eV
Density	٦.٢٠ g/cm^3
Lattice Constant	6.482 Å

Melting point	1092°C
Boiling point	1130°C
Refractive index	2.67
Specific Heat Capacity	0.21 J/gK
Dielectric Constant	low at 10

Atomic numbers 48 and 52 for, Cd and Te respectively can both be found in the fourth row of the table [30,31]. Cadmium telluride is a crystalline compound formed from cadmium and tellurium. It has very low solubility in water and is etched by many acids such as hydrobromic and hydrochloric acids. It is commercially available as powder or crystals. It can also be made into nanocrystals, the CdTe has a cubic structure as shown in Fig. (1.4) [32,33]. At room temperature, the vapor pressure of CdTe is zero. Due to its high melting point and insolubility, CdTe is more stable than its parent components, cadmium and tellurium, and most other Cd compounds [33].

Cadmium Telluride (CdTe) is becoming the most successful contender to Si photoactive material for the realization of solar cells due to its high efficiency and low-cost solar cell applications. The material is gaining great interest among researchers due to its crucial properties such as long-term performance stability [35,36]. And high optical absorption coefficient ($> 10^5$ cm^{-1}) to achieve nearly full absorption of the solar spectrum for thicknesses below 800 nm [36,37].

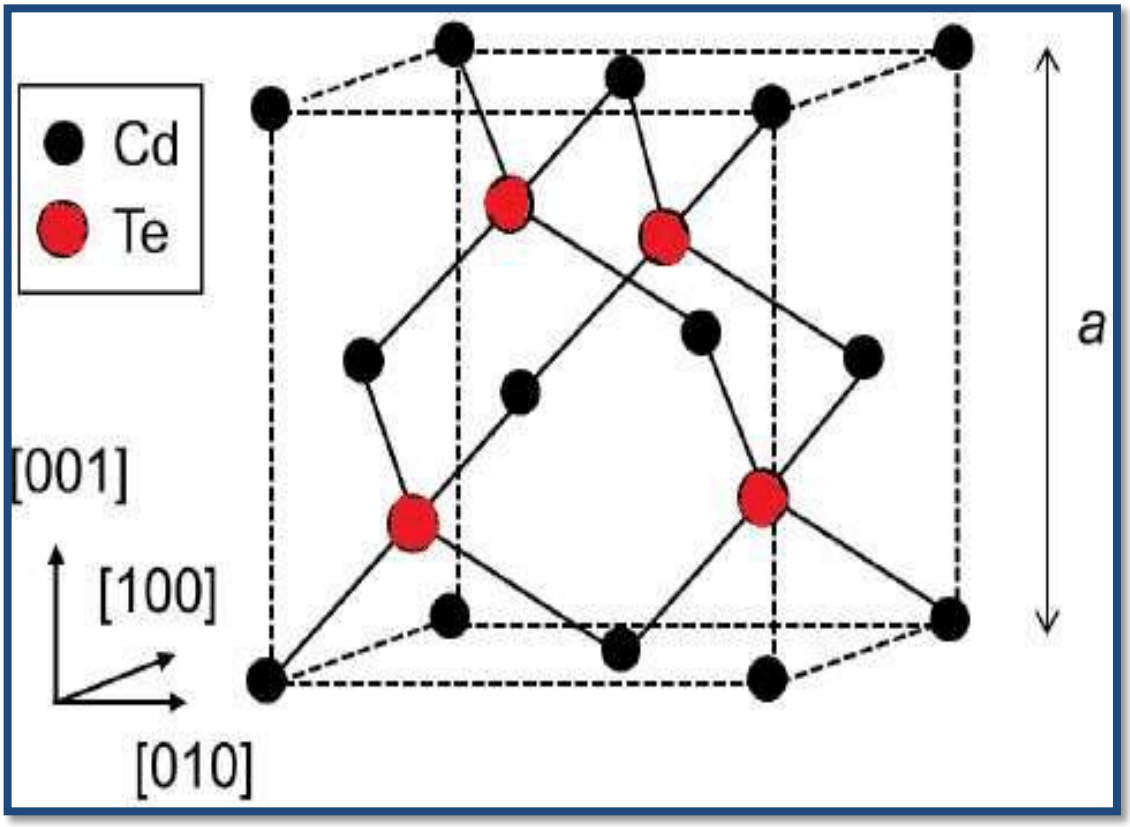

Fig. (1.4): Unit cell crystal structure of CdTe [38].

1.4 Review Of The Literature

In 2010, S. J. Ikhmayies and R. N. Ahmad-Bitar [39], studied, vacuum evaporation was used to create CdTe thin films on glass substrates. The XRD diffractogram revealed a zinc blend structure with a strong reflection from the (111) plane. The diameter of the nanocrystallites was estimated by using the XRD pattern and the Scherrer formula and found to be 23 nm. In the wavelength range of 600-1100 nm, measurements of transmittance and absorbance were taken. These distinct transitions between the valence and conduction bands of the quantum dots are used to explain these sharp lines. Vacuum evaporation was used to create CdTe thin films on glass substrates while the temperature was room temperature.

In 2014, E.R. Shaaban *et al.*[40], they purposed flexible optical devices, they studied CdTe thin films of varying thicknesses produced on polymer substrates. When various CdTe film thicknesses' X-ray diffractograms are

measured, their patterns reveal polycrystalline nature with a preference for orientation along the (111) plane. Using Swanepoel's approach, the optical constants of CdTe films were determined based on the observed transmittance spectral data in the 400–2500 nm range. After being determined, the refractive index n and absorption index k show a normal dispersion. The Wemple-DiDomenico model, which is based on a single oscillator, was followed by the data on refractive index dispersion. At zero photon energy, the refractive index number and oscillator dispersion parameters were calculated. In these films, it is discovered that the potential optical transition is permissible.

In 2015, K. Punitha, *et al.* [41], reported on post-deposition heat treatment (annealing)-induced change in optical properties derived from UV–vis study of CdTe thin films prepared on amorphous glass substrate by electron beam evaporation technique. The annealing effect gives rise to the enhancement in crystalline nature (zinc blende structure) of CdTe films with (111) preferred orientation. The average transmittance was increased with the annealing temperature and the slight shift in transmission threshold towards higher wavelength region revealed the systematic reduction in optical energy band gap. The existence of a shallow level just below the conduction band, within the band gap, was identified in the range of 0.23 and 0.14 eV for the films annealed at 200 and 450 ◦C, respectively. In addition, the scanning electron microscopic measurement supports the result of the X-ray diffraction study.

In 2016, M. T. Dejpasand, *et al.* [42], used the thermal evaporation technique to coat thin layers of cadmium telluride with an average thickness of 300 nm on glass substrates. Systematically examining the impact of substrate temperature on sample physical characteristics. A variety of characterization techniques, including X-ray diffraction (XRD), UV-vis, and atomic force microscopy, were used for the produced specimens. According to XRD analyses, the deposited layers had a cubic structure. The samples' crystallinity characteristics were found to be enhanced by raising the substrate temperature.

The specimens' refractive index increased and their band gap energy decreased as the substrate temperature increased, according to an optical study of the samples.

In 2017, P. K. K. Kumarasinghe, *et al.* [43]**,** studied the Microstructure and other physical properties of CdTe thin films are directly affected by the deposition conditions as well as post-deposition treatments. CdTe films were fabricated using the thermal evaporation technique at different substrate temperatures from 125 to 300° C and subjected to post-deposition air annealing and chemical etching to observe the alterations of structural, optical, and electrical properties.

In 2018, A. Arce-Plaza, *et al.* [44], studied the II-IV semiconductor compound, CdTe, which has suitable electrical and optical properties as photovoltaic and high-energy radiation sensor material. As an absorber material for thin film-based solar cells, CdTe holds the potential to fabricate high-efficiency solar cells using low-cost technologies. This chapter presents a comprehensive review of the CdTe thin-film deposition techniques as well as of the several configurations for the solar cell structures that have led to the best efficiency conversion, It has a bandgap of 1.42 eV (optimal for the solar spectrum) and is a semiconductor of direct band transitions that allows thin film applications. Another property is its absorption coefficient of 104 cm, which allows 90% absorption with a 1 μm thickness of the thin films.

In 2019, S. A. Fadaam, *et al,* [45], studied the effect of annealing temperature (200, 400) of CdTe heterojunction on solar cells efficiency prepared by thermal evaporation technique in vacuum with rate deposition (4.32 A°/sec) and thickness (≈ 400 ±10 nm), solar cells were realization with conversion efficiencies of (6.4% - 10.8%) . The main focus in this work was to study the annealing temperature dependent conduct of the expansion parameter and the

band gap energy of (CdTe) thin film in solar cells. Room temperature band gap for (CdTe) is found (Eg =1.5 to 2) eV for efficiency solar cells

In 2019, S. Ray, *et al.* [46], studied the synthesis and characterization of thin-film-based photovoltaic materials attract great research interest for the past few years as the efficiency of the photovoltaic cell can be improved systematically with a proper functionalization of the films and making multilayers. We have synthesized Cu-doped CdTe thin films with different doping concentrations using the PVD technique. The structural, morphological, and optical properties of synthesized films were carefully investigated. Our study shows that all the prepared films are polycrystalline with a cubic structure. Our investigation shows that the optoelectronic behavior of the doped CdTe sample can be improved by up to 3% Cu doping. Therefore, we anticipate that up to 3% Cu-doped CdTe would be suitable for the counterpart of highly efficient CdTe-based p-n junction solar cells

In 2020, S. S. Oluyamo, *et al.* [47], studied cadmium telluride (CdTe) thin films were fabricated using an electrodeposition technique at 1400 mV cathodic potential. CdTe films were deposited on fluorine-doped tin oxide (FTO) substrate of dimension 2.3 by 2.4 cm^2 at varied times of deposition. X-ray diffraction (XRD), scanning electron microscopy (SEM), ultraviolet-visible spectrophotometer (UV-vs), photoelectrochemical cell measurement (PEC), and energy dispersive X-ray spectroscopy (EDX) were used to characterize the structural, morphological, optical, electrical conductivity and elemental composition of electrodeposited films respectively. The particle average crystallite size was estimated as 11.98 nm

In 2021, H. T. Gaganpreet, *et al.* [48]**,** optimization of the physical properties of cadmium telluride (CdTe) thin films has been carried out to improve its performance by the influence of RF power. CdTe Nanocrystalline thin films were characterized by using various techniques such as atomic force

microscopy (AFM), scanning electron microscopemicroscopy (SEM), and X-ray diffraction (XRD). XRD study revealed that CdTe films are polycrystalline and have preferential growth in (111) direction. SEM images showed a continuous and dense morphology of CdTe films on glass substrates. The AFM result shows that the surface roughness of films increases with annealing. Optical properties were investigated with the help of the UV–visible absorption spectrum which showed that the bandgap decreases with an increase in Radio-frequency power.

In 2022, H. S. Patel *et al.* [49], studied thin films of CdTe with thickness around 4000Å have been deposited by the thermal evaporation method at room temperature. The structural characterization of this film was carried out using XRD (X-ray diffraction technique) and TEM (Transmission electron microscopy). The structure of CdTe film was found to be hexagonal. Also, the lattice parameters, grain size (D), dislocation density (ρ) and micro strain (ε), were taken from the XRD data. From TEM of CdTe thin films, the polycrystalline nature was confirmed. A surface morphology study was done by SEM (Scanning electron microscopy) technique. Atomic Force Microscopy (AFM) provides numerical data of surface height at digitized locations, which are usable for various surface characterizations.

In 2022, Ashith , *et al.* [50], CdTe thin films have been deposited on glass substrates by thermally evaporating CdTe powder under a high vacuum. The optimum film thickness for photovoltaic applications was determined by performing a detailed characterization of the films. The thermal evaporated CdTe films were found to be polycrystalline with a cubic structure. Considerable improvement in the crystallinity was observed with the increase in thickness. The lattice constant, dislocation density، strain, and stress have also been analyzed. The optical properties of the CdTe films have been observed to change with thickness. The maximum optical absorption was found in the near

infrared region. The photoluminescence spectra showed a prominent peak, corresponding to the band-edge transition of the CdTe films.

In 2023, H. M. Ali and M. H. Mustafa [51], ptical properties, structural makeup, and morphology of thin films of cadmium telluride (CdTe) with a thickness of 150 nm produced by thermal evaporation over glass. The X-ray diffraction study showed that the films had a crystalline composition, a cubic structure, and a preference for grain formation along the (111) crystallographic direction. The outcomes of the inquiry were used to determine these traits. With the use of thin films of CdTe that were doped with Ag at a concentration of 0.5%, the crystallization orientations of pure CdTe (23.58, 39.02, and 46.22) and CdTe:Ag were both determined by X-ray diffraction. orientations (23.72, 39.21, 46.40) For samples that were pure and those that were doped with silver, the optical band gap shrank by (1.52-1.47) eV (400–1100)nm resulting in a drop in the absorption coefficient. An incident power density of (100 mW/cm^2) was used to examine the I-V properties of heterojunctions created by light on a variety of clean and doped materials. In accordance with the X-ray diffraction analysis, the films had a cubic structure and dominated grain growth along the (111) crystallographic direction.

In 2023, Jena, I. and Singh, U.P [52], focuses on the study of influence of copper incorporation in the cadmium telluride (CdTe) films.. Copper incorporated CdTe films have been characterized by X-ray diffraction (XRD), Atomic force microscopy (AFM), scanning electron microscopy (SEM), UV–Vis spectroscopy, Raman spectroscopy and Hall Effect measurements. XRD analysis illustrated that all the CdTe thin films were of polycrystalline nature possessing cubic structure showing sharp peak at (111) orientation, while the intensities of peaks varied from sample to sample with respect to copper incorporation in the CdTe films**.**

1.5 Aim of the Work

1- Preparation of CdTe thin films by using the thermal evaporation technique with thicknesses less than the critical thickness.

2- Study some physical properties (morphology and structure, optical) of CdTe thin film to find out the appropriate application for these films.

3- Study the dispersion parameters using the Wemple–DiDomenico model of CdTe thin film to find its potential for use in communications and the design of optical devices.

CHAPTER TWO

Theoretical Part

2.1 Introduction

This chapter focuses on the theoretical part which represents thermal evaporation (optimization, advantages, disadvantages, specifications of the system), as well as structural and morphological properties by X-ray diffraction (XRD) , scanning electron microscopy (SEM), atomic force microscopy (AFM), optical properties of crystalline semiconductors the optical constant, fundamental Absorption Edge (electronic transitions).

2.2 Thermal evaopration

Thermal evaporation was devised by Faraday during the 1850s [53]. During this process, atoms and clusters of atoms or molecules are removed in the form of a vapor flux from a metal crucible, containing some bulk material (target) by heating the crucible, either by passing a current through it or by a heater filament [54]. Alternatively, during electron-beam (e-beam) evaporation, a beam of electrons bombards the bulk material in the crucible to generate the vapor flux. The crucible and its contents are placed in a vacuum chamber, with pressure typically below 10^{-4} Torr. The vapor flux condenses on a substrate [21]. Fig. (2.1) presents a schematic for the thermal evaporation technique.

The substrate is placed near the evaporating material, and the vapor condenses onto it, forming a thin film. The thickness of the film can be controlled by adjusting the rate of evaporation. Thermal evaporation is commonly used to deposit metals and oxide materials and can be used to create films with high purity and conformal coverage on various substrates. It is a relatively simple and low-cost technique, but it has limitations, such as poor adhesion and low deposition rates compared to other PVD techniques [55].

Thermal evaporation is a simple convenient process to evaporate and condense a wide range of materials in a vacuum on a substrate surface. So, it is one of the versatile techniques of PVD at present. Thermal evaporation is the

simplest way of depositing material onto a substrate under pressure $1x10^{-7}$ mbar and gives excellent purity of films [56].

The process involves three steps [57] :

(i) evaporation of the material to be deposited by a high energy source such as an electron beam or ions–this evaporates atoms from the surface.

(ii) transport of the vapor to the substrate to be coated.

(iii) deposition of the coating at the substrate surface.

PVD has several advantages including [56] :

(i) coatings formed by PVD may have improved properties compared to the material.

(ii) all types of inorganic materials and some types of organic materials can be used.

(iii) the process is environmentally friendly compared to many other processes such as electroplating. However, PVD has also some disadvantages including [58] :

1- problems with coating complex shapes.
2- high process cost and low output.
3- the complexity of the process.

Thermal evaporation is a physical vapor deposition (PVD) technique used to create thin films on a substrate. It involves heating a material (usually a metal) in a vacuum chamber until it melts and then evaporates, forming a vapor that condenses onto a substrate to create a thin film [59]. In the thermal evaporation process, the material to be deposited is placed in a high-temperature container called a crucible. The crucible is heated using an electron beam or resistive heating until the material reaches its melting point, and then the temperature is increased to produce a vapor [60].

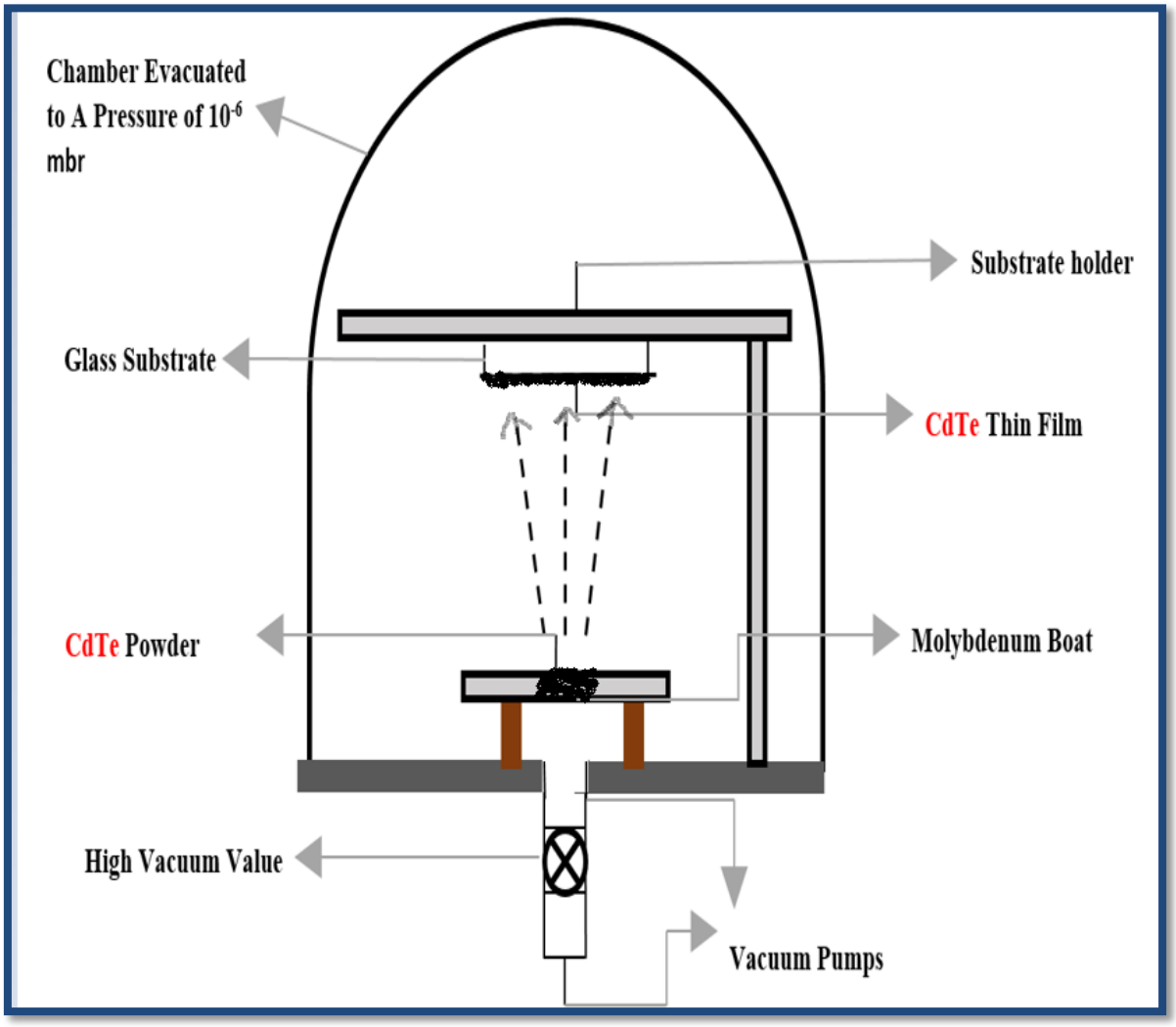

Fig. (2.1): The schematic diagram of the thermal evaporation setup [50].

2.3 Structural and Morphological Properties:

2.3.1 X-ray Diffraction (XRD)

The discovery of X-rays by Wilhelm Conrad Roentgen in 1895 allowed important innovations in all scientific disciplines, making the development of new medical and technical applications possible [61]. In particular, the research on X-ray diffraction (XRD) by crystals initiated by Laue, Friedrich, and Knapping in 1912 opened new possibilities in the study of crystalline materials [62]. It is possible to apply XRD to investigate the crystallization process, unit cell lattice parameter detail, crystal structure, crystal orientation, and crystallite size, which is

a fast and effective approach. The constructive interference of a monochromatic beam of X-rays is used to produce the XRD peaks after scattering each set of lattice planes in the sample at specific angles, where the distribution of the atoms determines the peak intensities within the lattice. Therefore, the periodic atomic fingerprint of materials is represented by the XRD pattern [63,64]. The XRD methods are based on the ability of crystals to diffract X-rays in a characteristic manner allowing a precise study of the structure of crystalline phases. Recorded diffraction patterns contain additive contributions of several micro- and macrostructural features of a sample. With the peak position, lattice parameters, space group, chemical composition, macro stresses, or qualitative phase analysis can be investigated [65].

X-rays are high-energy electromagnetic waves with a wavelength between (10^{-3} and 10^{1}) nm [66]. The sample holder, X-ray tube, and X-ray detector are the three basic components of an X-ray diffractometer. The cathode ray tube is responsible for creating X-rays, which are subsequently driven toward a target by a voltage and attack the target substance. When electrons with sufficient energy displace inner shell electrons of the target material, X-ray spectra are produced [67]. However, due to the periodic nature of a crystalline structure, constructive or destructive scattered radiation will result, leading to characteristic diffraction phenomena which can be studied to investigate the crystal structure of materials [68]. When X-ray light of wavelength (λ) is projected at an angle (θ) onto a crystal lattice, the incoming X-rays interact constructively with the sample if the circumstances meet Bragg's law Bragg Fig. (2.2) [69]. gives the details about the geometrical condition for diffraction and the determination of Bragg’s law. Bragg’s law is given in Eq. (2-1).

$$2d_{hkl}sin\theta = n\lambda \qquad (2\text{-}1)$$

Where $d_{hkl} = {}^{d}/_{n}$, θ is Bragg diffraction angle (degree) and λ is wavelength for incident X-ray beam (Å).

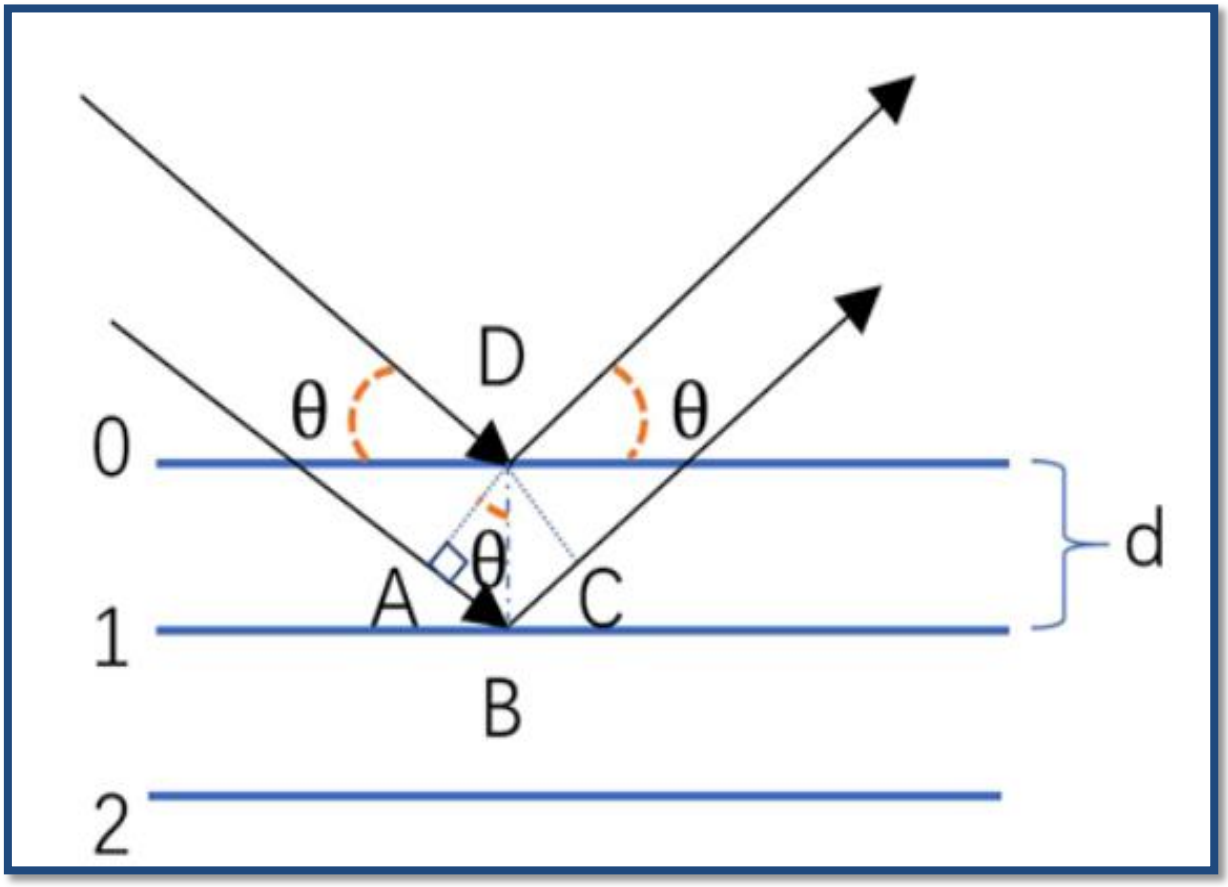

Fig. (2.2): Bragg's diffraction [67].

In general, diffraction data are represented as intensity distribution as a function of the 2θ angle. The information content that can be extracted is represented in Fig. (2.3).

The maximum peak intensity Imax can be defined as well as the integrated intensity Iint (area under the peak). The peak width can be generally characterized by the full width at half maximum (FWHM) [70].

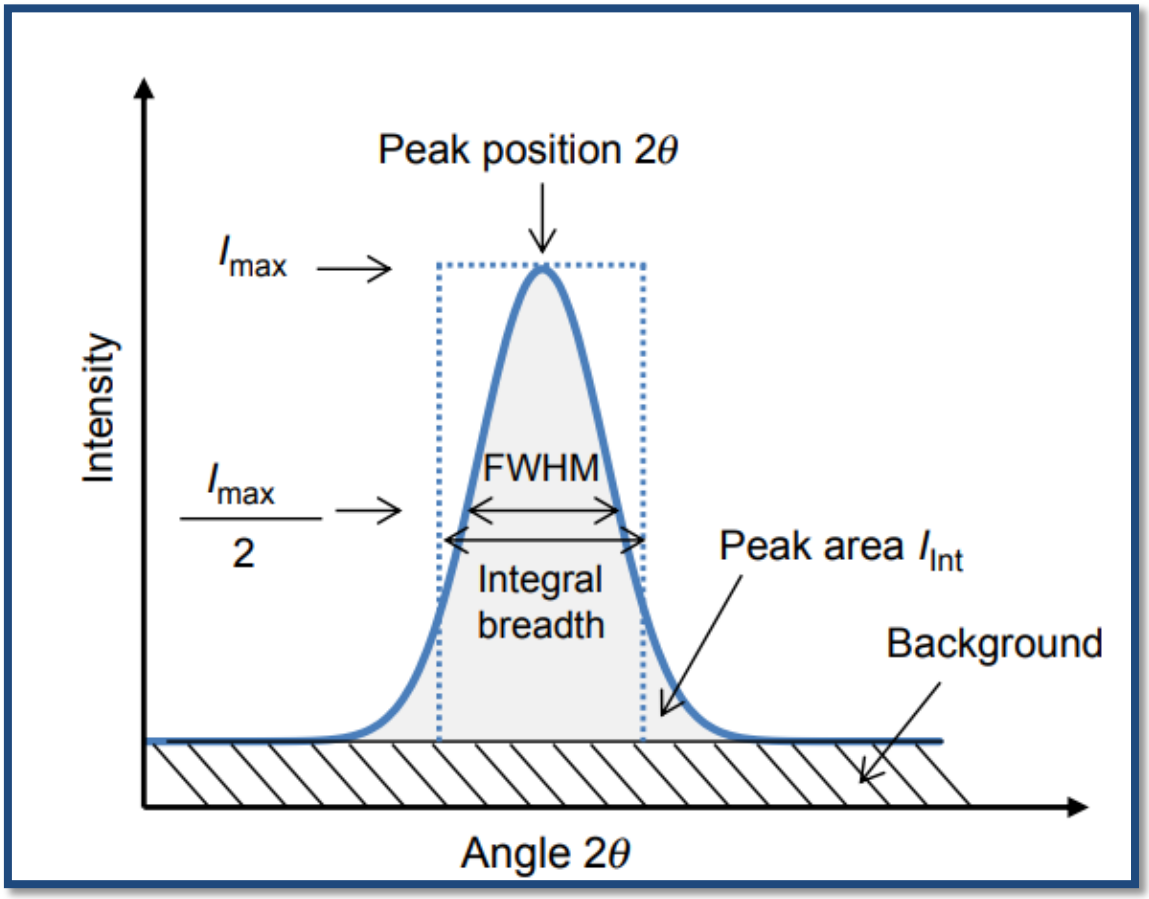

Fig. (2.3): Action peak and information content that can be extracted [67].

2.3.1.1 Parameters' Calculation

Normally, XRD is used to calculate different parameters, which could be used to clarify the studies of the deposited films, including:

1- Full width at half maximum (FWHM) (β).

The full width at half of the maximum intensity (FWHM) of the preferred orientation (peak), could be measured since it is equal to the width of the line profile (radian) at half of the maximum intensity [71].

2- Average crystallite size (Dav)

The crystallite size (D) can be estimated using Scherer's formula [61]:

$$D = k\lambda/\beta cos\theta \qquad (2\text{-}2)$$

Where k is constantly dependent on the type of crystal structure (0.9), λ is the x-ray wavelength (Å), β is the full width at half of the maximum intensity (FWHM)(radian), θ is the Bragg diffraction angle of the XRD peak (degree) [72].

2.3.2 Scanning Electron Microscope (SEM):

The Scanning electron microscope (SEM) is a powerful tool for analyzing nanometer to micrometer scale organic and inorganic materials. The great magnification of SEM, which may reach up to 1,000,000x in some of the newest models, allows it to create extremely detailed pictures of a wide variety of materials, potential to provide previously unknown details about the material composition of scanned specimens that are not obtainable by conventional laboratory analysis [73].

Fig. (2.4) depicts the scanning electron microscopemicroscope (SEM) used for the analysis [74].

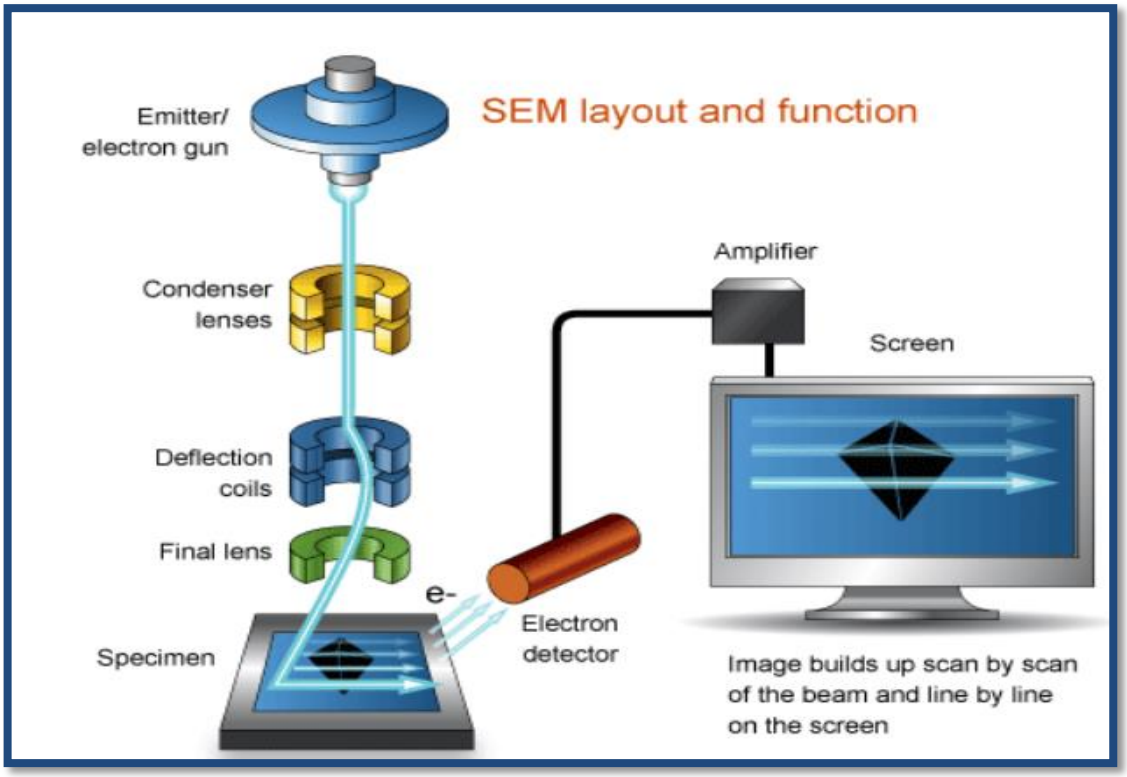

Fig. (2.4): SEM components [74].

High-resolution surface imaging is possible using a scanning electron microscope (SEM). The SEM creates a beam of incoming electrons in an electron column above the sample chamber, allowing for imaging to be performed using electrons. Thermal emission is the source of the electrons. The size, shape, density, and orientation of nanostructures may be estimated with its help [75].

The apparatus is a pressure-control system that can store any kind of sample, whether it's moist or requires minimal preparation. Samples up to 200 mm in diameter and 80 mm in height can be analyzed by the equipment. In Fig. (2.5), we see the device's magnification in action [76].

Electrons are generated at the top of the column, accelerated down, and passed through a combination of lenses and apertures to produce a focused beam of electrons that hits the surface of the sample. The main components of a SEM are the: electron source, the column down which electrons travel with electromagnetic lenses, the electron detector, the sample chamber, the computer, and the display to view the images [77]. Researchers and scientists in many domains, from materials science to biology, find SEM to be an invaluable tool because of the unique insights it gives into sample structure and behavior [78].

Scanning Electron Microscope (SEM) uses a focused beam of high-energy electrons to generate a variety of signals at the surface of specimens. The signals

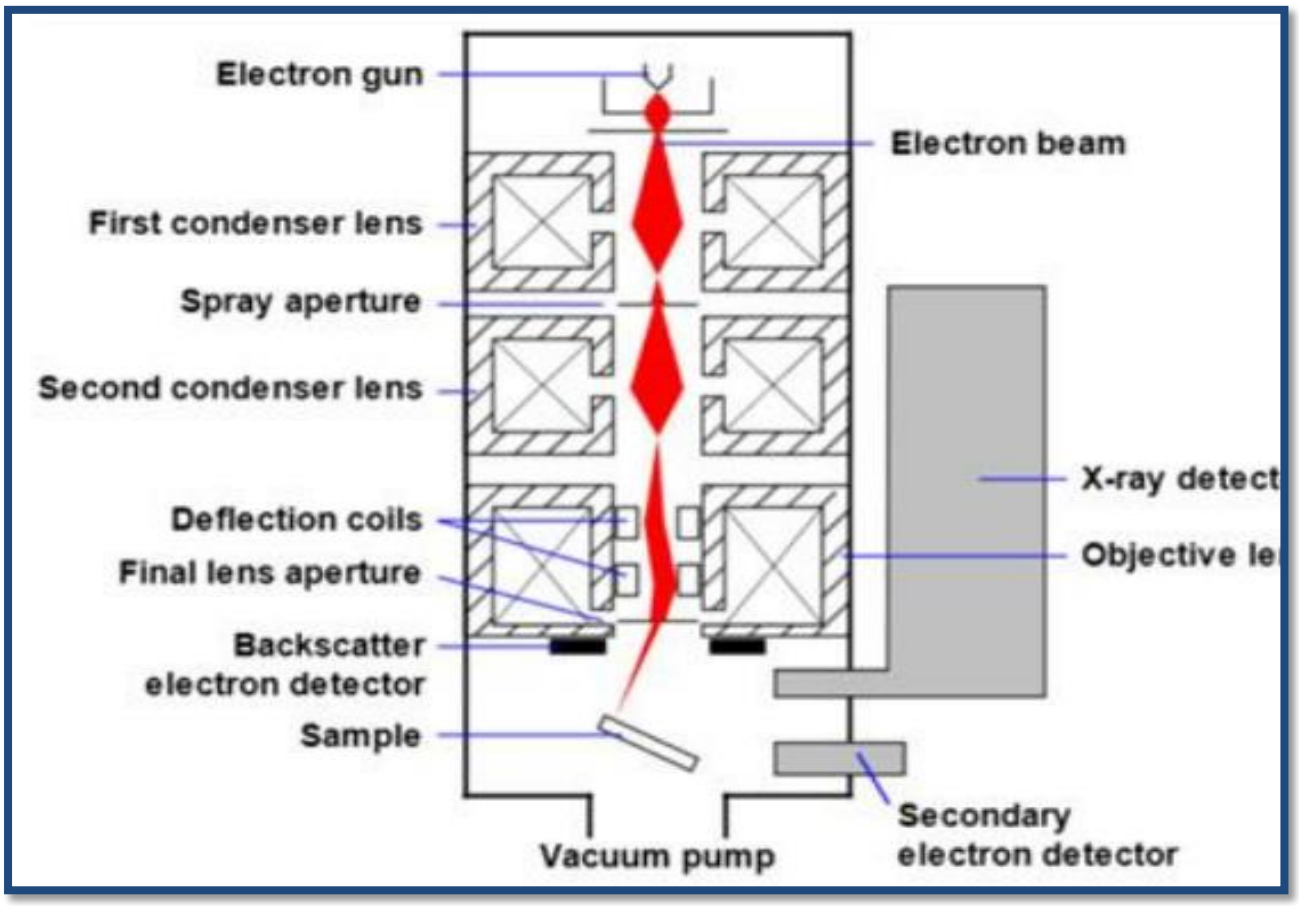

reveal information about the sample including external morphology (texture), chemical composition, and crystalline structure and orientation of materials making up the sample. In most applications, data are collected over a selected area of the surface of the sample and a 2-dimensional image is generated that displays spatial variations in these properties. SEM is routinely used to generate high-resolution images of the shapes of objects and to show spatial variations in chemical compositions [79].

Fig. (2.5): Schematic of scanning electron microscope [76].

2.3.3 Atomic Force Microscopy (AFM)

Is a high-resolution imaging technique first demonstrated by Binnig, Quate, and Gerber in 1985 [80]. Atomic force microscopy (AFM) has great potential as a tool for structural biology, a field in which there is increasing

demand to characterize larger and more complex biomolecular systems [81]. The atomic force microscope (AFM), a development of the scanning tunneling microscope (STM), is widely used for analyzing semiconductors, it is the perfect instrument for assessing morphology at the nanoscale [82]. It is possible to attain sub-Angstrom vertical resolution and 5 nm lateral resolution in an ambient environment, with no special sample conductivity or surface preparation needed [83]. AFM is one of the elected techniques for fine reconstruction of surface topographies with nanometer vertical and lateral resolution [84].

Atomic force microscopy is a high-resolution imaging technique where a small probe with a sharp tip is scanned back and forth in a controlled manner across a sample to measure the surface topography at up to atomic resolution [85]. Atomic force microscope techniques encompass a variety of scanning modes that enable scanning nanoscale [86,87].

Fig. (2.6) explains the block diagram of AFM. The atomic force microscope consists of a micro-scale cantilever with a sharp tip at its end that is used to scan the specimen surface The cantilever is typically silicon or silicon nitride with a tip radius of curvature on the order of nanometers [80].

Atomic Force Microscope principles include:

1- Surface Sensing: An AFM uses a cantilever with a very sharp tip to scan over a sample surface.

2- Detection Method: A laser beam is used to detect cantilever deflections from the surface of the sample.

3- Imaging: An AFM images the topography of a sample surface by scanning the cantilever over a region of interest [88].

Atomic Force Microscopy (AFM) , which uses a sharp tip to probe the surface features by raster scanning, can image the surface topography with

extremely high magnifications. The measurement of an AFM is made in three dimensions, the horizontal X-Y plane and the vertical Z-dimension [89].

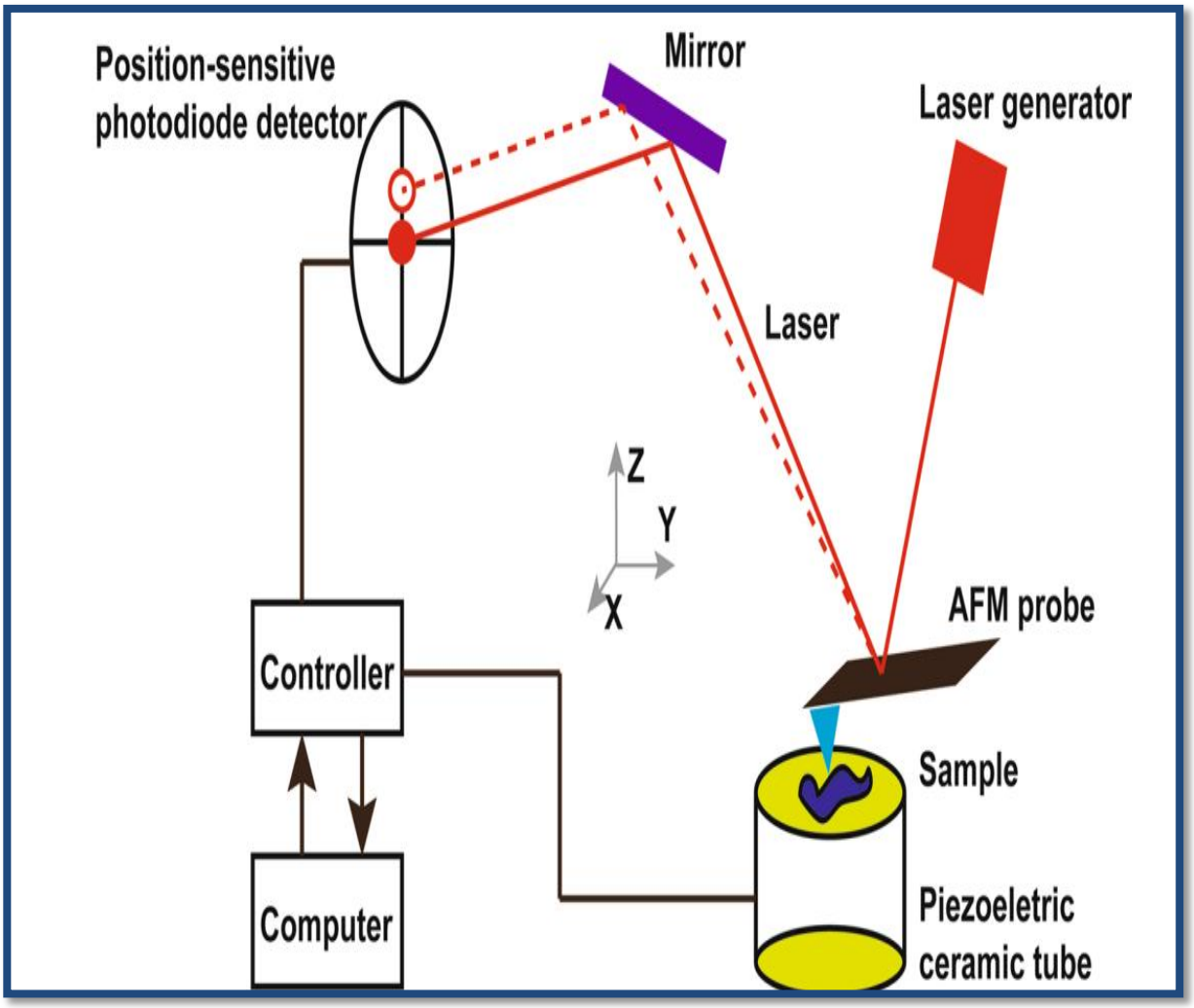

Fig. (2.6): Block diagram of atomic force microscopy [89].

2.4 Optical Properties of Semiconductors

The study of the optical properties of semiconductors is of great technical importance because it provides us with information on the energy packages and types of transitions occurring in the material and the knowledge of the properties of optoelectronic devices [90]. The optical properties of a material define how it interacts with light. The optical properties of matter include [91].

2.4.1 Absorbance (A) :

Absorption of electromagnetic radiation is how matter (typically electrons bound in atoms) takes up a photon's energy and so transforms electromagnetic

energy into internal energy of the absorber (for example, thermal energy) Equations (2-3) showing the absorbance [64] :

$$A = I_A / I_0 \qquad (2\text{-}3)$$

It is defined as the ratio between absorbed light intensity (I_A) by material and incident intensity of light (I_o).

2.4.2 Transmittance (T) :

The transmittance of the surface of a material is its effectiveness in transmitting radiant energy It is the fraction of incident electromagnetic power that is transmitted through a sample the transmittance is defined as [92].

$$T = I_T / I_0 \qquad (2\text{-}4)$$

Equation (2-4) shows the transmittance it is the ratio between the intensity of the beam from the membrane I_T to the intensity of the beam falling on the membrane $I_{0.}$

2.5 Optical Constants

2.5.1 Absorption Coefficient (α) :

The absorption coefficient determines how far into a material light of a particular wavelength can penetrate before it is absorbed. In a material with a low absorption coefficient, light is only poorly absorbed, and if the material is thin enough, it will appear transparent to that wavelength. The absorption coefficient depends on the material and also on the wavelength of light which is being absorbed. Semiconductor materials have a sharp edge in their absorption coefficient since light that has energy below the band gap does not have sufficient energy to excite an electron into the conduction band from the valence band. Consequently, this light is not absorbed [93].

The absorption coefficient (**α**) was calculated using the absorbance data by following the relation [93] :

$$\alpha = 2.303 \frac{A}{t} \quad (2\text{-}6)$$

The absorption coefficient, α, is related to the extinction coefficient, k by the following formula [93] :

$$\alpha = \frac{4\pi\, k_0}{\lambda} \quad (2\text{-}7)$$

Where λ is the wavelength. If λ is in nm, multiply by 10^7 to get the absorption coefficient in the units of cm^{-1} [94].

2.5.2 Extinction Coefficient (k_o) :

The coefficient of inertia represents the number of photons absorbed by the membrane, that is, the energy absorbed by the electrons of the material, and expresses the following relationship [92].

$$k_0 = \frac{\alpha\lambda}{4\pi} \quad (2\text{-}5)$$

Equation (2-5) shows the extinction coefficient (k_0) where (λ) is the wavelength of the incident radiation (α) absorption coefficient.

2.5.3 Refractive Index (n)

The refractive index is defined as the ratio between the speed of light in vacuum (c) and the speed of light in the matter, calculated from the amount of the following relationship [95].

$$n = \left(\frac{4R}{(R-1)^2} - k^2\right)^{1/2} + \frac{(R+1)}{(R-1)} \quad (2\text{-}16)$$

where (R) is the reflectance.

(R) is calculated from the following equation [93]:

$$R + T + A = 1 \quad (2\text{-}17)$$

2.5.4 Complex Dielectric Constant

The insulation constant is defined as the absorption of energy in the material due to the interaction of light with the charges of the medium, and that leads to the polarization of the charges, and this polarization is called the insulation constant is known as the following relationship [96].

$$\varepsilon_r = n^2 - k_0^2 \quad (2\text{-}18)$$

$$\varepsilon_i = 2nk_0 \quad (2\text{-}19)$$

$$\varepsilon = \varepsilon_r + i\varepsilon_i \quad (2\text{-}20)$$

Where ε_r is the real part of the dielectric constant, and ε_i is the imaginary part of the dielectric constant.

2.6 Fundamental Absorption Edge

The process of basic absorbance in crystalline semiconductors for incident rays happens when an electron in the valence band absorbs high energy from an incident photon to escape to the conduction band if the photon energy ($h\nu$) is equal to or larger than the forbidden energy gap (E_g) [97].

$$h\nu \geq E_g \quad (2\text{-}8)$$

where (ν) is the frequency in (Hz) and (h) Plank constant (6.625×10^{-34} $J.s$), Spectroscopy of incident ray's region which starts electrons in its transporting is called (fundamental absorption edge) is shown in Fig. (2.7). The fundamental absorption edge is one of the greatest striking features of the absorption spectrum of a semiconductor. It equals the difference between the top valence band and the bottom conduction band [98]. When ($E_g=h\nu_0$), where (ν_o) is called critical frequency and the wavelength facing it is called wavelength cut

off (λ_c) [99]. This process happens when the width of the forbidden energy gap equals to incident energy photon which can be expressed in the equation [97].

$$\lambda(nm) = \frac{hc}{E_g} = \frac{1.24}{E_g\ (eV)} \qquad (2\text{-}9)$$

Where (c) is the speed of light in a vacuum.

The study of the optical properties of semiconductors is of great technical importance because it provides us with information on the energy packages and types of transitions occurring in the material and the knowledge of the properties of optoelectronic devices.

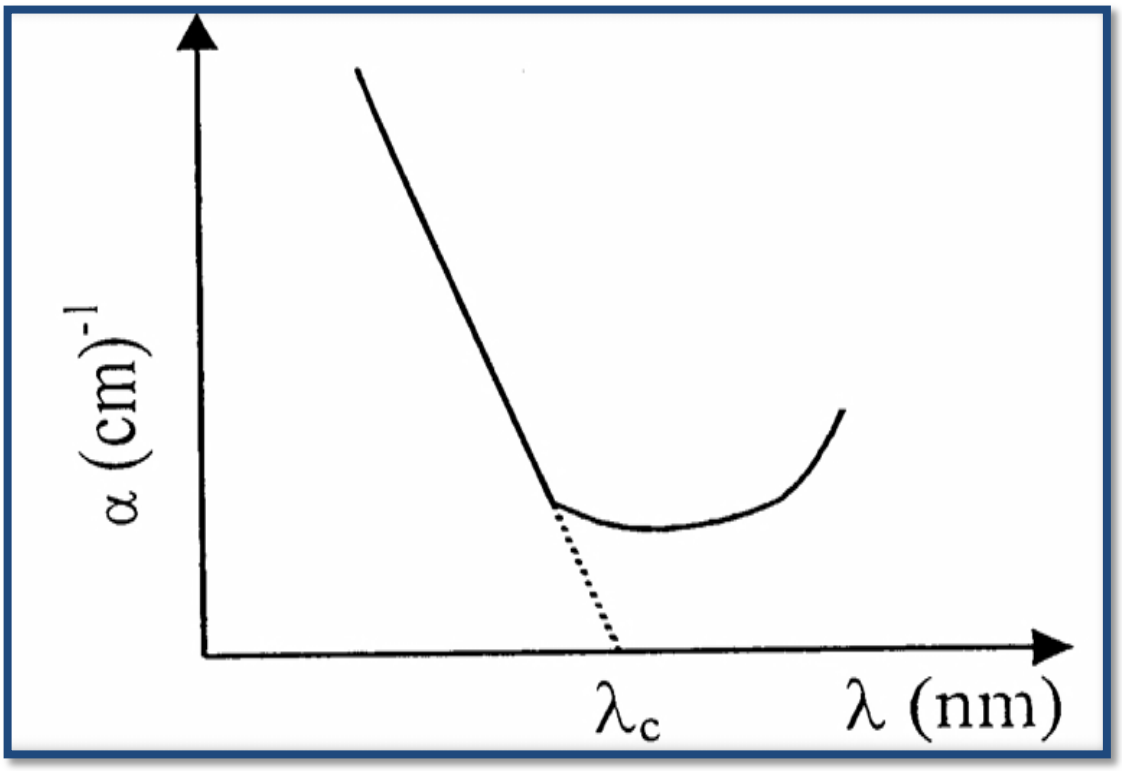

Fig. (2.7): Fundamental absorption edge of crystalline semiconductor [98].

2.7 The Electronics Transition

There are essentially two types of electronic transitions [100].

2.7.1 Direct transition

This transition happens in semiconductors when the bottom of the conduction band (C.B) is exactly over the top of the valence band (V.B). This means that they have the same value of wave vector (ΔK=0). In this state, the absorption seems when (Eg=hυ). This transition type needed the laws of conservation in energy and momentum. There are two types of direct transitions, they are [101]:

a) Allowed direct transition

Fig (2-8-a) shows this transition happens from the top points in the (V. B) and the bottom point in the (C. B.). The empirical relationship for this type of transition is given by the equation [101] :

$$\alpha h\nu \approx \left[h\nu - E_g\right]^{1/2} \qquad (2\text{-}10)$$

where (α) is the absorption coefficient.

b) Forbidden direct transitions

Fig (2-8-b) shows this transition happens from near the top points of (V. B) and the bottom points of (C.B). The empirical relationship which corresponds to this transition is given by the equation [102].

$$\alpha h\nu \approx \left[h\nu - E_g\right]^{3/2} \qquad (2\text{-}11)$$

2.7.2 Indirect Transitions

This transition happens when the bottom of (C.B) is not over the top of (V.B), in a curve (E-K). The electron transits from (V.B) is not perpendicularly where the value of the wave vector of electron before and after transition is not equal ($\Delta K \neq 0$). This transition type happens with the help of a like particle called "Phonon", for conservation of the energy and momentum law. Therefore, assistance of a phonon is necessary to conserve the momentum, so [103].

$$h\nu \approx E_g \pm E_P \qquad (2\text{-}12)$$

$$hk_f \approx hk_i \pm hk_P \quad (2\text{-}13)$$

Where E_p is the energy of absorbed or emitted phonon.

a) Allowed indirect transitions

Fig (2-8-c) shows this transition occurring between the top of (V.B) and the bottom of (C.B) which are found in the difference region of (K-space), so that [104].

$$\alpha h\nu \approx \left[h\nu - E_g\right]^2 \quad (2\text{-}14)$$

b) Forbidden indirect transitions

Fig (2-8-d) shows this transition occurring between near points at the top of (V.B) and near points at the bottom of (C.B). The absorption coefficient for transition with a phonon absorption is given by following equation [105].

$$\alpha h\nu \approx \left[h\nu - E_g\right]^3 \quad (2\text{-}15)$$

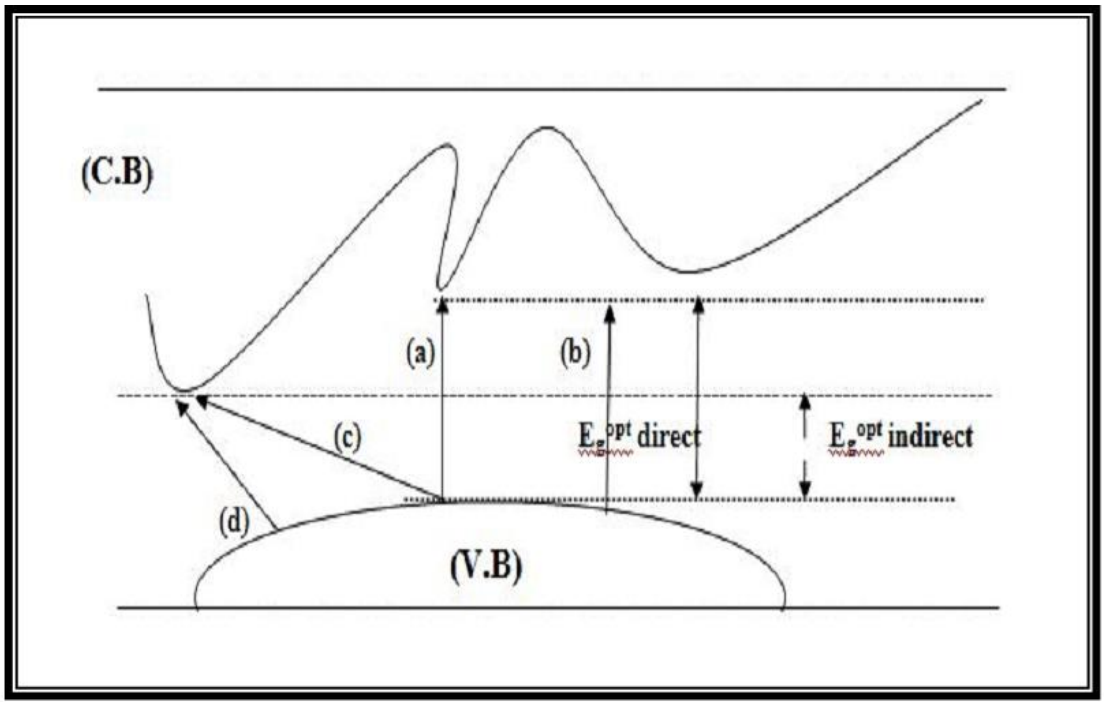

Fig. (2.8): The types of transition (a) allowed direct, (b) forbidden direct, (c) allowed indirect, (d) forbidden indirect [105].

2.8 Surface energy loss function (SELF) and Volume Energy Loss Function (VELF)

Surface energy loss function (SELF) and volume energy loss function (VELF) can be used to express these energy transfers using dielectric theory. By using the relationships (2-21) (2-22), one might compare both energy loss functions [106].

$$SELF = \frac{\varepsilon_r}{(\varepsilon_r+1)^2+\varepsilon_i^2} \quad (2\text{-}21)$$

$$VELF = \frac{\varepsilon_i}{(\varepsilon_r)^2+\varepsilon_i^2} \quad (2\text{-}22)$$

2.9 Dispersion Parameter

In optics and wave propagation in general, dispersion is the phenomenon in which the phase velocity of a wave depends on its frequency [107]. In numerous applications, including optical communication and the design of optical systems, dispersion parameters are crucial [108]. The single effective oscillator energy (E_O), dispersion energy (E_d), and estimated zero-frequency refractive index (n_0) and dielectric constant (ε_∞), as well as the optical moments, are calculated using the Wemple-DiDomenico (WDD) model in Equation [109,110] :

$$(n^2 - 1) = \frac{E_d\, E_0}{E_0^2-(h\nu)^2} \quad (2\text{-}23)$$

$$n_0^2 = 1 + E_d/E_O \quad (2\text{-}24)$$

where n denotes the refractive index. (E_o)(E_d) is the model's primary output. The energy (E_o), or average energy gap, provides quantitative information about the material's overall band structure. This differs from the information obtained from the optical gap which investigates the material's optical characteristics near its basic absorption edge. Despite the difference be showing that the oscillator energy, (E_o) is often twice the optical energy gap, (E_g) i.e. ($E_o \approx 2E_g$) [111]. On the other hand, the dispersion energy (Ed), which is a measure of oscillator strength, quantifies the average energy of interbond optical transitions and is associated with the sample's structural order, i.e, it is related to the ionicity,

anion valency, and coordination number of the material [112,113]. It's worth noting at this point that the dispersion energy (E_d) is almost completely independent of the effective single oscillator energy, (E_o). This is because Ed is proportional to the dielectric loss, whereas (E_o) is independent of the dielectric loss, either close or from afar. The static refractive index (n_o), has been calculated from WDD dispersion parameters, E_o, and, E_d, using the formula (2-23) and (2-24) M_{-1} M_{-3} moments of the optical spectra can be obtained from the relationships. The M_{-1} and M_{-3} moments of the optical spectra can be obtained from the relationships [114,115].

$$\varepsilon_\infty = n^2(0) \qquad (2\text{-}25)$$

$$E_0^2 = \frac{M_{-1}}{M_{-3}} \qquad (2\text{-}26)$$

$$E_d^2 = \frac{M_{-1}^2}{M_{-3}} \qquad (2\text{-}27)$$

The obtained values are given formula The (M_{-1} and M_{-3}) moments changed due to the formation coordination Wimple-DiDomenico.

2.10 The weight method

The thickness of the thin films has been calculated according to the following equation (3-1) :

$$t = \frac{m}{2\pi\rho R^2} \qquad (2\text{-}28)$$

Where:

t: is the thickness of the thin films (nm).

m: mass of the material in (g)

ρ: is the density of material (g/cm^3).

R: is the distance between the substrate and the boat (cm).

This method gives an approximate thickness because not all the material is deposited on the substrate but some of the material is lost or fleeing on the sides of the heater. We get this thickness (65, 72, 80, 88, 100, 110, 124, and 140 nm).

Chapter Three

Experimental And Measurement

3.1 Introduction

This chapter emphasizes the experimental details used in the fabrication and investigation of pure CdTe thin films with different thicknesses by thermal evaporation method on a glass substrate under pressure up to 1×10^{-7} mbar with a rate of deposition 0.5 nm/sec onto a glass substrate. The techniques used for preparation and testing the structure of the thin films are the investigation of the structural and morphological features by X-ray diffraction (XRD), scanning electron microscope (SEM), and atomic force microscope (AFM), and the determination of grain size are presented. The optical measurements of thin films such as (transmittance (T), absorbance (A), absorption coefficient (α), optical energy gap (E_g), refractive index (n), extinction coefficient (k_o), and the dielectric constants (ε_r and ε_i) and Surface Energy loss function (SELF), Volume Energy loss function (VELF) in addition of dispersion parameters. The schematic diagram of the experimental work starting from material up to film characterization is displayed in Fig (3.1).

3.2 Nanomaterial Used:

1- Cadmium telluride (CdTe) :

It was observed as a powder from Zhengzhou Dongyao nano materials Co. LTD China company, with a nano grain size of 44 μm, density of 6.20 g/cm^3, color black to brown, and high purity (99.99 %).

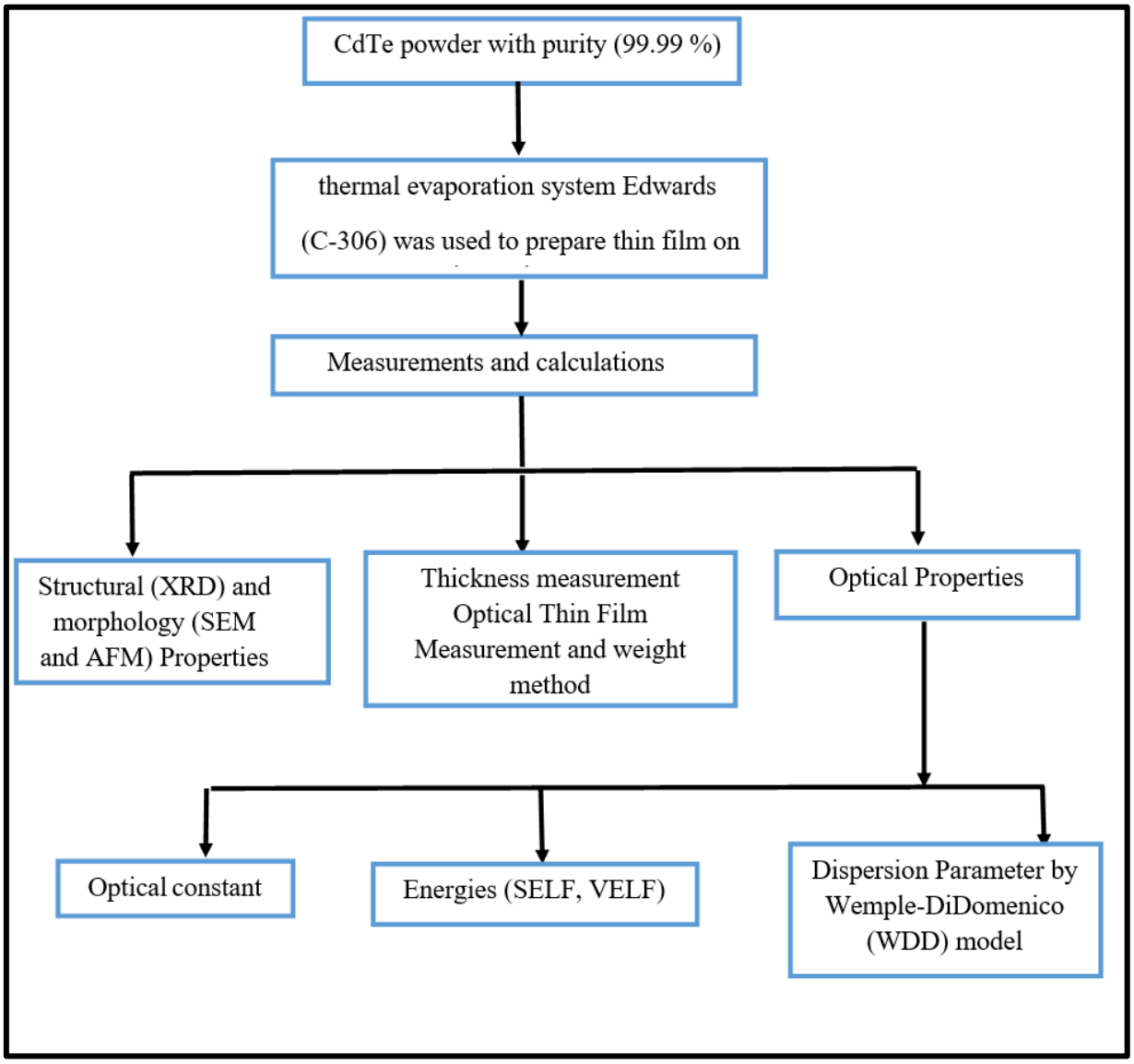

Fig. (3.1): Schematic diagram of experimental work

3.3 Substrate Preparation

The glass slides each of (2.54 × 7.62) cm^2 area was used as substrates with thickness (0.1-0.12) cm. These glass slides were subjected to the following steps:

1- The substrates were cleaned with alcohol.

2- The substrates were immersed in a clean beaker containing distilled water and then washed ultrasonically for 10 min .

3- Lastly, the glass substrates were dried by an air jet and rubbed with soft paper.

3.4 Evaporation Boat

The most commonly used materials for evaporation boats are metals with a high melting point, such as tungsten (W) (M.P = 3370 ^{o}C), and molybdenum (Mo) (M.P = 2622 ^{o}C). In this work, a molybdenum boat was used for the deposition of CdTe thin film, as shown in Fig. (3.2).

Fig. (3.2): Evaporation Boat Molybdenum boat

3.5 The Coating Unit

The vacuum unit system is:

1- Edwards Auto 306 that modified its chamber.

2- Uses tungsten or Molybdenum filaments to heat evaporates.

3- Ultimate chamber pressure 1×10^{-7} mbar.

4- Typical filament currents are (100-200) A.

5- Maximum deposition thickness that can be achieved is 1.5 μm.

The main constructions of the typical vacuum coating unit are shown in Fig (3.3). This calculation was carried out Department of Physics, University of Babylon/College of Education for Pure Sciences.

Fig. (3.3): Thermal evaporation system.

3.6 Thin Film Growth

In the present work, thin films of CdTe have been (powder, purity 99.99%). The deposition of CdTe thin films has been performed by electrical resistance heated thermal evaporation process. In this process, the electrical power is passed through the boat to create a vapor that travels in straight-line paths to the substrate. In general, there are three steps in any vacuum deposition process; creation of an evaporate from the source material; transport of the evaporator from the source to the substrate; and condensation of the evaporator

onto the substrate to form the thin film deposited. In this work, the evaporation processes have been performed at room temperature (R.T). The pressure during the evaporation was approximated to 10^{-7} mbar with a rate of deposition of 0.5 nm. s^{-1}. The distance between the source and substrate was kept at 15 cm.

3.7 Films Thickness Measurement

Thickness is one of the most important thin film parameters. There are several methods used for measuring the thickness of the thin film. In this work, the thickness of the films was measured using the optical measurement and weight method, the measurements from the two methods were comparable**.**

3.7.1 Optical measurement method

Film thickness measurements by Optical Thin Film Measurement have been obtained. This method is based on interference of the light beam reflected from the thin film surface and substrate bottom, as shown in Fig. (3.4). This calculation was carried out Department of Physics, University of Babylon/College of Education for Pure Sciences.

With the optical interferometer and the weight method from both methods, the thickness measurements were close**.**

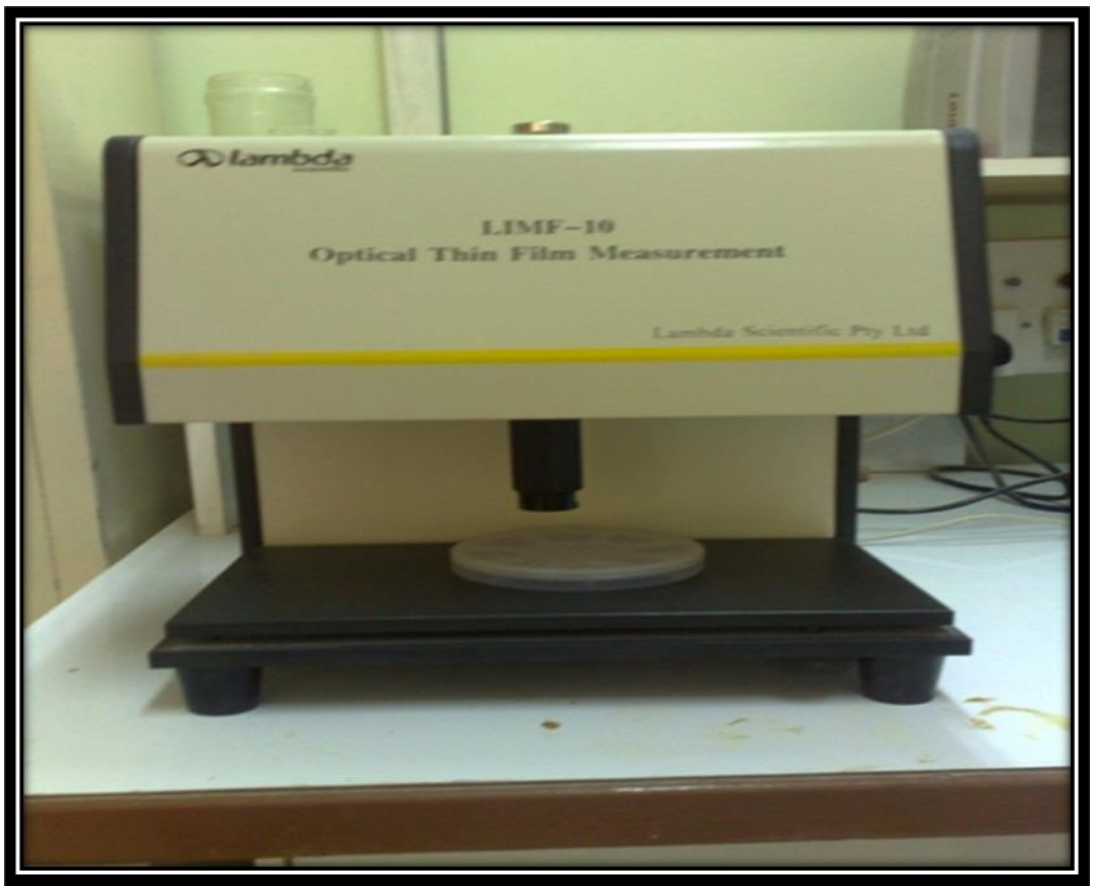

Fig. (3.4): Optical thin film measurement.

3.8 Structural and Morphological Measurements

3.8.1 X-ray diffraction (XRD)

These measures' primary goal is to look at the kind of structure that exists in the prepared thin films. The general structure of bulk solids can be analyzed using this experimental method, including lattice constants, the identification of unknown materials, the orientation of single crystals and polycrystals, flaws, stresses, etc. employing an X-ray diffracts meter system (XRD-6000) from SHIMADZU to measure X-ray intensity as a function of Bragg's angle The system's conditions were as follows:

Source CuK_{α} with radiation of wavelength $\lambda = 1.5406$ Å.

Target: Cu

Current = 30 mA.

Voltage = 40 kV.

Scanning speed = 0.25 deg/min

The X-ray scans are performed between 2θ values of 5^{o} and 80^{o} as shown in Fig. (3.5).

Fig.(3.5): The system of the XRD.

3.8.2 Scanning Electron Microscope (SEM)

SEM is an electron microscope that images the sample surface with a high-energy beam of electrons in a raster scan pattern. After the preparation of the sample, the part of each sample with dimensions (5 mm × 10 mm) was cut and pleased into the SEM sample holder for examination. The surface morphology of CdTe is observed using (INSPECT S50, company, Japan origin, type FEI customer ownership SEM), as shown in Fig. (3.6). This calculation was carried out in Iran at the University of Tehran.

Fig. (3.6): The system of SEM

3.8.3 Atomic Force Microscope (AFM).

Surfaces can be examined at the molecular level using an atomic force microscope (AFM). Real topography data are obtained rather than just images. Using an atomic force microscope (AFM), researchers may analyze the size and other properties of produced nanoparticles. Fig. (3.7). illustrates the AFM's basic operating principle. The thin-scope AFM is used to examine each sample. It is

located at the University of Babylon/College of Education for Pure Sciences-Department of Physics.

Fig. (3.7): The system of AFM

3. 9 Optical Measurement

The optical measurements of CdTe thin films are acquired using a spectrophotometer (Shimadzu UV- 1650 PC) made by Phillips, a Japanese firm, as shown in Fig. (3.8), for the wavelength range of 200 to 1100 nm. From these optical measurements, the optical characteristics are computed. It is located at the University of Babylon/College of Education for Pure Sciences-Department of Physics.

Fig. (3.8): Shows a photo of a UV-VIS-NIR spectrophotometer

Chapter Four

Results And Discussion

4.1 Introduction

This chapter presents the results and discussion of the structural, morphological, and optical properties of CdTe thin films (Dispersion parameters were also investigated using the Wemple-Didominco model) for different thicknesses (65, 72, 80, 88, 100, 110,124 and 140) nm . These are deposited on glass substrates by the thermal evaporation technique. The samples were diagnosed by XRD, SEM, AFM, and UV-Visible spectrophotometer.

4.2 Thin Films Test and Results

After the deposition of the thin films on glass slides were completed, structural and optical tests and performed to determine the effect of the preparation parameters used to prepare them in this study.

4.2.1 Structural and Morphological Properties

Structural and morphological properties include the X-ray Diffraction (XRD), scanning electron microscopeMicroscope (SEM), and Atomic Force Microscope (AFM).

4.2.1.1 X-ray Diffraction of CdTe Thin Films

To investigate the structural nature of CdTe films, the X-ray diffraction was recorded between 5^{o}-80^{o}. The XRD spectra of CdTe thin films with different thicknesses were prepared by thermal evaporation technique at R.T.

The XRD pattern of CdTe thin films is shown in Fig. (4.1- 4.8). The low-intensity peak that appeared at $2\theta=23.03^{o}$ corresponding to (111) was correlated with a value obtained by Sotelo-Lermaetal [39]. A gradual rightward shift in the angles represents a crystalline structure on a tiny scale. It was noticed that the CdTe films produced through thermal evaporation were a cubic phase. From the Fig., no sharp peaks were noticed in the prepared films making the concluded films amorphous. Similar behavior was reported in [50,116].

The XRD patterns were used to calculate the crystallite size and other microstructural characteristics. The crystallite size (D) was calculated using Scherrer formula eq. (2-2) from the low intensity peaks [69].

It was found that when the film thickness increased to the optimum value, the size of the crystallites increases. The improvement in crystallinity due to the elimination of grain boundaries with some weak aggregations, a further factor that influences crystallinity enhancement is the atoms' mobility after on the surface. When a substrate undergoes thermal evaporation, more atoms settle evenly throughout its surface as the substrate's thickness grows [117,50].

The smallest crystallite size (D=4.14) was found in the 72 nm thickness, and on the other hand, the biggest (D=14.33 nm) was found at 140 nm. From figures (4.1- 4.8), the values of crystallite size and FWHM are tabulated in Table (4.1), it can note that the broadening in full width at half maximum (FWHM) indicates the small particle size [118].

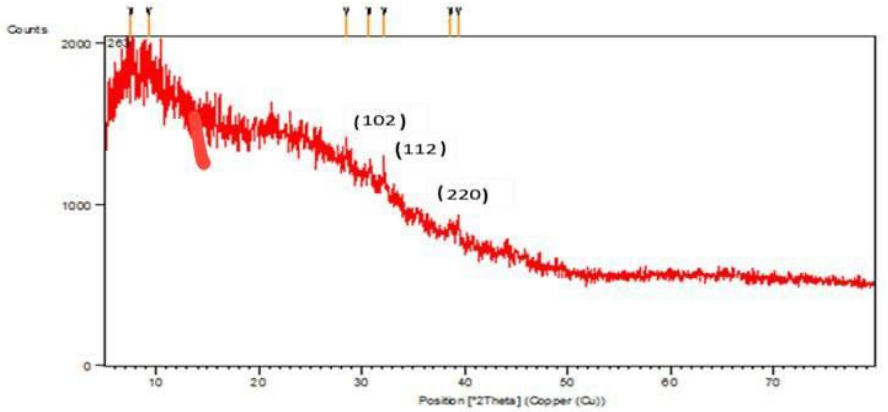

Peak List

Pos.[°2Th.]	Height [cts]	FWHMLeft[°2Th.]	d-spacing [Å]	Rel. Int. [%]
7.53(8)	115(34)	0.9(3)	11.72350	95.98
9.3(1)	120(29)	1.4(4)	9.52233	100.00
28.47(5)	62(12)	0.7(2)	3.13267	51.89
30.71(4)	61(12)	0.5(2)	2.90915	50.96
32.14(2)	96(17)	0.3(1)	2.78291	80.08
38.64(5)	43(9)	0.5(2)	2.32828	35.49
39.36(2)	92(18)	0.25(7)	2.28741	76.47

Thickness=65nm

Fig. (4.1): The XRD patterns of CdTe thin films at t=65nm

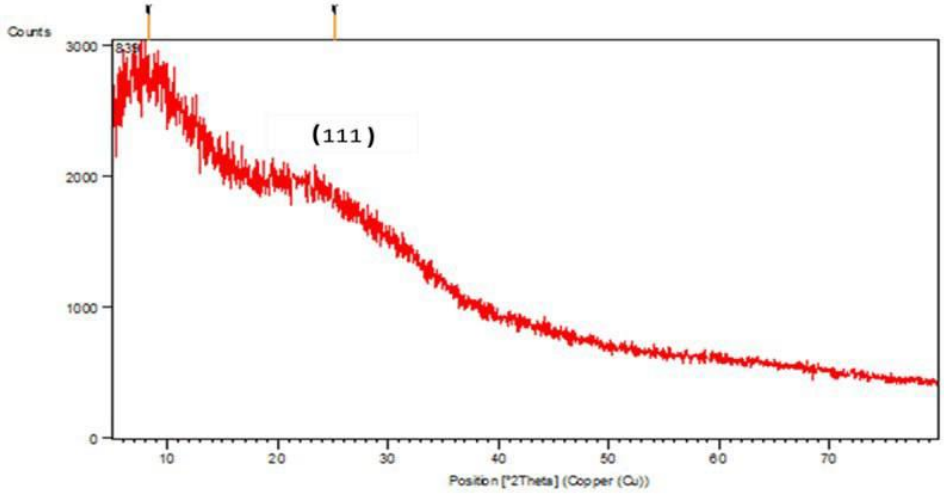

Peak List

Pos.[°2Th.]	Height [cts]	FWHMLeft[°2Th.]	d-spacing [Å]	Rel. Int. [%]
8.223594	255.269800	9.942400	10.74294	100.00
25.085440	181.599400	9.491552	3.54703	71.14

Thickness=72nm

Fig. (4.2): The XRD patterns of CdTe thin films at t=72 nm

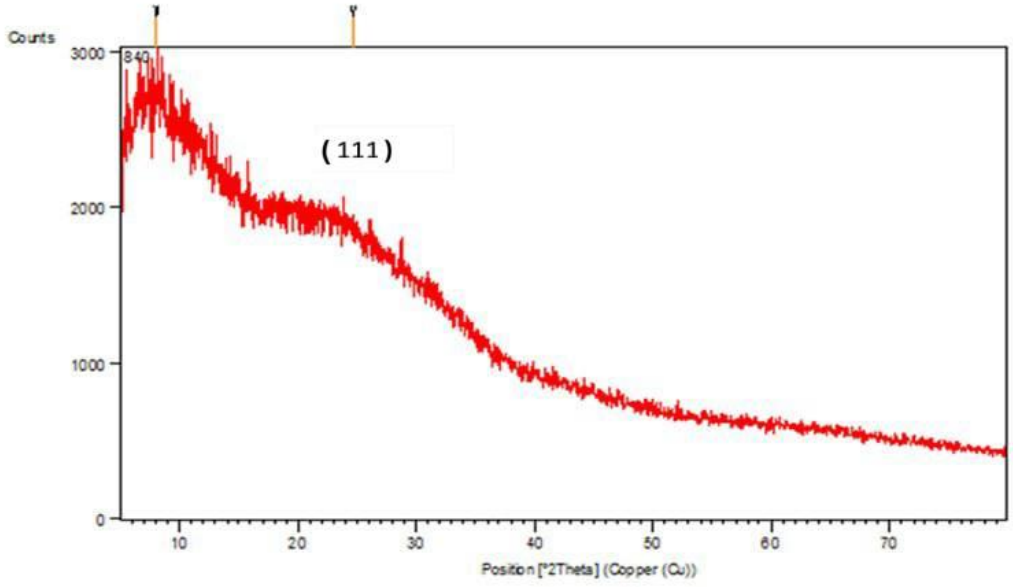

Peak List

Pos.[°2Th.]	Height [cts]	FWHMLeft[°2Th.]	d-spacing [Å]	Rel. Int. [%]
8.069888	232.577900	9.796800	10.94721	100.00
24.682070	200.585800	9.428833	3.60407	86.24

Thickness=80nm

Fig. (4.3): The XRD patterns of CdTe thin films at t=80 nm

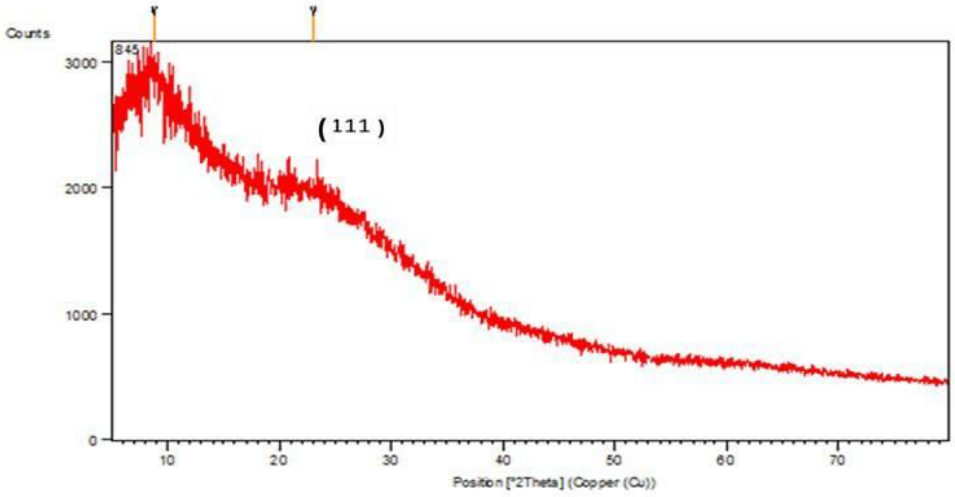

Peak List

Pos.[°2Th.]	Height [cts]	FWHMLeft[°2Th.]	d-spacing [Å]	Rel. Int. [%]
8.778170	311.794600	4.100680	10.06544	100.00
23.030950	86.857000	3.850212	3.85858	27.86

Thickness=88nm

Fig. (4.4): The XRD patterns of CdTe thin films at t=88 nm

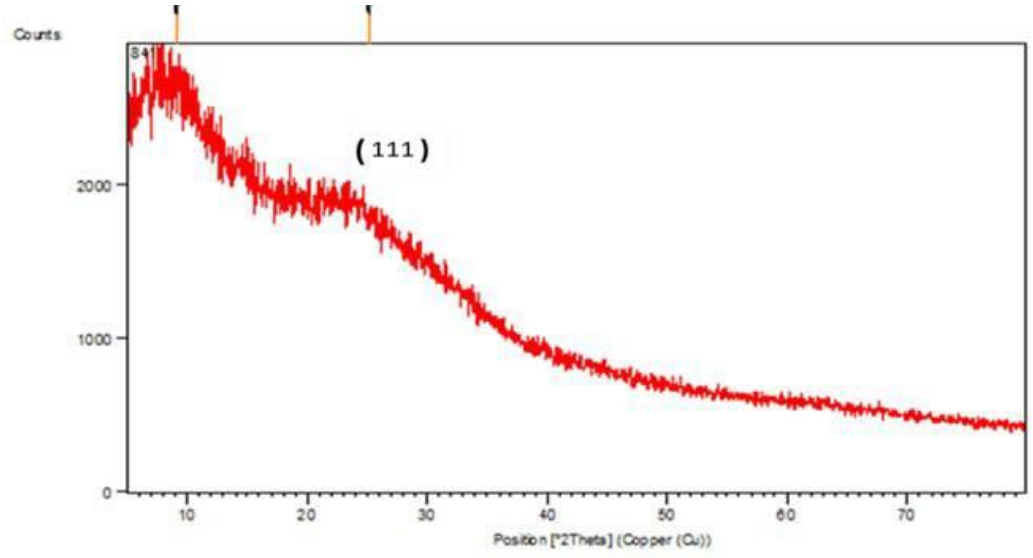

Peak List

Pos.[°2Th.]	Height [cts]	FWHMLeft[°2Th.]	d-spacing [Å]	Rel. Int. [%]
9.057738	195.495800	8.819200	9.75539	100.00
25.117930	190.289000	8.426194	3.54251	97.34

Thickness=100nm

Fig. (4.5): The XRD patterns of CdTe thin films at t=100 nm

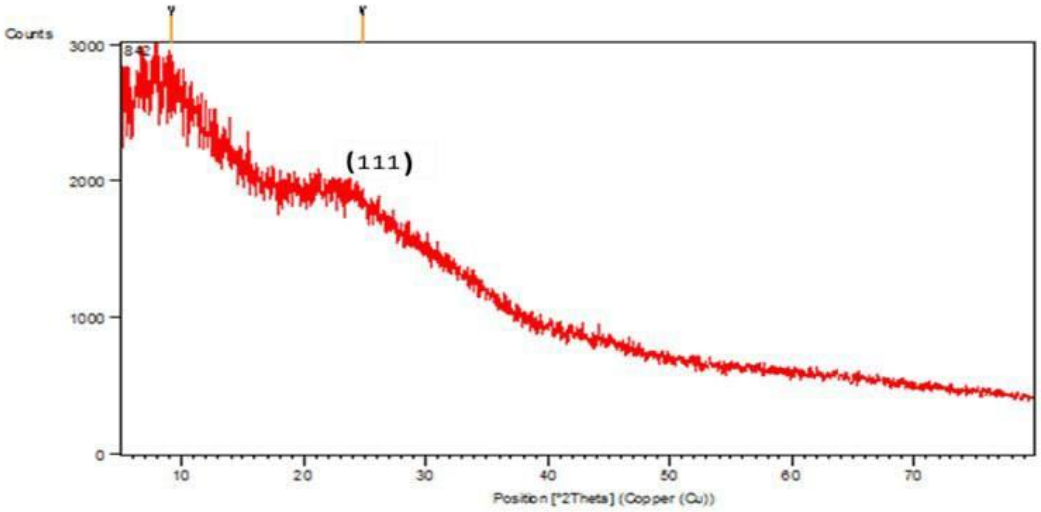

Peak List

Pos.[°2Th.]	Height [cts]	FWHMLeft[°2Th.]	d-spacing [Å]	Rel. Int. [%]
9.116132	157.235000	6.978066	9.69303	84.19
24.811500	186.757200	7.177198	3.58557	100.00

Thickness=110nm

Fig. (4.6): The XRD patterns of CdTe thin films at t=110 nm

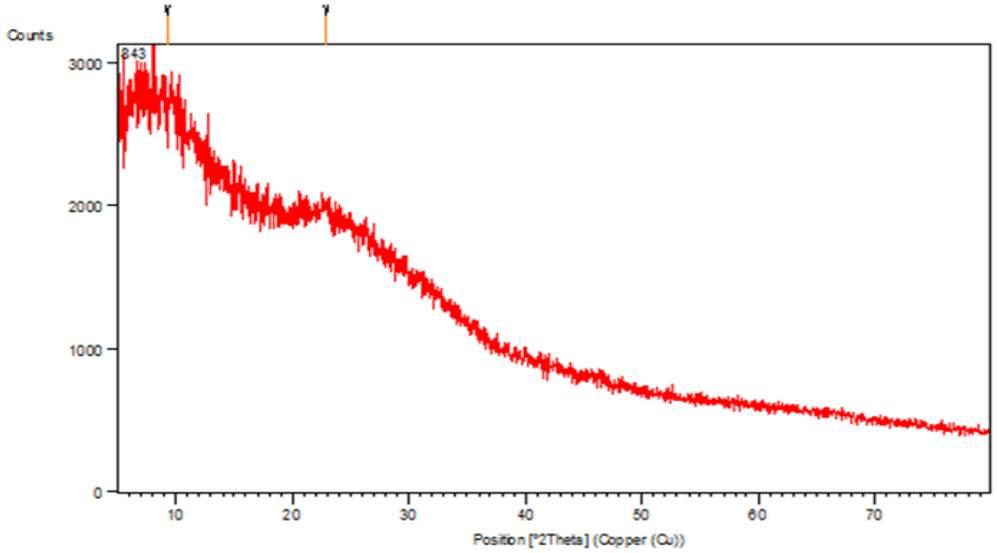

Peak List

Pos.[°2Th.]	Height [cts]	FWHMLeft[°2Th.]	d-spacing [Å]	Rel. Int. [%]
9.249421	195.720600	4.317846	9.55365	100.00
22.914450	105.045300	3.626126	3.87794	53.67

Thickness=124nm

Fig. (4.7): The XRD patterns of CdTe thin films at t=124 nm

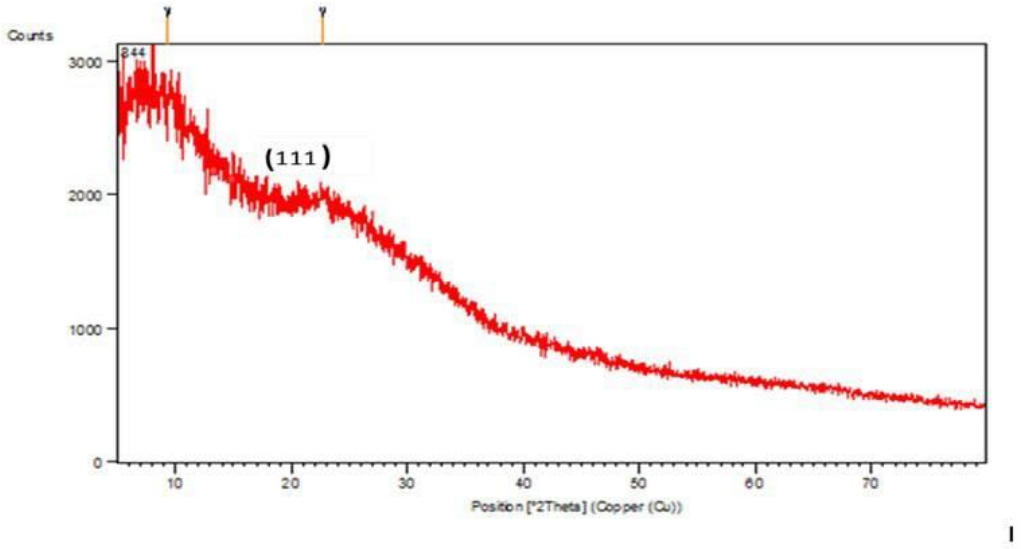

Peak List

Pos.[°2Th.]	Height [cts]	FWHMLeft[°2Th.]	d-spacing [Å]	Rel. Int. [%]
9.327972	207.211200	4.583607	9.47337	100.00
22.685610	116.568100	2.029466	3.91654	56.26

Thickness=140nm

Fig. (4.8): The XRD patterns of CdTe thin films at t=140 nm

Table (4.1): The average crystallite size, FWHM, and peak position of the different thicknesses of CdTe thin film samples

Thickness (nm)	peak position (2θ°)	FWHM (β°)	D (nm)	The average the crystallite size (nm)
65	32.14	3	27.5706	4.6797
	9.3	14	5.6961	
	7.53	9	8.8505	
72	8.22359	9.9424	8.01498	4.1484
	25.0854	9.491552	8.57863	
80	8.06989	9.7968	8.13332	4.190
	24.6821	9.42883	8.62899	
88	8.77817	4.10068	19.4399	10.126
	23.031	3.85021	21.0675	
100	9.05774	8.8192	9.04072	4.831
	25.1179	8.42619	9.66387	
110	9.116132	6.978066	11.426	5.691
	24.8115	7.177198	11.3389	
124	9.24942	4.3178	18.4681	10.208
	22.9145	3.62613	22.3648	
140	9.32797	4.58361	17.3983	14.335
	22.6856	2.029466	39.944	

4.2.1.2 Scanning Electron Microscope (SEM):

Scanning Electron Microscope (SEM) was used to investigate the surface morphology of samples and the dispersion of CdTe thin film on the surface. SEM showed the morphology of the CdTe films on the glass slide at 50kx and the scale was 200 nm.

The deposited CdTe samples on the glass substrate are shown in Figures (4.9 and 4.10). Figures show that the CdTe thin films at different thicknesses exhibit a smooth surface consisting of small spherical grains, the increase of thickness leading to changes in the morphology of the surface, and an increase in the roughness. This enhanced crystallinity points to due to the coalescence of atoms on the substrate surface. This inference is consistent with the result of the XRD measurement and the results of the previous researchers [119].

From images in the Fig. (4.9 and 4.10), uniform morphology reveals a rather smooth surface and the increase in thickness led to changes in the morphology of the surface, the average grain size increased with increasing thickness, in increased 17.86 nm at a thickness of 65 nm, and appear some agglomerations at increasing thickness of thin film.

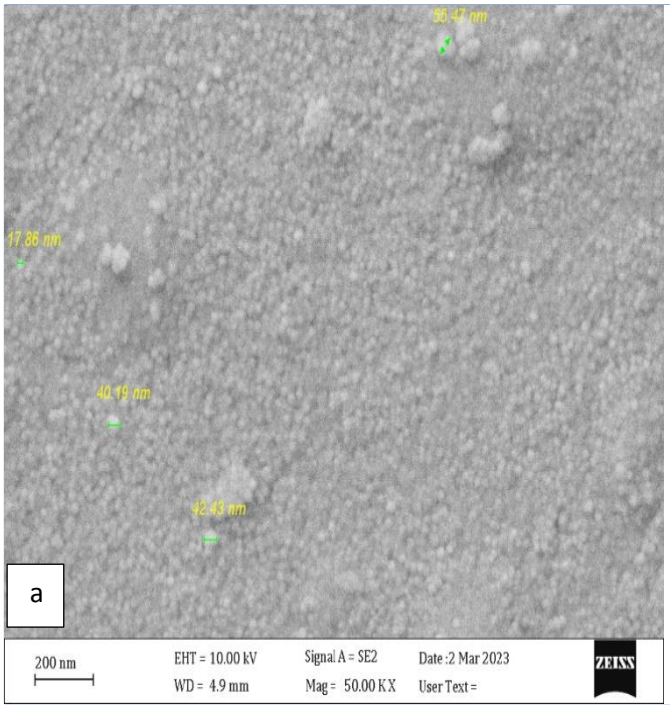
86.47 nm
17.86 nm
40.19 nm
42.43 nm
a
200 nm
EHT = 10.00 kV
WD = 4.9 mm
Signal A = SE2
Mag = 50.00 K X
Date :2 Mar 2023
User Text =
ZEISS

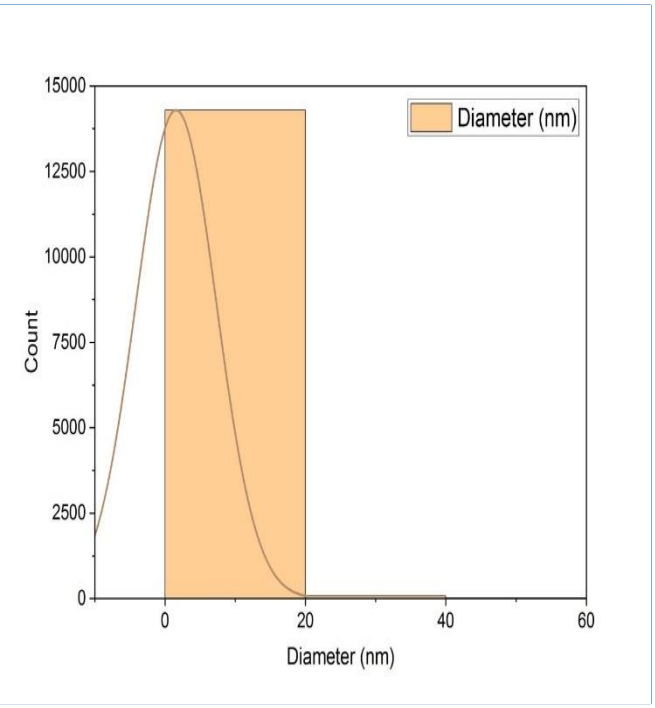
Diameter (nm)
Count
Diameter (nm)
15000
12500
10000
7500
5000
2500
0
0
20
40
60

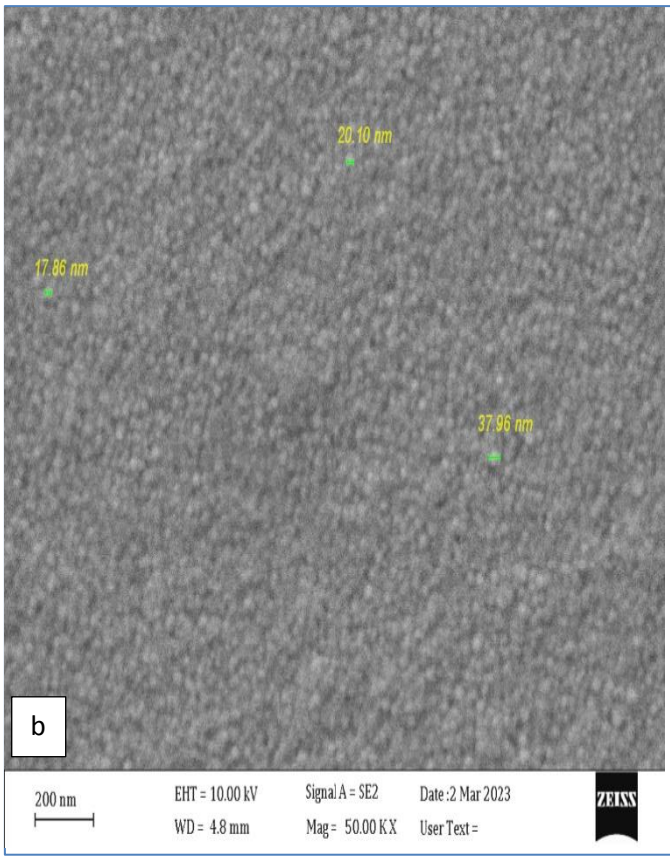
20.10 nm
17.86 nm
37.96 nm
b
200 nm
EHT = 10.00 kV
WD = 4.8 mm
Signal A = SE2
Mag = 50.00 K X
Date :2 Mar 2023
User Text =
ZEISS

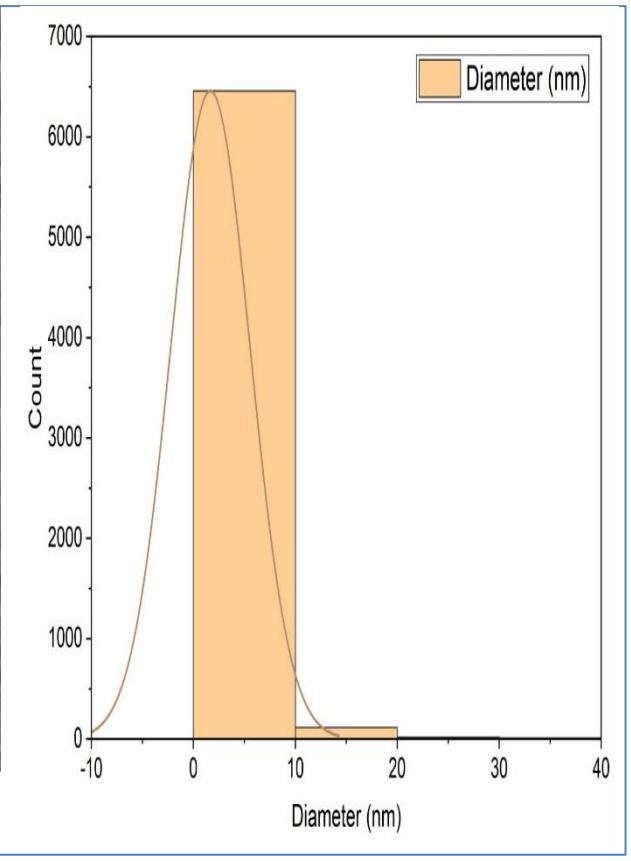
Diameter (nm)
Count
Diameter (nm)
7000
6000
5000
4000
3000
2000
1000
0
-10
0
10
20
30
40

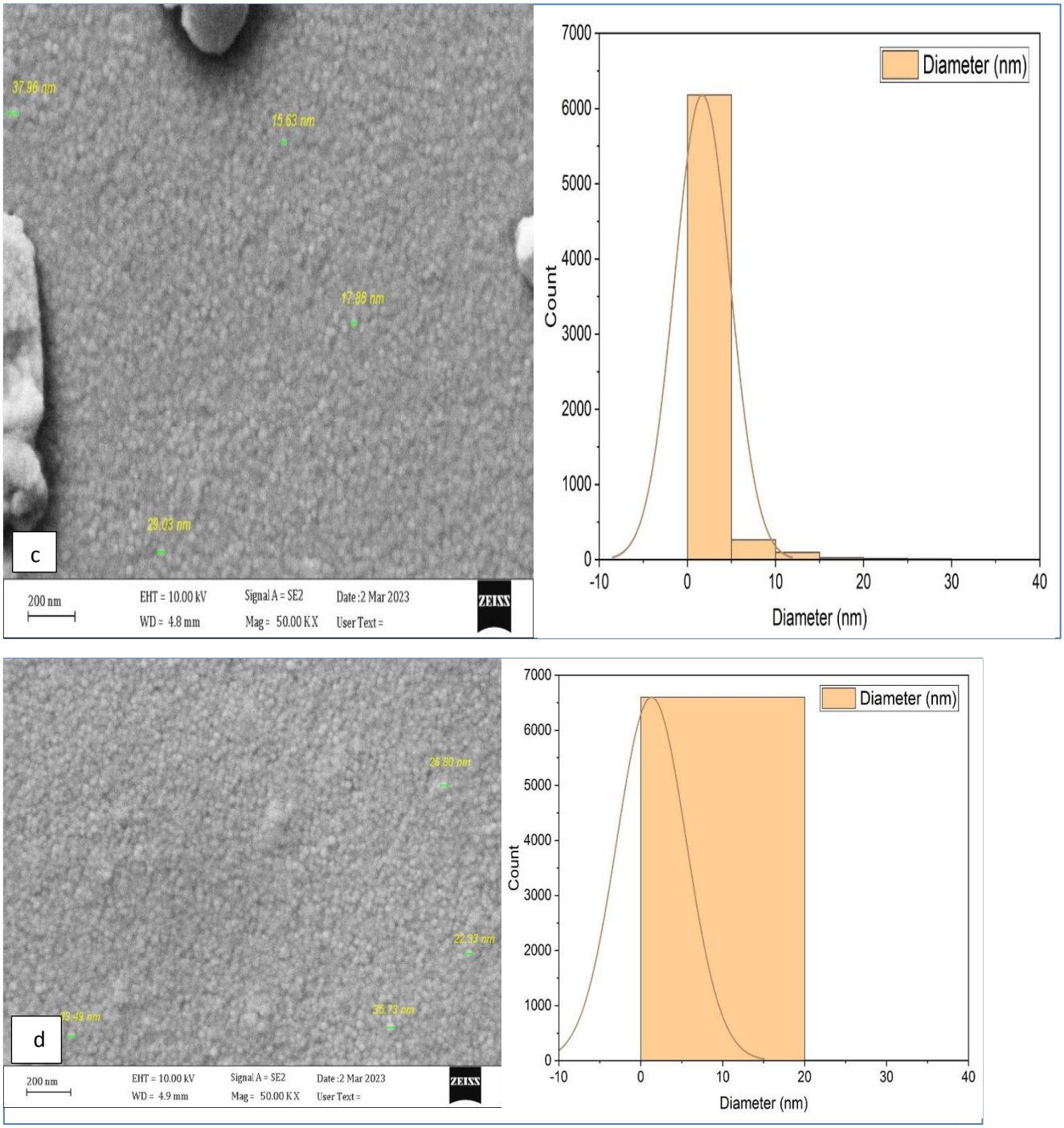

Fig. (4.9): *SEM* images and grain distribution function of the CdTe thin films at thickness a=65 nm,b=72 nm, c=80 nm, d=88 nm

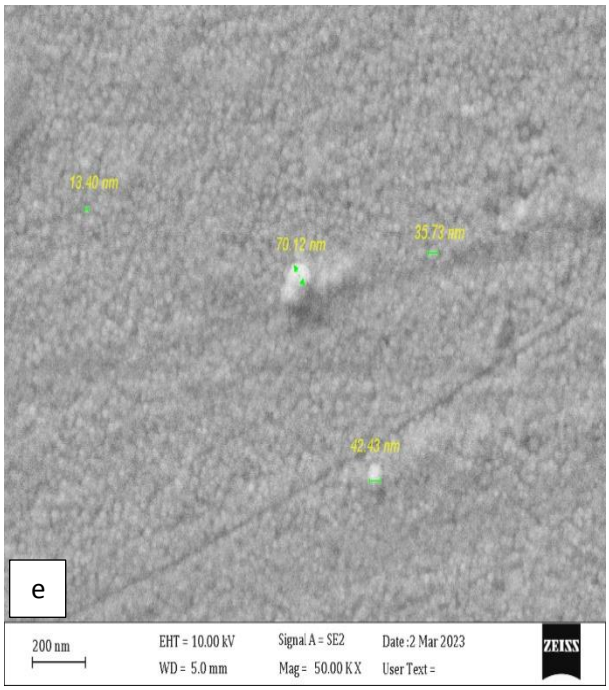
13.40 nm
70.12 nm
35.73 nm
42.43 nm
e
200 nm
EHT = 10.00 kV
WD = 5.0 mm
Signal A = SE2
Mag = 50.00 K X
Date :2 Mar 2023
User Text =
ZEISS

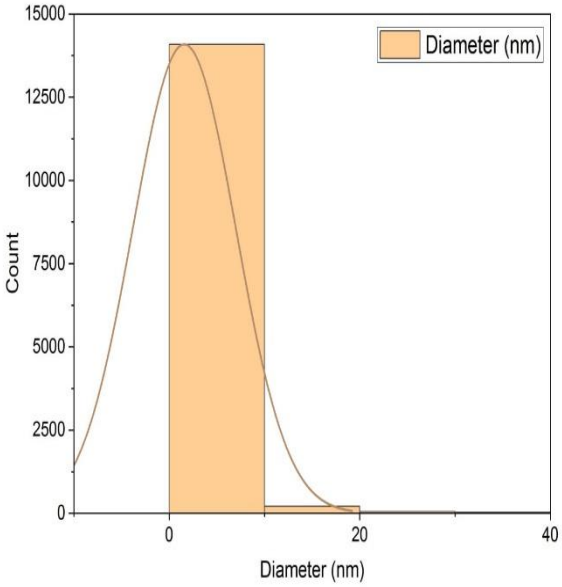
Diameter (nm)
Count
Diameter (nm)
15000
12500
10000
7500
5000
2500
0
0
20
40

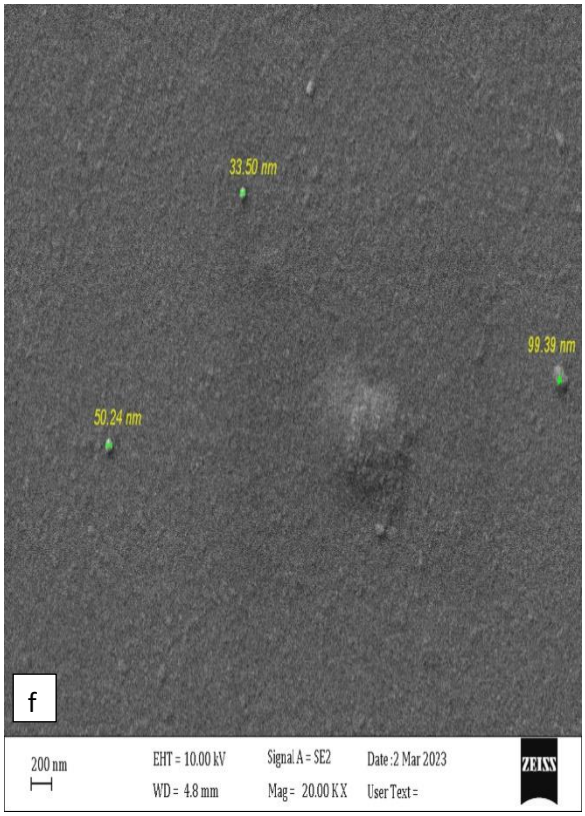
33.50 nm
99.39 nm
50.24 nm
f
200 nm
EHT = 10.00 kV
WD = 4.8 mm
Signal A = SE2
Mag = 20.00 K X
Date :2 Mar 2023
User Text =
ZEISS

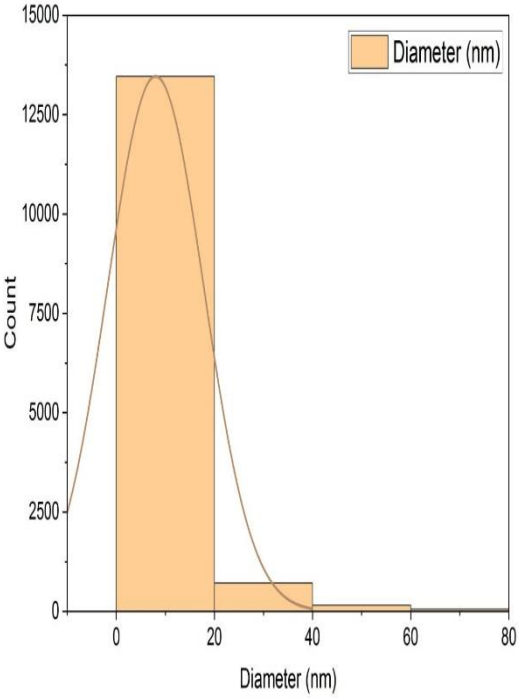
Diameter (nm)
Count
Diameter (nm)
15000
12500
10000
7500
5000
2500
0
0
20
40
60
80

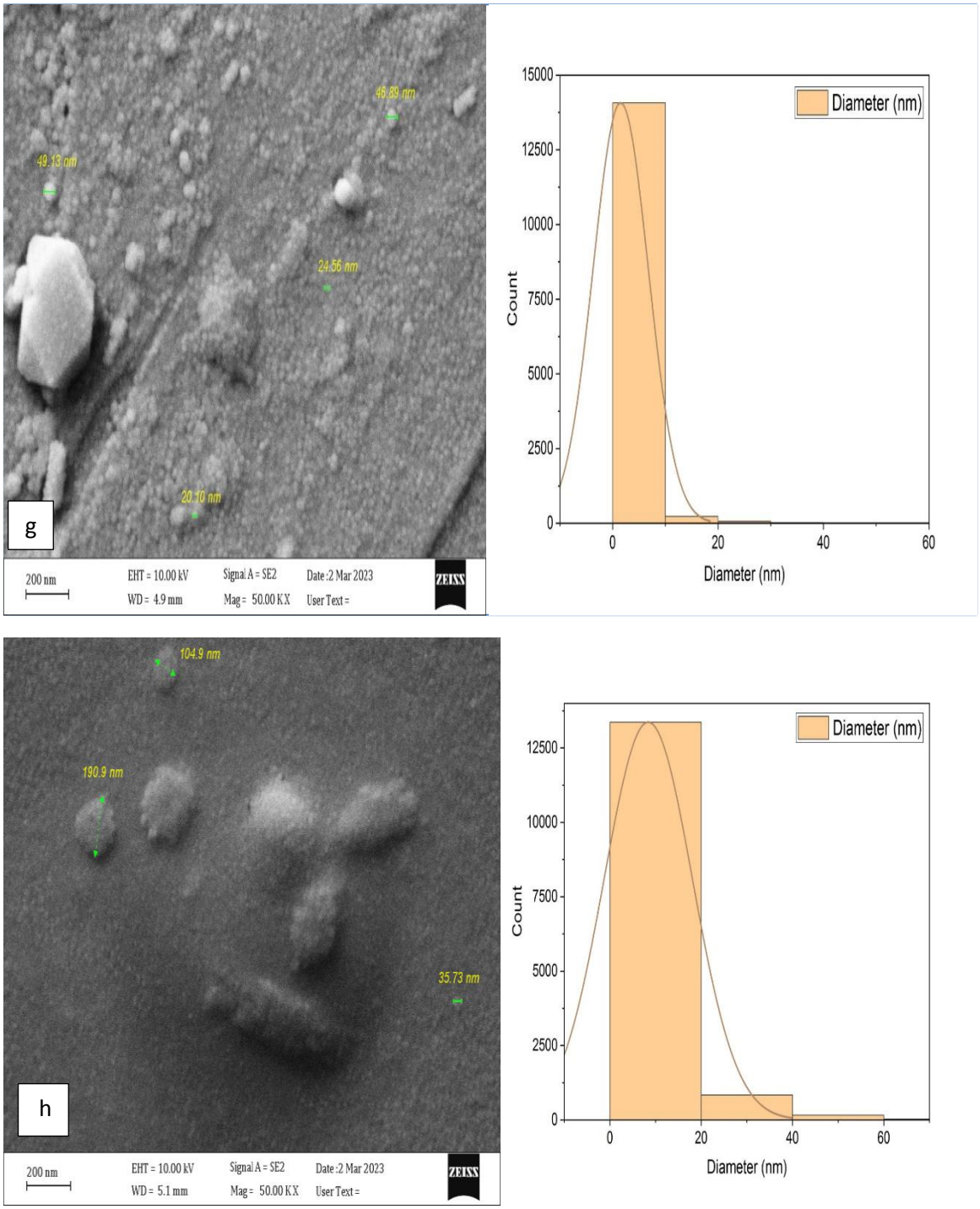

Fig. (4.10): *SEM* images grain distribution function of the CdTe thin films at thickness a=100 nm,b=110 nm, c=124 nm, d=140 nm.

4.2.1.3 Atomic Force Microscopy (AFM)

The AFM images of CdTe thin film with different thicknesses prepared by the thermal evaporation technique are shown in Figs. (4.11- 4.18). From the figures, of these images, the CdTe thin film shows a high surface homogeneity as in SEM in which the distribution of crystalline granules is uniform which is

evident from the convergence of the roughness and root mean square (RMS). The white areas of the images indicate that there are a set of crystalline granules one on top other, so it can be believed that the adjacent granules come together to form large clusters; therefore, we find that the granules in the white areas are larger than that in other regions From the images, the high homogeneity of the films appeared from the values of roughness average.

The results that come from the figures were listed in Table (4.2). With increasing film thickness from (65 -72) nm the (Sq) it is seen to increase, from (0.311-0.549) with increasing film thickness from (80-88) nm it is seen to decrease, from (0.451-0.312), and with increasing film thickness from (100-110) nm it is seen to increase, from (0.366 - 0.38) with increasing film thickness from (124 -140) nm it is seen to increase, from (0.420-465), which is attributed to the fact that aggregate forms bigger grains at higher thicknesses. Therefore, the surface morphology of thin film is strongly affected by the degree of aggregation. The increase in RMS leads to an increase in crystalline growth in a vertical direction more than a horizontal direction. It noticed the roughness averages (Sa) increase in thickness with abnormalities in the thickness (65-80) nm. Also, Table (4.2) contains the ten-point height and the average diameter, the average diameter There have also been reports of such roughness increases with film thickness by researchers [120-122].

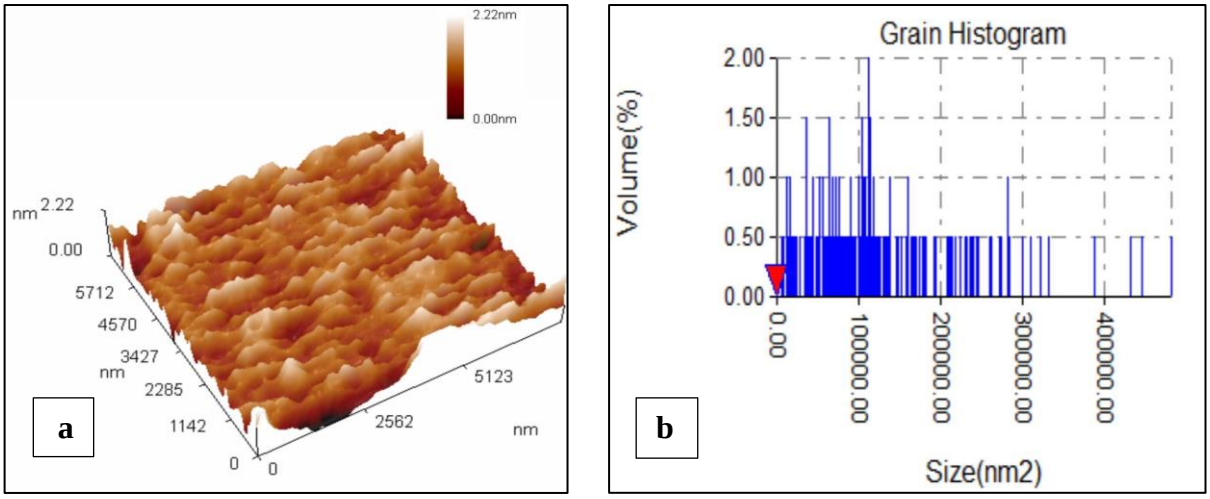

Fig. (4.11): AFM images of CdTe thin films at thickness 65 nm for a) 2D , b) Grain Histogram.

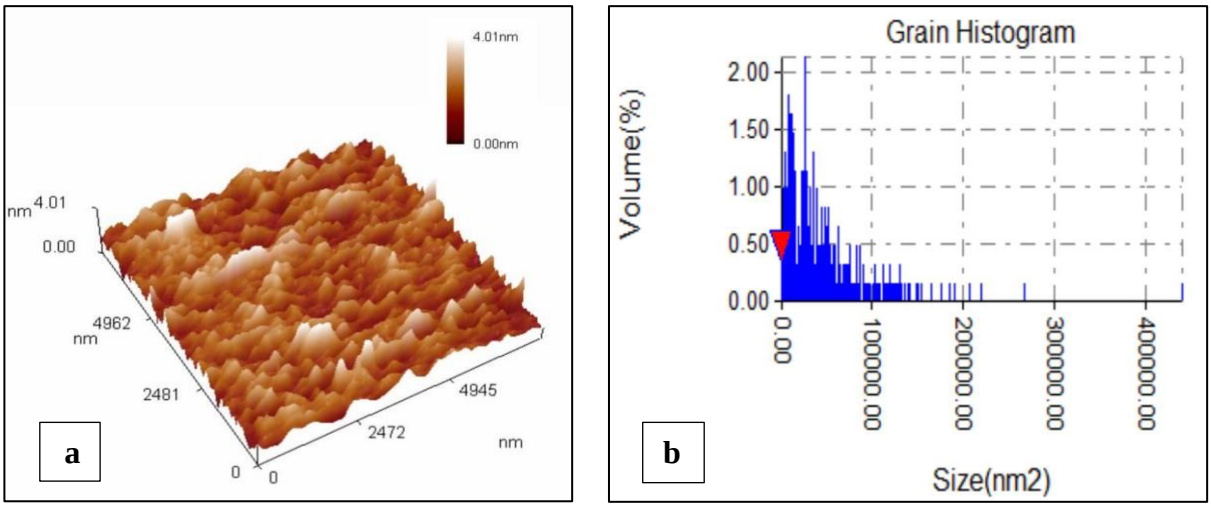

Fig. (4.12): AFM images of CdTe thin films at thickness 72 nm for a) 2D , b) Grain Histogram.

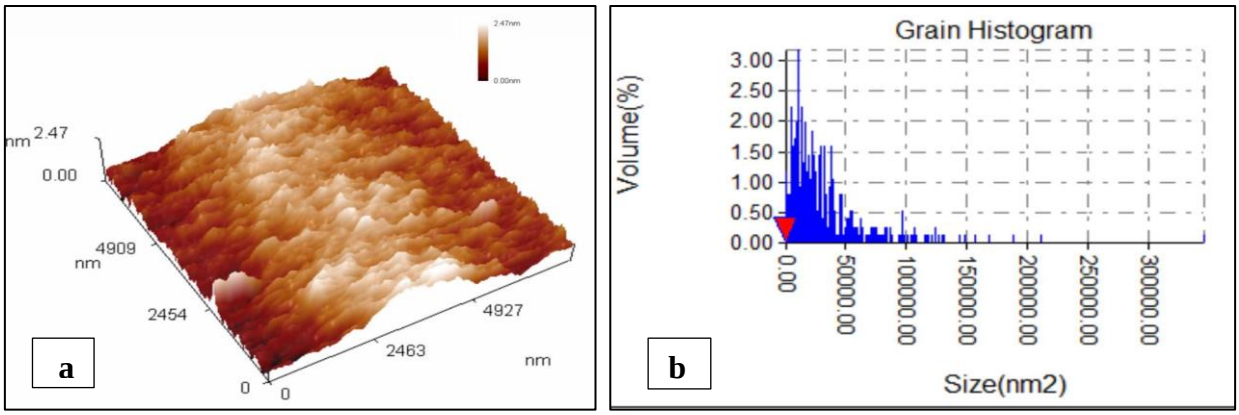

Fig. (4.13): AFM images of CdTe thin films at thickness 80 nm for a) 2D, b) Grain Histogram.

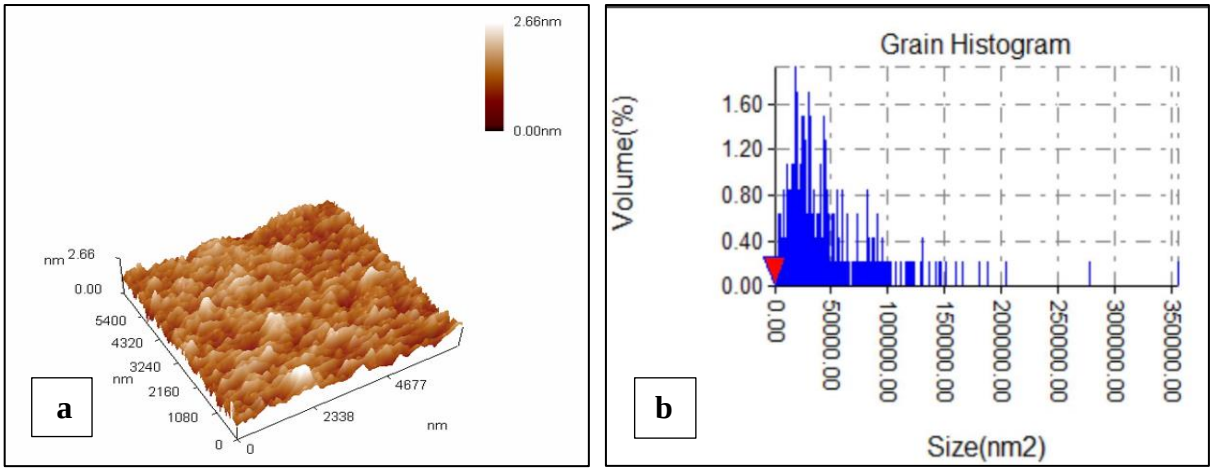

Fig. (4.14): AFM images of CdTe thin films at thickness 88 nm for a) 2D, b) Grain Histogram.

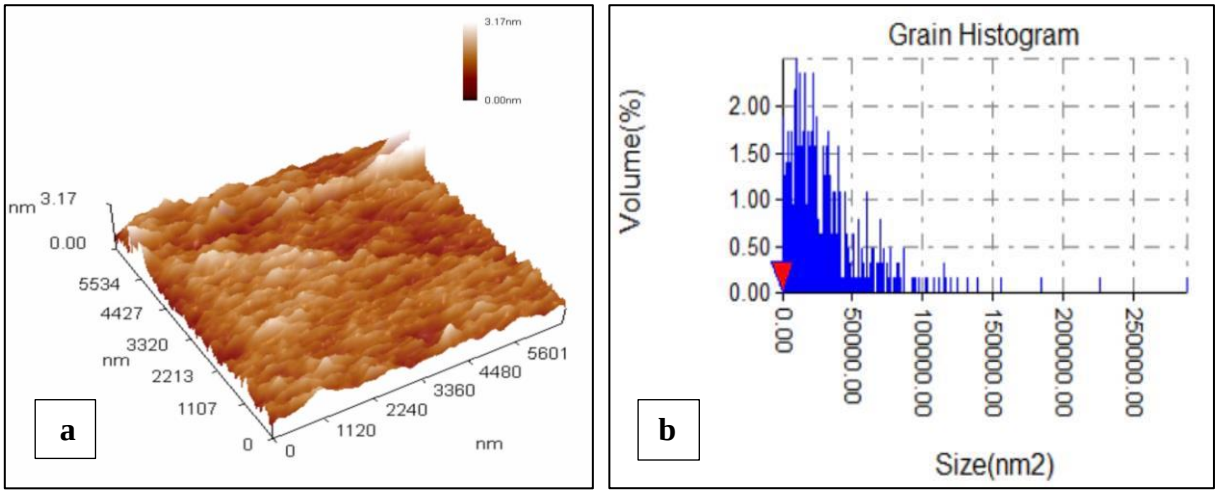

Fig. (4.15): AFM images of CdTe thin films at thickness 100 nm for a) 2D, b) Grain Histogram.

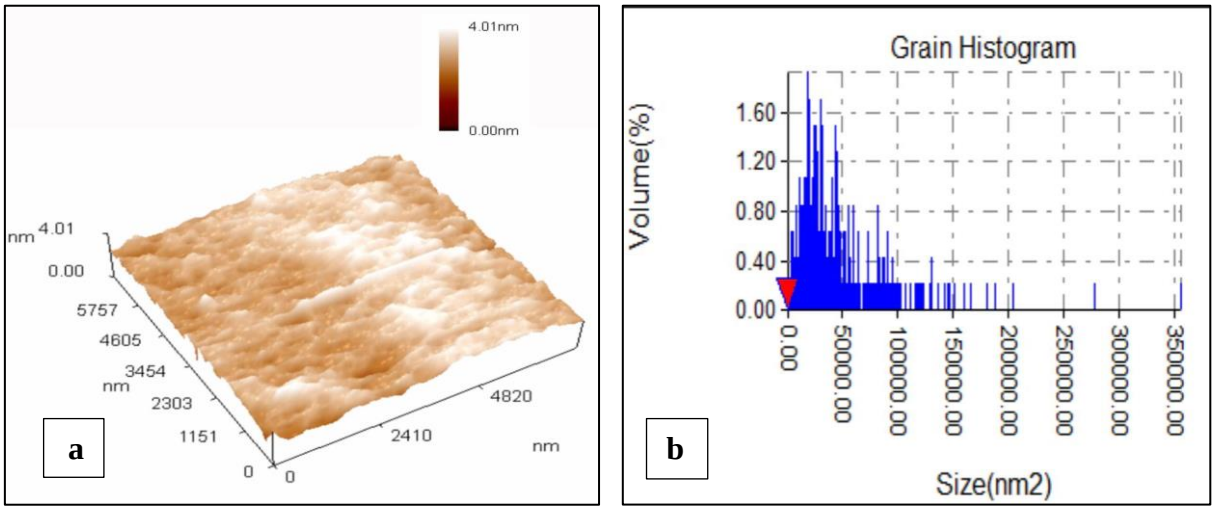

Fig. (4.16): AFM images of CdTe thin films at thickness 110 nm for a) 2D, b) Grain Histogram.

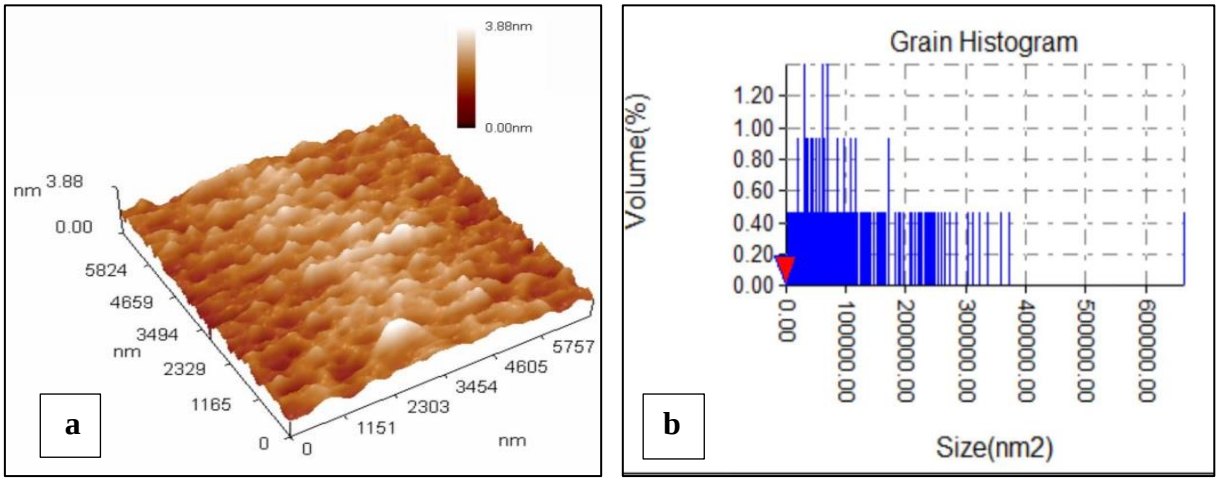

Fig. (4.17): AFM images of CdTe thin films at thickness 124 nm for a) 2D, b) Grain Histogram.

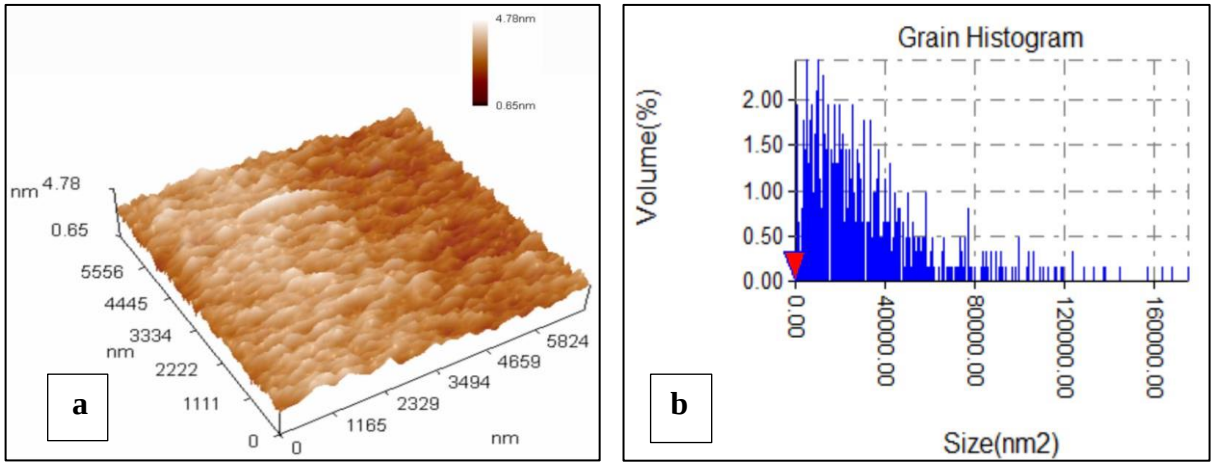

Fig. (4.18): AFM images of CdTe thin films at thickness 140 nm for a) 2D, b) Grain Histogram.

Table (4.2): Morphological characteristics of CdTe thin film with different thicknesses prepared by thermal evaporation technique

Thickness (nm)	Roughness averages (Sa) (nm)	Root means square (Sq) (nm)	Ten points height (Sz) (nm)	Average diameter (nm)
65	0.238	0.311	1.4	392.8
72	0.425	0.549	3.98	231.5
80	0.369	0.451	2.38	200.1
88	0.244	0.312	2.62	198.2
100	0.277	0.366	3.02	234.7
110	0.312	0.38	2.16	346.7
124	0.332	0.429	2.19	376.2
140	0.380	0.465	4.09	206.6

4.2.2 Optical Properties

4.2.2.1 Absorbance (A)

The absorbance of CdTe thin film with different thicknesses was recorded at room temperature and calculated from the relation (2-3), Fig. (4.19) displays the variation of optical absorbance with a wavelength of CdTe thin film. It can be observed that the absorbance spectra of the CdTe thin film increased with the increasing thickness of the films this behavior can be attributed to the increase in the grain size with increased thickness, at high wavelengths, the incident photons don't have enough energy to interact with atoms and thus the photon will be transmitted. When the wavelength decreases (at the neighborhood of the fundamental absorption edge), the interaction between an incident photon and material will occur, and the photon will be absorbance. This indicates that thicker CdTe thin films absorb more light compared to thinner ones. The relationship between thickness and absorbance can be used to optimize the performance of CdTe thin film-based devices such as solar cells and photodetectors. This finding is consistent with previous studies conducted on CdTe thin films, which have shown that the absorption coefficient is proportional to the thickness of the film [123,40].

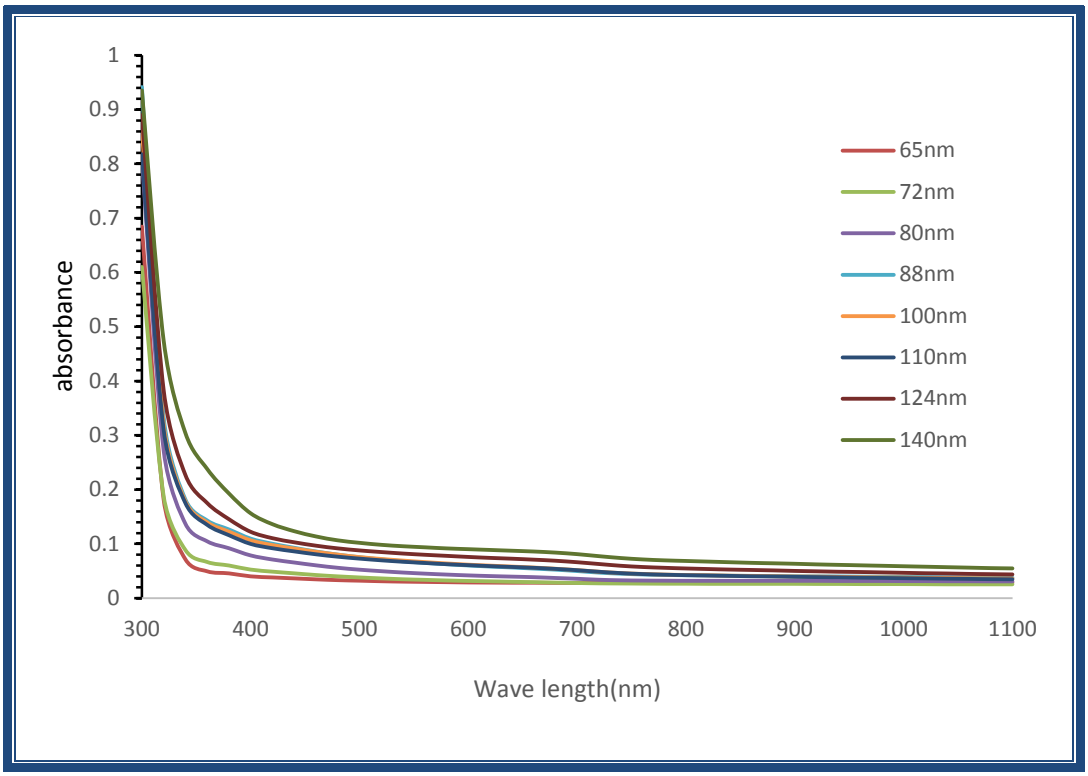

Fig. (4.19): Absorbance spectra as a function of the wavelength of CdTe thin films with various thicknesses

4.2.2.2 Transmittance (T)

Fig. (4.20) explain the variation of transmittance of CdTe thin film with different thicknesses with wavelength and calculating from the relation (2-4). It can be observed that the transmittance is decreased with the increase of thickness. This phenomenon is explained by a rise in the thickness of atoms, which increases the frequency of collisions between incident photons and atoms and causes a decrease in transmittance. When greater crystallite sizes are deposited and more atoms are present in the film, more states will be accessible for the photons to be absorbed, which results in a less pronounced fall in transmittance caused by the start of the absorption edge for films, the frequency of collisions between light photons and film atoms increases as wavelength increases which result in increased absorption, are to blame for the declines in transmittance films this finding is consistent with the researchers [124].

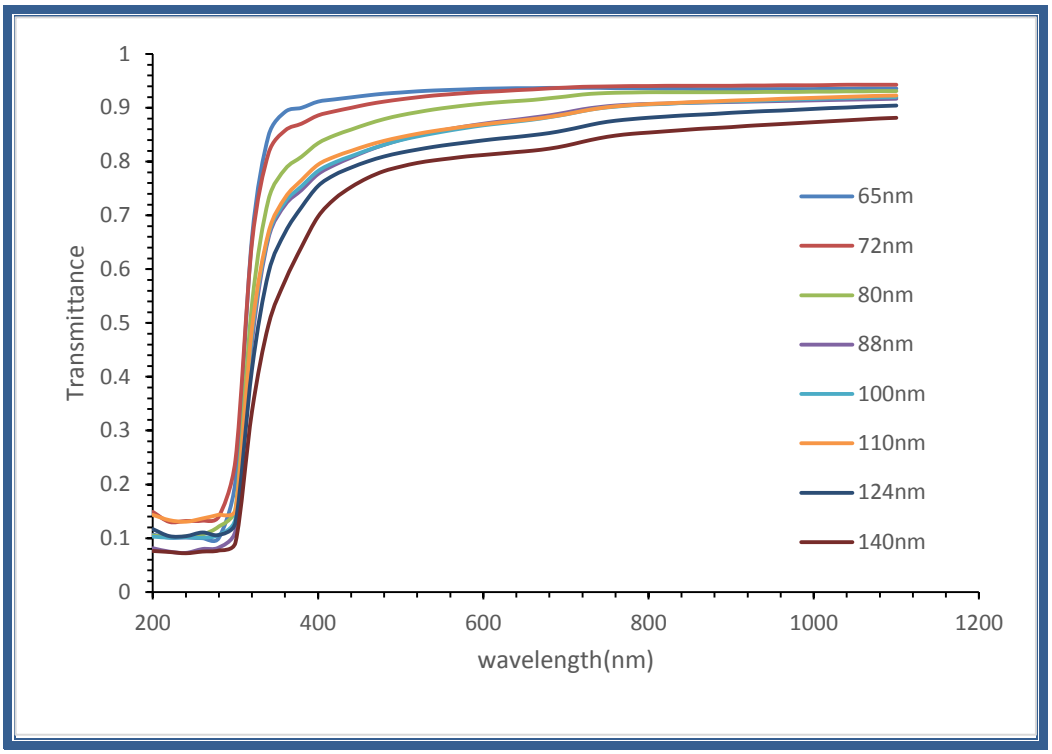

Fig. (4.20): Transmittance spectra as a function of the wavelength of CdTe thin films with various thicknesses

4.2.2.3 Absorption coefficient (α)

The absorption coefficient (α) of CdTe thin films is calculated by using the equation (2-6). The variation of the absorption coefficient versus wavelength of CdTe thin films with different thicknesses is presented in Fig. (4.21). From the figure, it can be observed that the absorption coefficient is increased with the increase in thickness. Its value is larger than (10^4 cm^{-1}), which causes an increase in the probability of the occurrence of direct transitions. This can be linked with the increase in grain size and it may be attributed to the light scattering effect for its high surface roughness, which is in agreement with the finding of researchers [125,126]. These results could have important implications for the development of optoelectronic devices that rely on CdTe, helping to optimize design parameters and improve device performance.

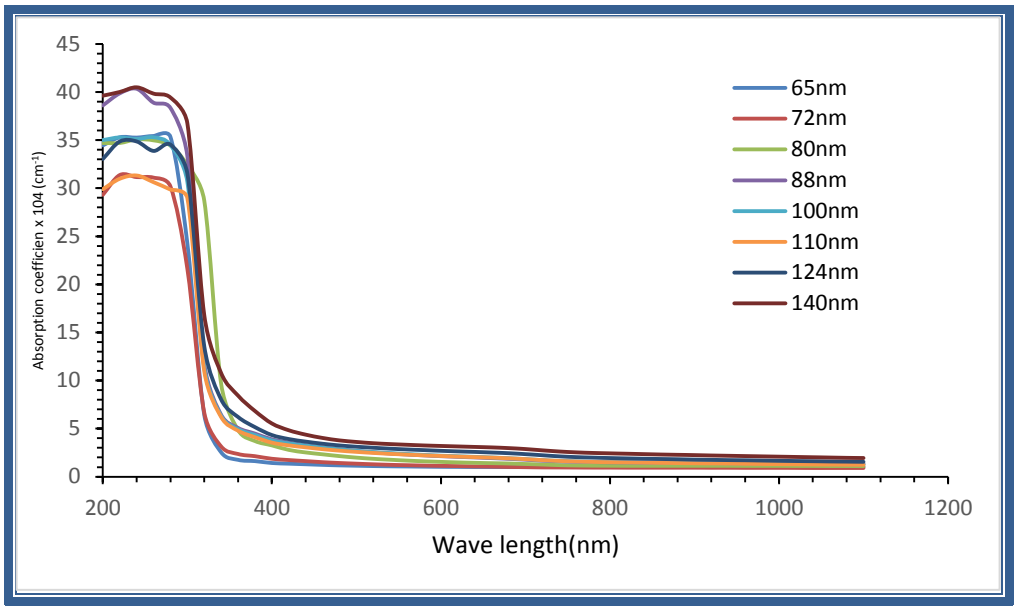

Fig. (4.21): absorption coefficient (α) as a function of the wavelength of CdTe thin films with various thicknesses

4.2.2.4 Extinction Coefficient (k_o)

The extinction coefficient (k_o) of CdTe thin films is determined by using equation (2-5). From Fig. (4.22), it can be observed that the extinction coefficient increases with the increase in thickness. The behavior explanation is the increased absorbance or the absorption coefficient and consequently, k_o will be increased This observation is attributed to the greater number of potential scattering centers that exist within a thicker material, the results agree with the results of the previous researchers [129,130].

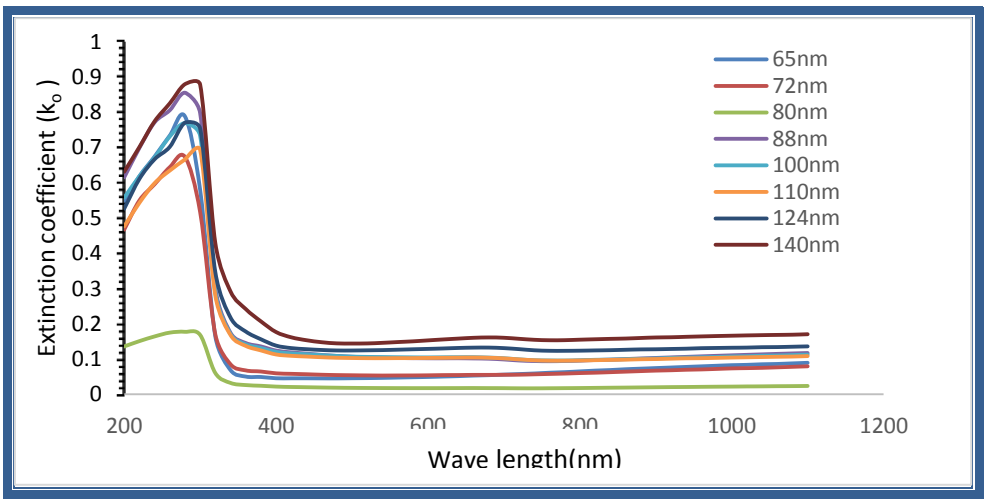

Fig. (4.22): Extinction coefficient as a function of the wavelength of CdTe thin films with various thicknesses

4.2.2.5 Refractive Index (n)

The refractive index was calculated from equation (2-16). Fig. (4.23) show the change of refraction index of CdTe thin films with different thicknesses as a function of wavelength

From Fig. (4.23), it can be observed that the refractive index (n) of the CdTe thin film increases with increasing thicknesses, also it is decreased with the increase of the wavelength. The behavior explanation is the increases of the absorbance or the absorption coefficient and consequently, (n) will be increased, when the incident light interacts with a material that has a high number of particles then the refractivity of the films increases. The results are in agreement with the research [129].Therefore, understanding how the refractive index of CdTe thin film changes with thickness is crucial for designing and optimizing these devices [132,133].

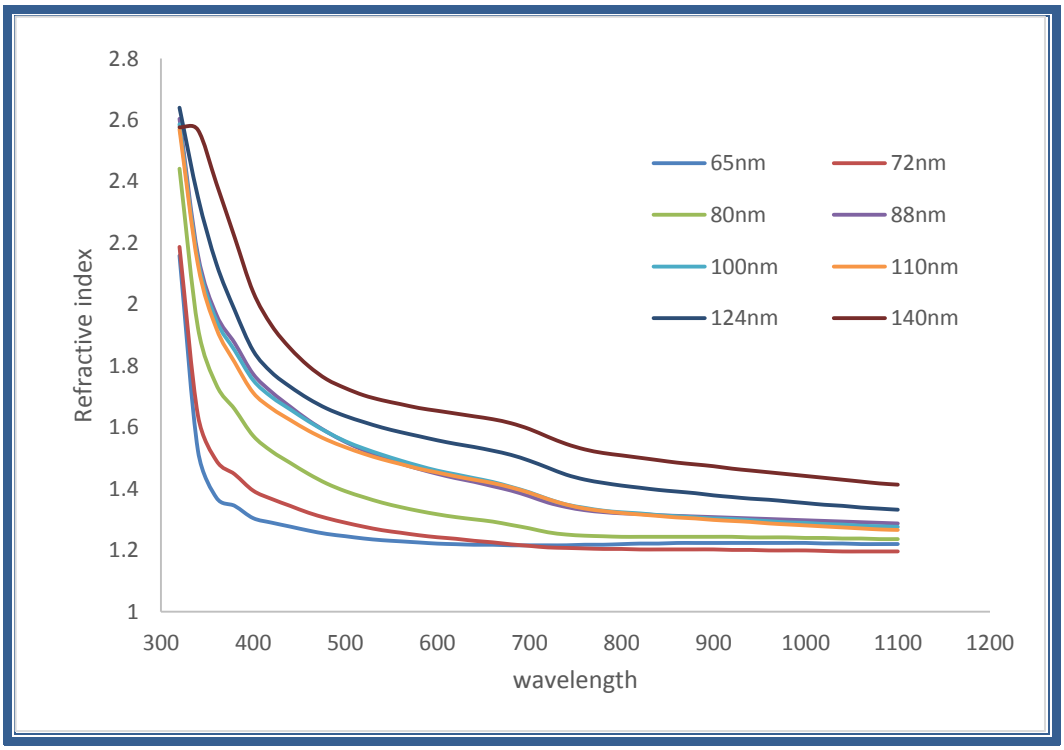

Fig. (4.23): Refractive index as a function of the wavelength of CdTe thin films with various thicknesses.

4.2.2.6 The Dielectric Constants (ε_r and ε_i)

The real (ε_r) and imaginary (ε_i) dielectric constants for CdTe thin films system are determined by using equations (2-18, 2-19), The variation of real (ε_r) and imaginary (ε_i) parts of dielectric constant values versus wavelength for CdT.From the Fig.s (4.24) and (4.25), it is found that ε_r and ε_i increase with increasing thickness of CdTe thin film. The behavior of ε_r is similar to that of the refractive index because of the smaller value of k_o compared with n, while ε_i is mainly dependent on the k_o values.

One important finding in the research of CdTe thin films is that the values of ε_r and ε_i have been reported to increase with increasing thickness of the CdTe thin film. This phenomenon has been attributed to the increase in polarizability of the CdTe lattice with increasing thickness, resulting in a higher dielectric constant (ε_r) and a higher imaginary component of the dielectric constant (ε_i). This increase in the values of ε_r and ε_i with increasing thickness is due to the larger number of atomic layers within the CdTe lattice, which leads to a stronger polarization response This behavior is in agreement with the results of the researchers [132]. The increase in ε_r and ε_i with increasing thickness of CdTe thin films is a significant observation, as it suggests that the dielectric properties of CdTe thin films can be controlled by manipulating their thickness [133].

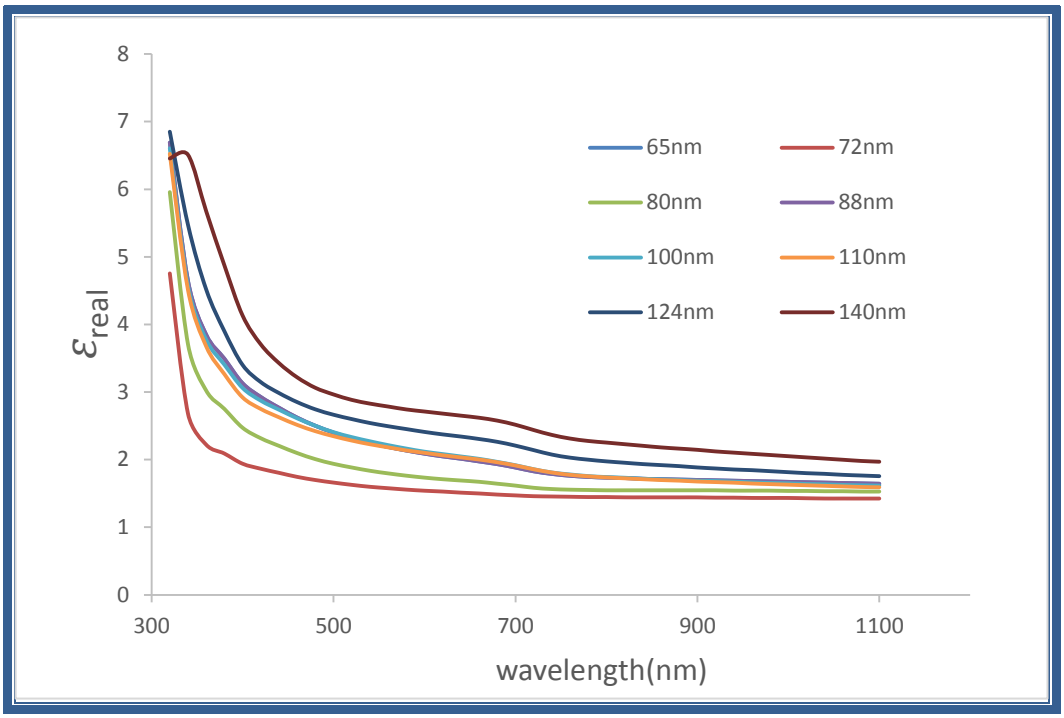

Fig. (4.24): Constant dielectric real as a function of the wavelength of CdTe thin films with various thicknesses

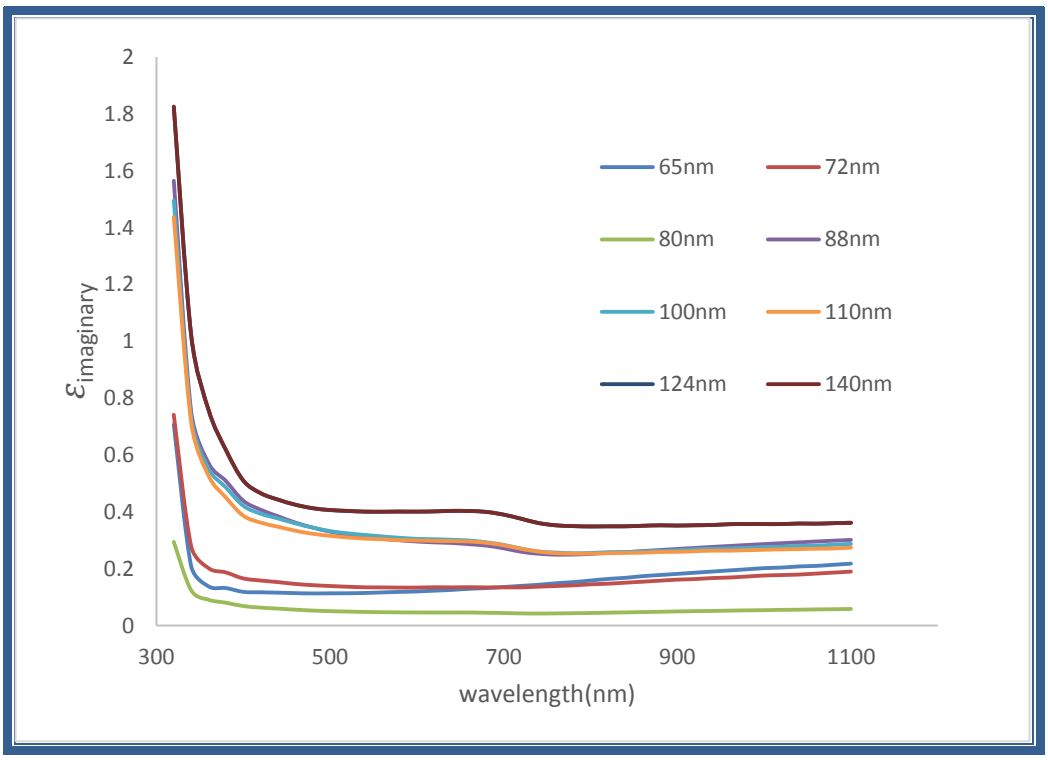

Fig. (4.25): Imaginary dielectric constants as a function of the wavelength of CdTe thin films with various thicknesses

4.2.2.7 Optical Energy Gap of the Allowed Direct Transition

The optical energy gap for CdTe thin films is calculated by using equation (2-10). The plot of $(\alpha h\,\nu)^2$ with energy $(h\,\nu)$ indicates that CdTe films are in direct transition. The band gap of the material is determined by extrapolating the linear region of the graph to the $h\,\nu$ axis. The curve can be fitted with a straight line very well for a higher energy range. From Fig. (4.26), it is clear that the direct energy gap of CdTe films increased from (3.44 eV – 3.62 eV) at the thickness (140 - 65) nm, the values of Eg are listed in Table (4.3). According to recent studies, the direct energy gap of CdTe films has been observed to decrease with an increase in thickness. This is due to the increase in the localized density of states near the band edges and in turn, decreased the value of Eg with thickness. Also, the decrease of the direct band gap with the increase in thickness can be attributed to an increase in particle size, These results are in good agreement with the findings of the researchers [134]. It is important to accurately measure and understand this effect to optimize the performance of CdTe-based solar cells and other optoelectronic devices [135].

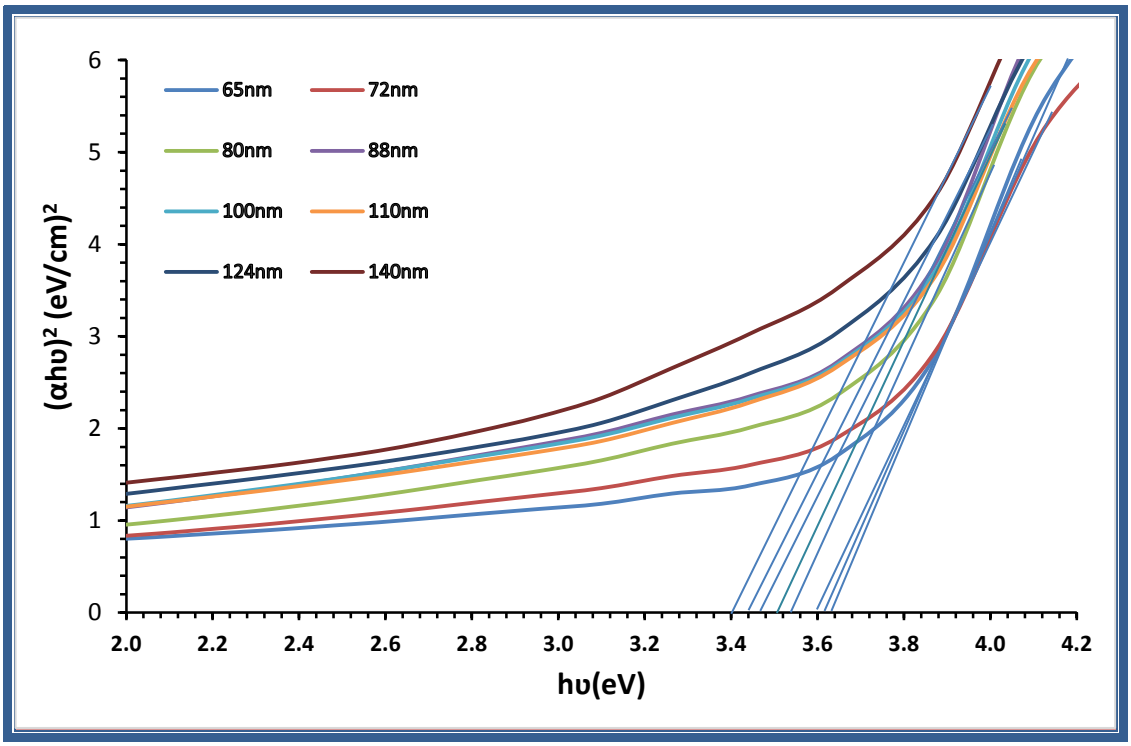

Fig. (4.26): The allowed energy gap versus photon energy of CdTe thin films with different thickness.

Table (4.3): The values of the energy gap of the allowed direct transition of CdTe thin film with different thicknesses.

The thickness of CdTe (nm)	Optical energy gap (eV)
65	3.62
72	3.60
80	3.56
88	3.52
100	3.51
110	3.50
124	3.46
140	3.44

4.2.2.8 Surface energy loss function (SELF) and volume energy loss function (VELF).

The Surface Energy Loss Function (SELF) and Volume Energy Loss Function (VELF) were calculated from the relations (2-21) and (2-22) respectively. Fig.s (4.27) and (4.28) display the wavelength dependence of the SELF and VELF values of CdTe thin films with different thicknesses. The volume energy loss function (VELF) and surface energy loss function (SELF) are two key parameters that determine the amount of energy lost by CdTe thin films. The VELF describes the energy loss due to electron-phonon interactions within the bulk of the CdTe material, while the SELF accounts for energy loss at the surface interface. Both VELF and SELF are dependent on the thickness of the CdTe thin film. Research has shown that as the thickness of CdTe thin films increases, both VELF and SELF also increased, this is because the increased thickness leads to more surface interactions, resulting in a greater amount of energy loss [136].

On the other hand, when the film is very thin and can spread itself on a certain substrate, it is the best possible because it will disappear several energies, including the elastic energy, and it can be neglected because it controls by neglecting this energy, and thus there will be a direct interaction between the

nanomaterial and the surface. Also, the potential energy will be neglected, and this will lead to the formation of a first layer on the substrate and then a second surface energy will come to form a second layer and thus a volume will be formed. The volume appears because it is a surface with thickness. It will be volume, and therefore the volume energy will appear. Therefore, the volume energy according to this figure does not show a large difference, while the surface energy will have a difference due to the very little thickness of the film.CdTe thin films have gained considerable attention in recent years due to their outstanding electronic and optical properties. One important aspect of studying CdTe thin films is understanding their energy loss mechanisms.

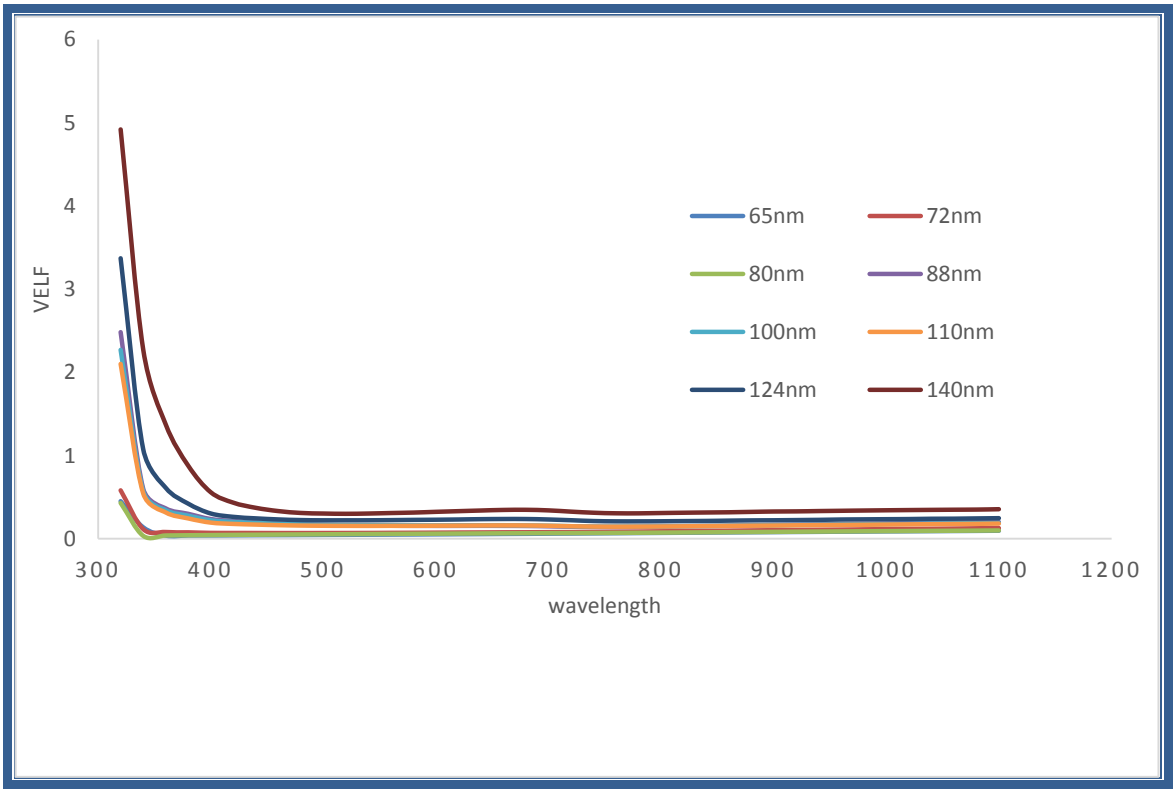

Fig. (4.27): volume Energy loss function of a wave of CdTe thin films (VELF).

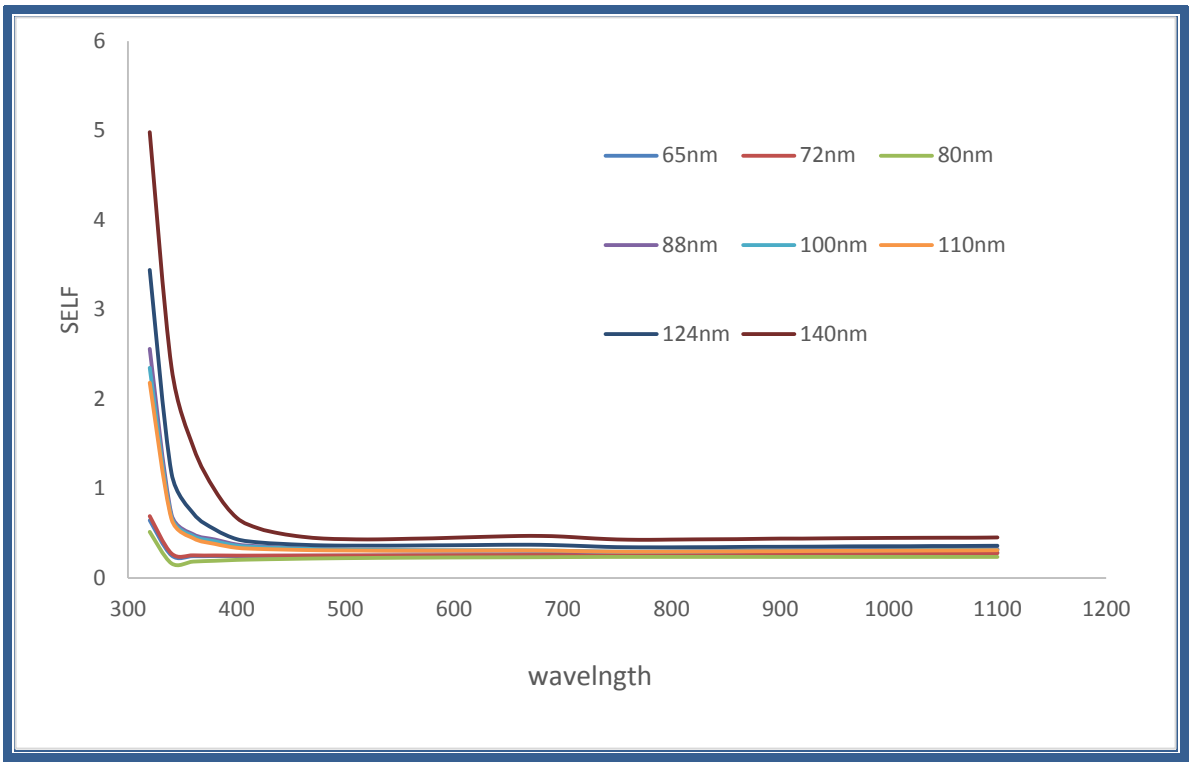

Fig. (4.28): Surface Energy loss function of a wave of CdTe thin films (SELF)

4.2.2.9 Dispersion Parameters and dispersion energies

Dispersion parameters were studied and diagnosed using the Wemple-DiDomenico model with different thicknesses. One of the primary outputs of the WDD model includes the calculation of single effective oscillator energy (E_o), dispersion energy (E_d), and estimated zero-frequency refractive index and dielectric constant ($\mathcal{E}_\infty$), as well as the optical moments. The physical explanation of the measured quantities is provided by the Wemple-DiDomenico (WDD) model in Equation (٢-٢٣).

The values of E_d and E_o can be derived directly from the intercept on the vertical axis (E_o/E_d) and slope ($E_d . E_o)^{-1}$ of the plot, respectively, by showing the plot of $(n2-1)^{-1}$ as a function of $(h\upsilon)^2$ and fitting it to the straight line taken from the figures (4.29 - 4.36). Further, the static refractive index (n_o) and static dielectric constant (ε_o) were also evaluated using the equation (2-24). Table (4.4) includes the computed values of the dispersion parameters, which are shown to decrease as the thickness increases. The obtained values of ($E_o \approx 2E_g$) are proportional to the Tauc bandgap. Due to the free electrons on the film surface,

the manufactured films produced a conductive layer with very low values of E_g, which had a high reflectivity [111,112].

It can also calculate the moments M_{-1} and M_{-3} of the optical spectra of thin films by using the relations (2-26), (2-27). Values of M_{-1} and M_{-3} are recorded in Table (4.4). From the Table, it could be noticed that optical moments (M_{-1}) and (M_{-3}) increases by decreasing the thickness of the CdTe film.

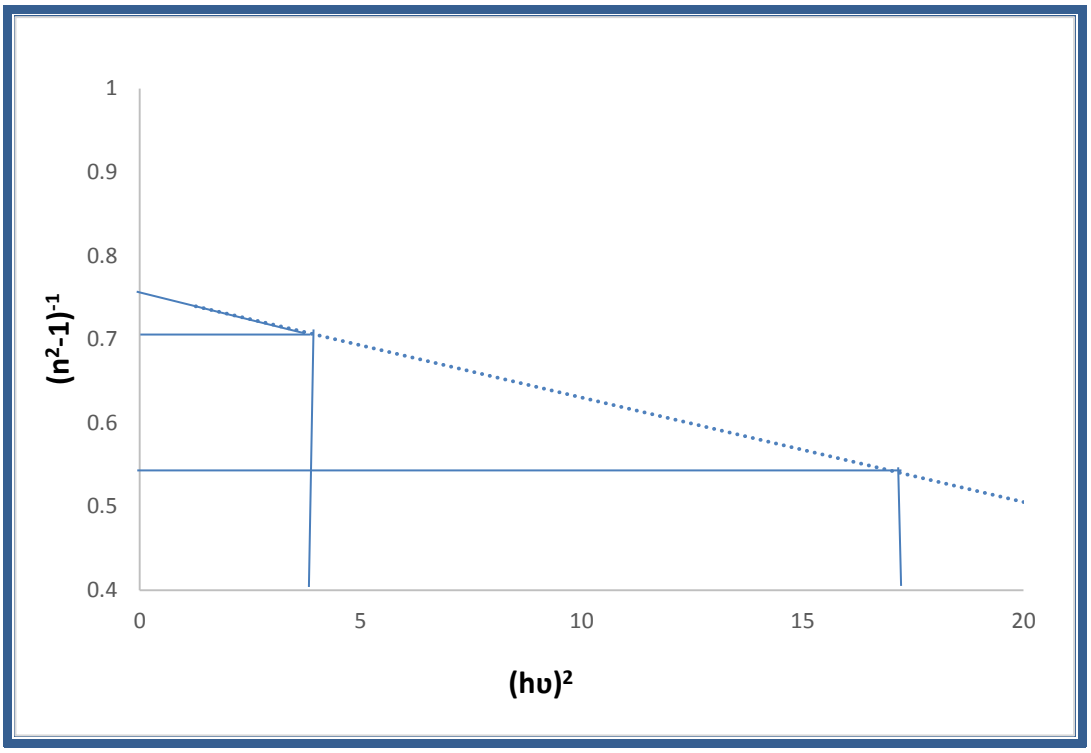

Fig. (4.29) : The relationship between $(n^2 -1)^{-1}$ and $(h\upsilon)^2$ for thickness 65 nm

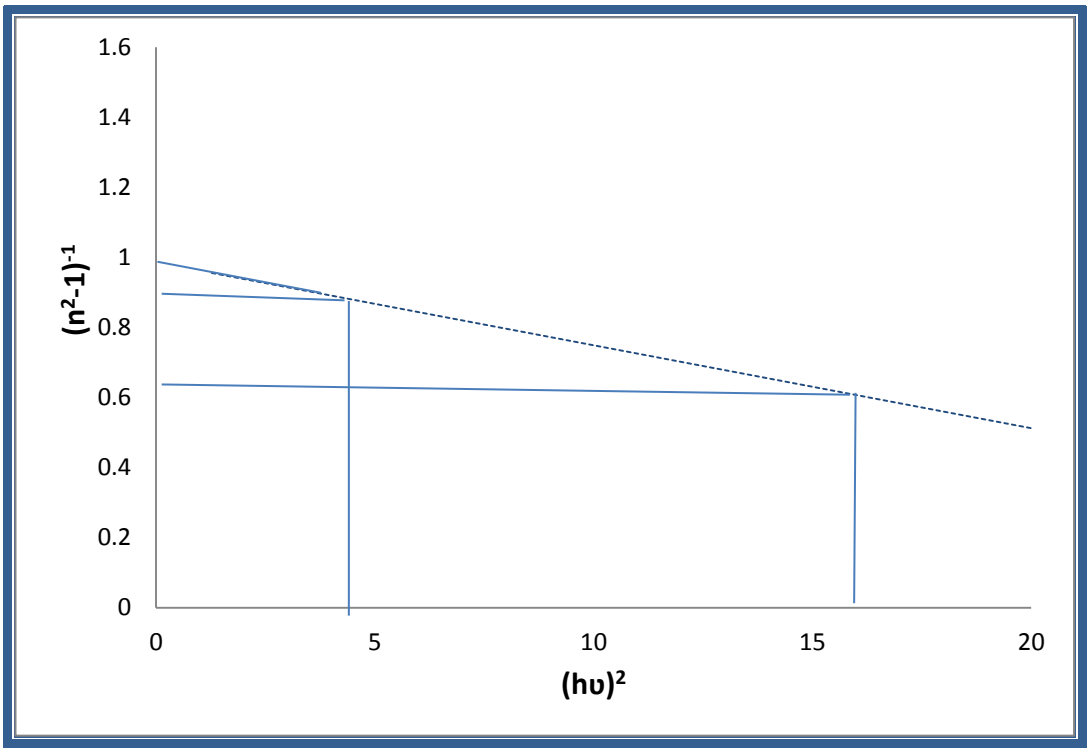

Fig. (4.30): The relationship between $(n^2 -1)^{-1}$ and $(h\upsilon)^2$ for thickness 72 nm

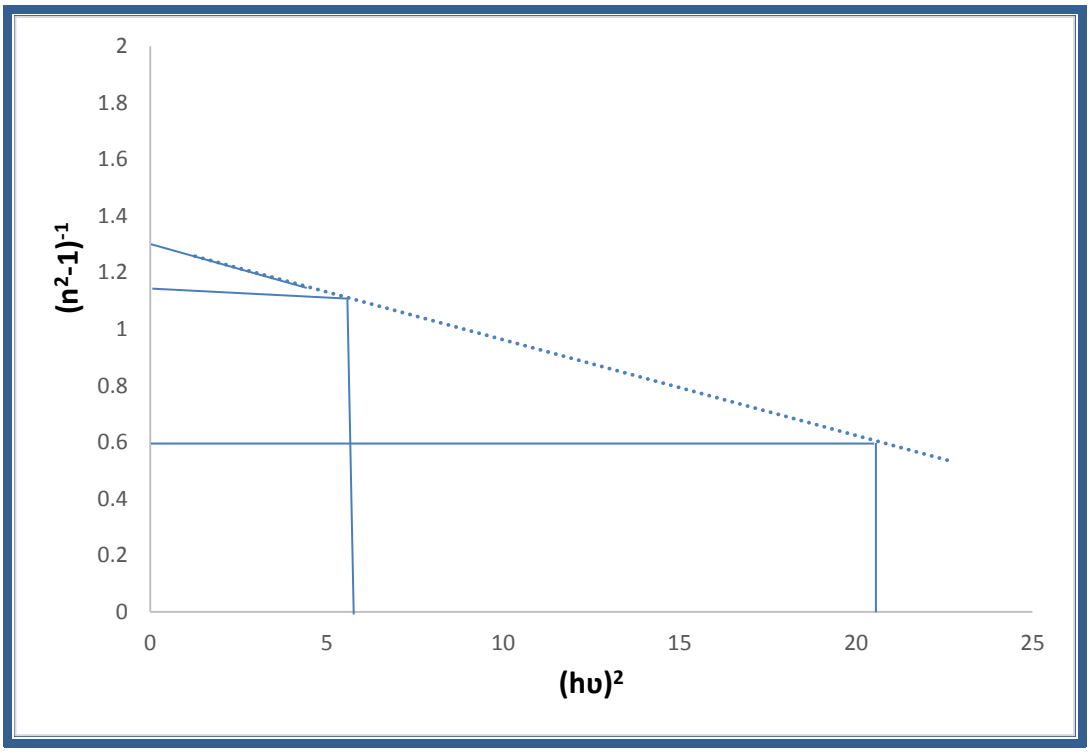

Fig. (4.31): The relationship between $(n^2 -1)^{-1}$ and $(h\upsilon)^2$ for thickness 80 nm

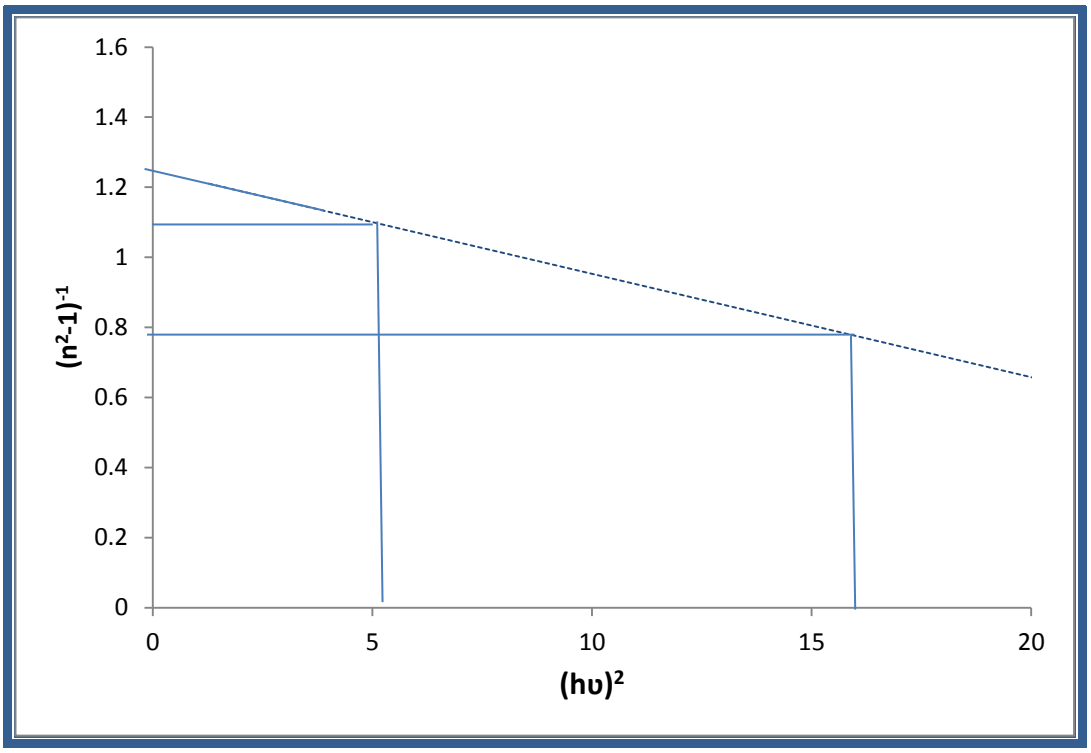

Fig. (4.32): The relationship between $(n^2 -1)^{-1}$ and $(h\upsilon)^2$ for thickness 88 nm

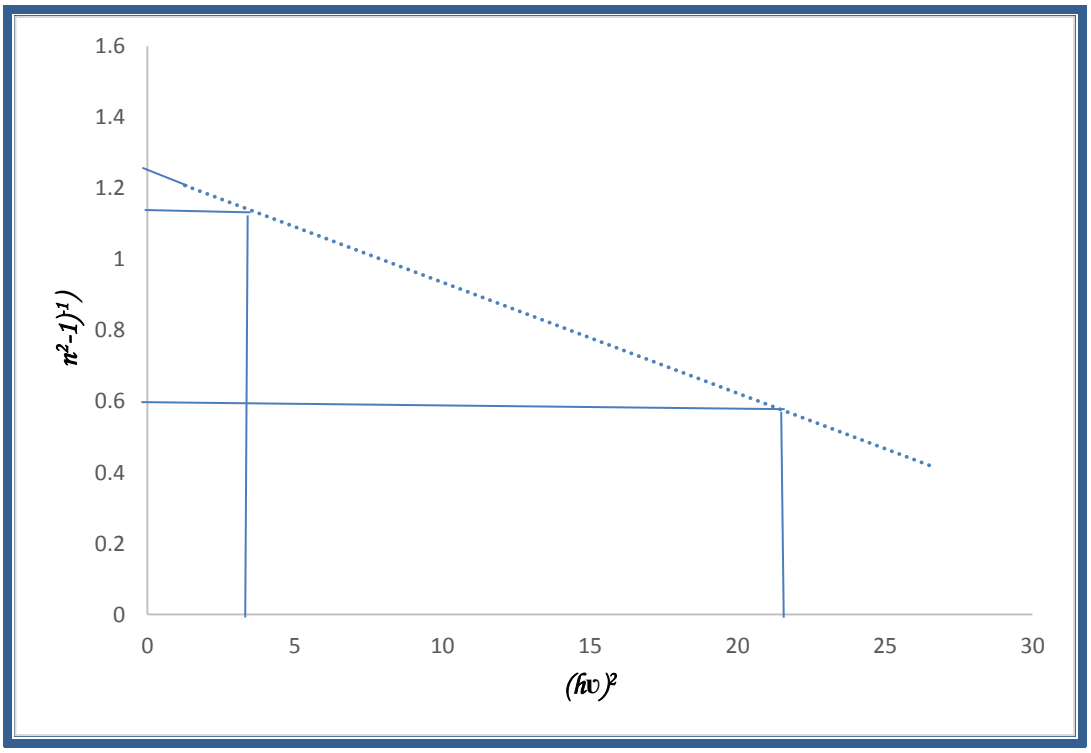

Fig. (4.33): The relationship between $(n^2 -1)^{-1}$ and $(h\upsilon)^2$ for thickness 100 nm

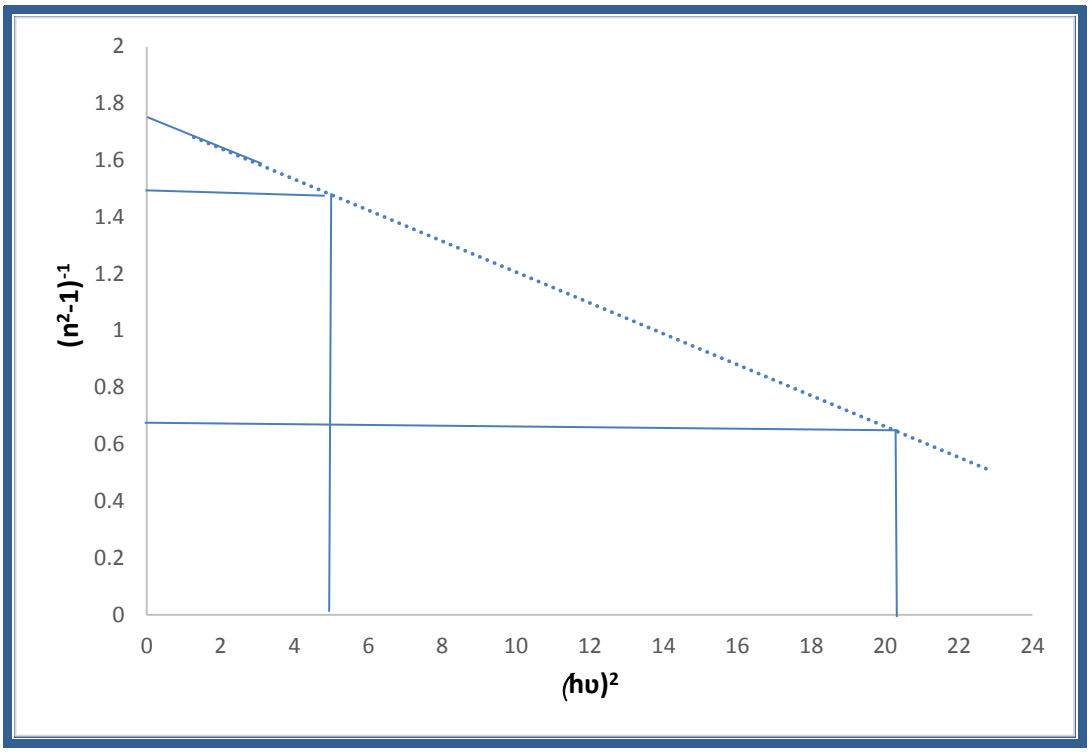

Fig. (4.34): The relationship between $(n^2 -1)^{-1}$ and $(h\upsilon)^2$ for thickness 110 nm

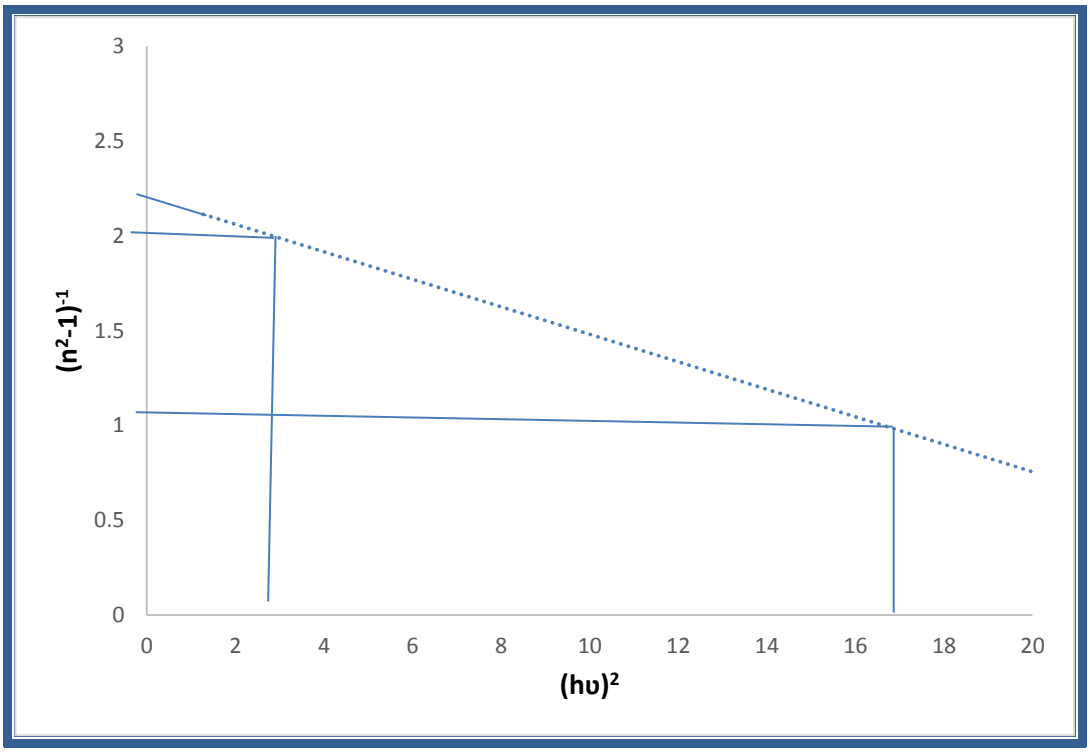

Fig. (4.35): The relationship between $(n^2-1)^{-1}$ and $(h\upsilon)^2$ for thickness 124 nm

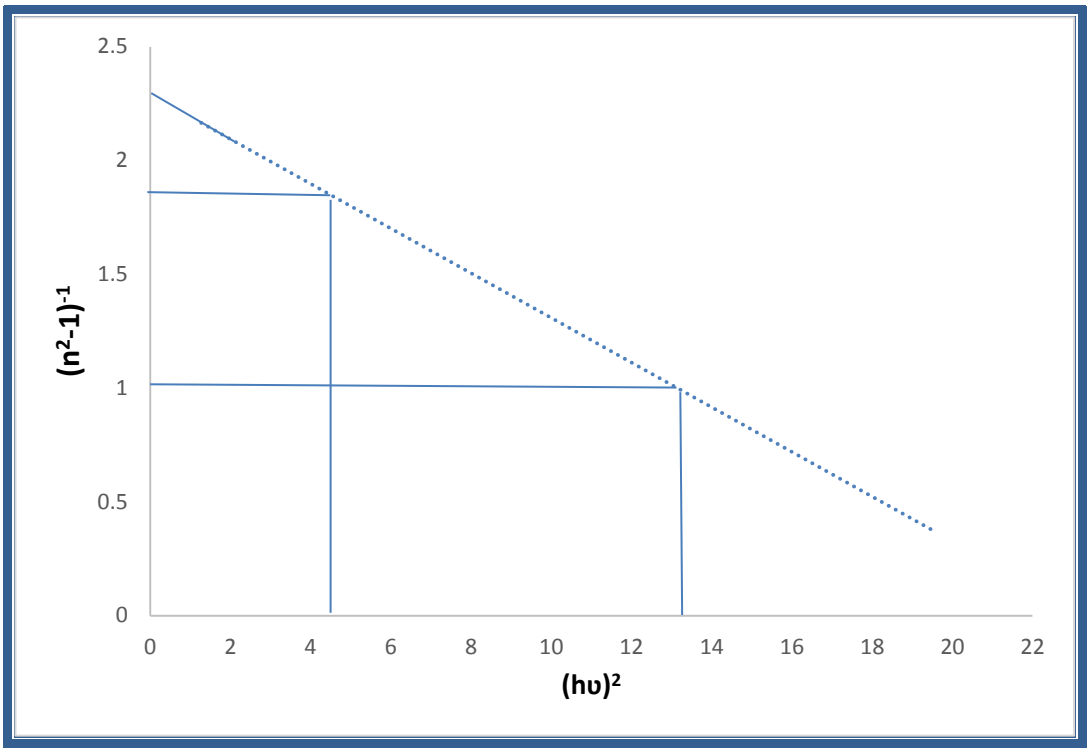

Fig. (4.36): The relationship between $(n^2-1)^{-1}$ and $(h\upsilon)^2$ for thickness 140 nm

Table (4.4): Dispersion parameters and moments of CdTe thin films deposited at different thickness values

thin film (nm)	E_0(meV)	E_d(meV)	E_g(eV)	ε_∞	n($_0$)	M_{-1}	M_{-3}
65	7.654655	10.20621	3.827328	2.33333	1.527525	1.333333	0.022756
72	6.793662	6.793662	3.396831	2	1.414214	1	0.021667
80	6.499231	4.92366	3.249615	1.7577576	1.325736	0.757576	0.017935
88	6.281172	5.024938	3.140586	1.8	1.341641	0.8	0.020277
100	6.065905	4.972053	3.032952	1.819672	1.348952	0.819672	0.022277
110	5.804663	3.242829	2.902332	1.558659	1.248463	0.558659	0.01658
124	5.700877	2.533723	2.850439	1.44444	1.20185	0.444444	0.013675
140	5.029911	2.186918	2.514955	1.434783	1.197824	0.434783	0.017185

4.3 Conclusions

The summarized results from this work are the following :

1- A successful thermal evaporation technique used to prepare CdTe thin films with fine thicknesses.

2- The X-ray diffraction (XRD) results showed that the prepared films were amorphous. With increasing thickness, peaks of XRD were attributed to the CdTe that corresponded to the (111) cubic phase.

3- From Atomic Force Microscopy (AFM), the roughness averages and root mean square increase with thickness increase.

4- Scanning Electron Microscopy (SEM) uniform morphology revealing a rather soft surface and with an increase in thickness led to changes in the surface morphology and increased roughness.

5- Optical properties results showed the absorbance, absorption coefficient, extinction coefficient, refractive index, and real and imaginary dielectric constants increased with the increase of film thicknesses, while the transmittance and optical energy gap decreased. The CdTe thin films have allowed a direct energy gap that was decreased from 3.62 eV – 3.44 eV with increased thickness.

6- The surface energy loss function (SELF) and volume energy loss function (VELF) values observed increased with the increment thickness.

7- Dispersion parameters were provided by the Wemple-DiDomenico model. The values of the energy gap were estimated by a decrease as the thickness increased, which was comparable with that calculated by the Tauc equation.

4.4 Future Works

1. The effect of thickness as antireflection coating of CdTe films for solar cell application.

2. Thin film fabricated of CaF2-doped CdTe for optoelectronic applications.

References

References

[1] J. E. Greene, "Review Article: Tracing the recorded history of thin-film sputter deposition: From the 1800s to 2017." Journal of Vacuum Science & Technology A: Vacuum, Surfaces, and Films, Vol. 35, No. 5, P. 05C204, (2017).

[2] G. Abadias, E. Chason, J. Keckes, M. Sebastiani, G. B. Thompson, E. Barthel, G. L. Doll, C. E. Murray, C. H. Stoessel, and L. Martinu, "Review Article: Stress in thin films and coatings: Current status, challenges, and prospects," Journal of Vacuum Science & Technology A: Vacuum, Surfaces, and Films Vol. 36, No. 2, P. 020801, (2018).

[3] N. W. Park, W. Y. Lee, J. E. Hong, T. H. Park, S. G. Yoon, H. Im, H. S. Kim, and S. K. Lee, "Effect of grain size on thermal transport in post-annealed antimony telluride thin films," Nanoscale Res Lett, Vol. 10, No. 1, (2015).

[4] S. Tiwari and R. Gebauer, "Optical optimization of thin-film polymer " Solar Cells (2020).

[5] H. A. Youssef, H. A. El-Hofy, and M. H. Ahmed, "Handbook of thin-film" Engineering Materials and Their Applications (2020).

[6] S. Kumar and D. K. Aswal, "Thin Film and significance of its thickness,", pp. 1–12, (2020).

[7] T. Osaka and T. Homma, "Thin films," Electrochemical Society Interface vol. 4, no. 2, pp. 42–46,(1995).

[8] M. Benelmekki and A. Erbe, "Nanostructured thin films–background", Preparation and Relation to the Technological Revolution of the 21st Century vol. 14, (2019).

[9] S. Badilescu, D. Raju, S. Bathini, and M. Packirisamy, "Gold nano-island platforms for localized surface plasmon resonance sensing: A short review," Molecules Vol. 25, No. 20. MDPI AG, Oct. 01, (2020).

[10] M. Alshami, A. Wabby, and M. F. Mousselly, "Design and development

of binary diffractive Germanium lens by thin film deposition," Journal of the European Optical Society, vol. 10, Nov, (2015).

[11] S. Abdallah, N. Al-Hosiny, and A. Badawi, "Photoacoustic study of CdS QDs for application in quantum-dot-sensitized solar cells," J Nanomater, vol. 2012, (2012).

[12] D. Dobrocky, Z. Pokorny, Z. Studeny, and T. Van Doan, "Analyse of tribological properties of layers created by plasma nitriding + DLC," Manufacturing Technology**,** vol. 18, no. 3, pp. 379–386, (2018).

[13] A. H. Ali, S. M. Hasony, A.-A. A. Al, and A. Lecturer, " effect of spin coating speed and deposition parameters on the crystalline size of ZNO thin films " Vol. 6, (2013).

[14] A. Nazar and A. Al-Gaffar, "Java Applet Technology for Design Interference Optical Coating" *Int J Environ Res Public Health*, Vol. 95, No. 8, pp. 18-27, (2009).

[15] M. M. Bellah, S. M. Christensen, and S. M. Iqbal, "Nanostructures for medical diagnostics," J Nanomater Vol. 2012, (2012).

[16] E. Hasani and D. Raoufi, "Effect of substrate and post-deposition annealing on nanostructure and optical properties of CdTe thin films,"Mater Res Express, Vol. 5, (2018).

[17] X. Cheng, Nanostructures: Fabrication and Applications (Woodhead Publishing Limited, (2013).

[18] N. Nasiri and C. Clarke, "Nanostructured gas sensors for medical and health applications: Low to high dimensional materials," Biosensors (Basel), Vol. 9, No. 1, pp. 1–22, (2019).

[19] T. Thomas, I.A. Ovid'ko, and A. K. Vasudevan. "Nanostructures : synthesis , functional properties and applications NATO science series," Physics (College Park Md).

[20] Z. Chai, A. Childress, and A. A. Busnaina, "Directed Assembly of Nanomaterials for Making Nanoscale Devices and Structures: Mechanisms and Applications," ACS Nano (2022).

[21] M. López-Alonso, B. Díaz-Soler, M. Martínez-Rojas, C. Fito-López, and M. D. Martínez-Aires, "Management of occupational risk prevention of nanomaterials manufactured in construction sites in the EU," Int J Environ Res Public Health,vol. 17, no. 24, pp. 1–27, Dec. (2020).

[22] G. Alberti, C. Zanoni, L. R. Magnaghi, and R. Biesuz, "Disposable and low-cost colorimetric sensors for environmental analysis," Int J Environ Res Public Health, Vol. 17, No. 22. MDPI AG, pp. 1–23, Nov. 02, (2020).

[23] A. Martirosyan and Y. J. Schneider, "Engineered nanomaterials in food: Implications for food safety and consumer health," Int J Environ Res Public Health**,** vol. 11, no. 6. MDPI, pp. 5720–5750, May 28, (2014).

[24] L. Pan, B. Li, J. Chen, H. Zhang, X. Wang, J. Shou, D. Yang, and X. Yan, "Nanotechnology-Based Weapons to Combat Human Papillomavirus Infection Associated Diseases," Front Chem**,** Vol. 9. Frontiers Media S.A., Nov. 17, (2021).

[25] A. Al-Samydai, M. Al Qaraleh, W. Alshaer, L. K. Al-Halaseh, R. Issa, F. Alshaikh, A. Abu-Rumman, H. Al-Ali, and E. A. S. Al-Dujaili, "Preparation, Characterization, Wound Healing, and Cytotoxicity Assay of PEGylated Nanophytosomes Loaded with 6-Gingerol," Nutrients**,** Vol. 14, No. 23, Dec. (2022).

[26] A. A. Ellakany, M. Abouelatta, A. Shaker, G. T. Sayah, and M. El-Banna, " TCAD simulation of a proposed 3D CdZnTe detector," The Journal of Engineering, Vol. 2017, No. 10, pp. 574–576, Oct. (2017).

[27] N. Deyneko, O. Semkiv, I. Khmyrov, and A. Khryapynskyy, "Investigation of the combination of ito/Cds/Cdte/Cu/Au solar cells in micro assembly for electrical supply of field cables," Eastern-European Journal of Enterprise Technologies, Vol. 1, No. 12–91, pp. 18–23, (2018).

[28] K. Taneja, A. V. Madiraju, M. Kumar, R. Seelaboyina, A. K. Keshri, and S. Mahajan, Conference Papers in Energy, Vol. 2013, pp. 1–4, May (2013).

[29] N. Kishore, V. Nagarajan, and R. Chandiramouli, "Substrate Rotation

Chemical Bath Deposition of Cadmium Sulfide Buffer Layers for Thin Film Solar Cell Application," Processing and Application of Ceramics, Vol. 13, No. 2, Pp. 124–131, (2019).

[30] A. J. Strauss, A. J. S. The, and D. P. Appliquee, "The physical properties of cadmium telluride To cite this version :,", Vol. 12, No. 2, pp. 167–184 (1977).

[31] R. Y. Petrus, H. A. Ilchuk, A. I. Kashuba, I. V. Semkiv, E. O. Zmiiovska, and F. M. Honchar, "Optical Properties of CdS Thin Films," J Appl Spectrosc, Vol. 87, No. 1, pp. 35–40, (2020).

[32] R. Kulkarni, S. Rondiya, A. Pawbake, R. Waykar, A. Jadhavar, V. Jadkar, A. Bhorde, A. Date, H. Pathan, and S. Jadkar, "Structural and Optical Properties of CdTe Thin Films Deposited Using RF Magnetron Sputtering," Energy Procedia, Vol. 110, No. December 2016, pp. 188–195, (2017).

[33] Aneka Gas, "Material Safety Data Sheet Induex-25 MATERIAL SAFETY DATA SHEET," Material Safety Data Sheet, pp.1–5, (2012).

[34] V. M. Fthenakis, Life Cycle Impact Analysis of Cadmium in CdTe PV Production, Vol. 8, No. 4. (2004).

[35] D. H. Rose and H. F. S., "Fabrication Procedures and," Progress in Photovoltaics: Research and Applications, Vol. 340, No. November 1998, pp. 331–340, (1999).

[36] V. Barrioz, G. Kartopu, S. J. C. Irvine, S. Monir, and X. Yang, "Material utilisation when depositing CdTe layers by inline AP-MOCVD," J Cryst Growth, Vol. 354, No. 1, pp. 81–85, Sep. (2012).

[37] S. Chun, K. S. Han, J. H. Shin, H. Lee, and D. Kim, , "Fabrication and characterization of CdTe nano pattern on flexible substrates by nano imprinting and electrodeposition," Microelectron, Vol. 87, No. 11, Pp. 2097–2102, Nov. (2010).

[38] O. Vigil-Galán, L. Vaillant, R. Mendoza-Pérez, G. Contreras-Puente, J. Vidal-Larramendi, and A. Morales-Acevedo, "Influence of the growth

conditions and postdeposition treatments upon the grain boundary barrier height of CdTe thin films deposited by close space vapor transport," J Appl Phys, Vol. 90, No. 7,pp. 3427–3431, (2001).

[39] S. J. Ikhmayies and R. N. Ahmad-Bitar,"Optical properties of nanocrystalline CdTe thin films," Physica B Condens Matter, Vol. 405, No. 15, p-p. 3141–3144, (2010).

[40] E. R. Shaaban, I. S. Yahia, N. Afify, G. F. Salem, and W. Dobrowolski, "Structural and the optical dispersion parameters of nano-CdTe thin film/flexible substrate," Mater Sci Semicond Process, Vol. 19, No. 1, pp. 107–113, Mar. (2014).

[41] K. Punitha, R. Sivakumar, C. Sanjeeviraja, and V. Ganesan, "Influence of post-deposition heat treatment on optical properties derived from UV-vis of cadmium telluride (CdTe) thin films deposited on the amorphous substrate," Appl Surf Sci, Vol. 344, pp. 89–100, (2015).

[42] M. T. Dejpasand, M. H. Ehsani, and H. Rezagholipour Dizaji, "Substrate temperature effect on the structural, morphological and optical properties of CdTe films," Materials Research Innovations, Vol. 22, No. 2, pp. 91–98, (2018).

[43] P. K. K. Kumarasinghe, A. Dissanayake, B. M. K. Pemasiri, and B. S. Dassanayake, Mater Res Bull, Vol. 96, pp. 188–195, Dec. (2017).

[44] A. Arce-Plaza, F. Sánchez-Rodriguez, M. Courel-Piedrahita, O. Vigil Galán, V. Hernandez-Calderon, S. Ramirez-Velasco, and M. Ortega López, "CdTe Thin Films: Deposition Techniques and Applications,"Coatings and Thin-Film Technologies (2019).

[45] S. A. Fadaam, M. H. Mustafa, A. H. A. AlRazaK, and A. A. Shihab, “Enhanced efficiency of CdTe Photovoltaic by thermal evaporation Vacuum,” in Energy Procedia, Elsevier Ltd, pp. 635–643, (2019).

[46] S. Ray, K. V. Bangera, and K. Tarafder, "Synthesis and characterization of Cu doped CdTe thin films for solar cell application," Mater Today Proc, Vol. 39, no. xxxx, pp. 2000–2004, (2019).

[47] S. S. Oluyamo, A. A. Faremi, O. I. O. Olusola, and Y. A. Odusote, "Tunability of conductivity type and energy band gap of CdTe thin film in the electrodeposition technique," Mater Today Proc, Vol. 38, no. xxxx, pp. 558–563. (2020).

[48] H. Trivedi, Gaganpreet, A. Boochani, N. Shagya, J. Lahiri, Z. Ghorannevis, and A. S. Parmar, "Investigating optical, structural and morphological properties of polycrystalline CdTe thin-film deposited by RF magnetron sputtering," Materials Letters: X, Vol. 11, p. 100087, Sep. (2021).

[49] H. S. Patel, J. R. Rathod, K. D. and V. M. Pathak, " Structural and Surface Studies of Vacuum Evaporated Cadmium Telluride Thin Films", American Journal of Materials Science and Technology, vol. 1, p-p. 11-21 (٢٠٢٢)

[50] V. K. Ashith, K. Priya, and G. K. Rao, "Effect of thickness on structural, electrical, and spectral response properties of thermal evaporated CdTe films," Indian Journal of Physics, May.(٢٠٢٢)

[51] H. M. Ali and M. H. Mustafa, "Optimization physical properties of CdTe/Si solar cell devices fabricated by vacuum evaporation," *Chalcogenide Letters*, vol. 20, no. 6, pp. 431–437, Jun. (2023).

[52] I. Jena and U. P. Singh, " Impact of thin layer of copper on cadmium telluride and cadmium sulfide thin films", Journal of Materials Science: Materials in Electronics, Vol. 37 .(٢٠٢٣)

[53] M. Faraday, "Experimental Relations o f Gold (and other Metals) to Light.," Phil. Trans. R. Soc., Vol. 147, No. 0, pp. 145–181 (1857).

[54] R. J. Martín-Palma and A. Lakhtakia, Vapor-Deposition Techniques (Elsevier Inc., 2013).

[55] A. E. B. Alwany, O. M. Samir, M. A. Algradee, M. M. Hafith, and M. A. Abdel-Rahim, "Investigation of the Effect of Film Thickness and Heat Treatment on the Optical Properties of TeSeSn Thin Films," World Journal of Condensed Matter Physics, Vol. 05, No. 03, pp. 220–231,

(2015).

[56] P. Rahi, "Challenges in PVD technique (Thin film formation by thermal evaporation)," International Journal of Advance Research and Development, Vol. 2, pp. 30–37, (2017).

[57] G. Shen, Y. Bando, and C. J. Lee, "Synthesis and evolution of novel hollow ZnO urchins by a simple thermal evaporation process," Journal of Physical Chemistry B, Vol. 109, No. 21, pp. 10578–10583, (2005).

[58] A. S. H. Makhlouf, Current and Advanced Coating Technologies for Industrial Applications (Woodhead Publishing Limited, 2011).

[59] V. Nirupama, M. Chandra Sekhar, K. Subramanyam, and S. Uthanna, "Structural and electrical characterization of magnetron sputtered MoO 3 thin films," in J Phys Conf Ser (Institute of Physics Publishing, 2010).

[60] " Nano-Scale Topographic Modification of Commercial Pure Titanium Dental Implant to Improve Osseointegration," International Journal of Science and Research (IJSR), Vol. 6, No. 1, pp. 1475–1482, Jan. (2017).

[61] C. A. Billur, G. Şahin, E. Güneri, B. Saatçi, and M. Ç. Soylu, "The effect of films thickness on structural and optical properties of amorphous Sn2O thin films deposited by ink jet printing method," J Mol Struc, (2020).

[62] V. V Tetyorkin, A. V Sukach, S. V Stariy, and V. A. Boiko, Photoluminescence Studies of CdTe Polycrystalline Films (2012).

[63] W. Schulz, F. Köhn, M. Balzer, M. Fenker, and J. Albrecht, "Properties of Wear-Resistant MoN Films on Microengineered Substrates," Coatings, Vol. 12, No. 9, pp. 1–10, (2022).

[64] X. Liu and B. Li, "IR variable angle spectroscopic ellipsometry study of high dose ion-implanted and annealed silicon wafers," J Appl Phys, Vol. 105, No. 1, (2009).

[65] S. Karvinen, "The effects of trace elements on the crystal properties of TiO_2," Solid State Sci, Vol. 5, No. 5, pp. 811–819, (2003).

[66] L. Stöber, J. P. Konrath, V. Haberl, F. Patocka, M. Schneider, and U. Schmid, "Nitrogen incorporation in sputter deposited molybdenum nitride

thin films," Journal of Vacuum Science & Technology A: Vacuum, Surfaces, and Films, Vol. 34, No. 2, p. 021513, (2016).

[67] I. C. Noyan and J. B. Cohen, "Measurement by Diffraction and Interpretation," New York: Springer p. 24, (1987).

[68] J. Epp, X-Ray Diffraction (XRD) Techniques for Materials Characterization (Elsevier Ltd, 2016).

[69] R. A. Kyle and M. A. Shampo,"William Lawrence Bragg.," J Am Med Assoc, Vol. 240, No. 8, p. 777, (1978).

[70] C. Gümüş, O. M. Ozkendir, H. Kavak, and Y. Ufuktepe, "Structural and optical properties of zinc oxide thin films prepared by spray pyrolysis method," Journal of Optoelectronics and Advanced Materials, Vol. 8, No. 1, pp. 299–303, (2006).

[71] C. J. Brinker and G. Cao, "Annual Review of Nano Research," (2006).

[72] A. A. Bunaciu, E. G. UdriŞTioiu, and H. Y. Aboul-Enein, "X-ray diffraction instrumentation and applications," Crit. Rev. Anal. Chem., Vol. 45, No. 4, pp. 289–299, (2015).

[73] E. Beygelzimer and Y. Beygelzimer, "Generalized estimates for thermal expansion of oxide scale in the range from 0°C to 1300°C with account for the movability of phase transitions in its components."

[74] L. A. Giannuzzi, "Scanning Electron Microscopy and X-Ray Microanalysis 4th Edition, Joseph I. Goldstein, Dale E. Newbury, Joseph R. Michael, Nicholas W.M. Ritchie, John Henry J. Scott, David C. Joy, Springer, 2018, 550 pp. ISBN:978-1-4939-6674-5.," Microscopy and Microanalysis, Vol. 24, No. 6, pp. 768–768, (2018).

[75] R. Wiesendanger, "Contributions of scanning probe microscopy and spectroscopy to the investigation and fabrication of nanometer-scale structures," Journal of Vacuum Science & Technology B: Microelectronics and Nanometer Structures, Vol. 12, No. 2, p. 515, (1994).

[76] H. N. Southworth, Scanning Electron Microscopy and Microanalysis

(1975).

[77] A. Albino, F. D. Nobre, and F. A. Da Costa, "The spin-1 Ising spin glass: A renormalization-group approach," Journal of Physics Condensed Matter, Vol. 12, No. 26, pp. 5713–5725, (2000).

[78] A. Abdullah and A. Mohammed, "Scanning Electron Microscopy (SEM): A Review," Proceedings of 2018 International Conference on Hydraulics and Pneumatics – HERVEX, pp. 77–85 (2019).

[79] R. J. Beane, "Using the scanning electron microscope for discovery-based learning in undergraduate courses," Journal of Geoscience Education, Vol. 52, No. 3, pp. 250–253, (2004).

[80] R. Splinter, "Action potential transmission and volume conduction," Handbook of Physics in Medicine and Biology, Vol. 56, No. 9, pp. 5-1-5–9, (2010).

[81] H. Jason, C. L. Cheung, A. T. Wooley, C. M. L. Structural, and C. Link, "Structural and Functional Imaging with Carbon Nanotube AFM Probes Citation Accessed Structural and functional imaging with carbon nanotube AFM probes," Science (1979), Vol. 77, pp. 73–110,

[82] J. S. Lacasa, L. Almonte, and J. Colchero, Beilstein, "In situ characterization of nanoscale contaminations adsorbed in air using atomic force microscopy," Journal of Nanotechnology, Vol. 9, No. 1, pp. 2925–2935, (2018).

[83] A. Karbach and D. Drechsler, "Atomic force microscopy - a powerful tool for industrial applications," Surface and Interface Analysis, Vol. 27, No. 5, pp. 401–409, (1999).

[84] F. Marinello, P. Bariani, S. Carmignato, and E. Savio, "Geometrical modelling of scanning probe microscopes and characterization of errors," Meas Sci Technol, Vol. 20, No. 8, (2009).

[85] H. S. Gadow and M. M. Motawea, "Investigation of the corrosion inhibition of carbon steel in hydrochloric acid solution by using ginger roots extract," RSC Adv, Vol. 7, No. 40, pp. 24576–24588, (2017).

[86] I. Muševič, "Atomic force microscopy," Informacije MIDEM, Vol. 30, No. 4, pp. 223–227, (2000).

[87] L. Li, C. Zhang, Z. Yuan, H. Hao, and C. Zhao, "Density functional theory and atomic force microscopy study of oleate functioned on siderite surface," Minerals, Vol. 8, No. 1, Jan. (2018).

[88] F. J. Giessibl, "Advances in atomic force microscopy," Rev Mod Phys, Vol. 75, No. 3, pp. 949–983, (2003).

[89] S. Kantorovitz, "Basic theory," Progress in Mathematics, Vol. 281, pp. 3–48, (2010).

[90] E. Finkman and Y. Nemirovsky, "Infrared optical absorption of Hg1-xCdxTe," J Appl Phys, Vol. 50, No. 6, pp. 4356–4361, (1979).

[91] F. Flory, "Optical properties of nanostructured materials: a review," J Nanophotonics **5**, 052502 (2011).

[92] J. R. Bolton, "The IUPAC Compendium of Chemical Terminology.", Vol. 2223, p. 6484, (2008).

[93] S. Chander and M. S. Dhaka, " Thermal evolution of physical properties of vacuum evaporated polycrystalline CdTe thin films for solar cells," Journal of Materials Science: Materials in Electronics, Vol. 27, No. 11, pp. 11961–11973, (2016).

[94] A. Chukwuemeka and N. N. Mishark, "Optical and solid state characterization of chemically deposited CuO/PbS double-layer thin film," Mater Res, Express, Vol. 5, No. 2, (2018).

[95] R. Dalven, "PbTe , PbSe , PbS AND PbO," Infrared Phys, Vol. 9, pp. 141–184, (1969).

[96] M. H. Shinen, S. A. A. Alsaati, and F. Z. Razooqi, "Preparation of high transmittance TiO2 thin films by sol-gel technique as antireflection coating," J Phys Conf Ser, Vol. 1032, No. 1, (2018).

[97] Y. N. Al-Jamal, "Solid state physics", Al-Mosel University, 2nd ed., Arabic Version, (2000).

[98] N. K. Abbas, L. K. Abbas, and S. A-Muhameed, "Effect Of Thickness On

Structural And Optical Properties Of ZnxCd1-xS Thin Films Prepared By Chemical Spray Pyrolysis," International Journal of Thin Films Science and Technology, Vol. 2, No. 2, pp. 127–132, (2013).

[99] M. Abdullah, "The Influence of Different Thickness on The Physical Properties of TiO_2 Thin Films Prepared by Chemical Thermal Evaporation," The Journal of the University of Duhok, Vol. 24, No. 1, pp. 107–118 (2021).

[100] D. H. Al Refaei, L. M. Al Taan, and L. A. Najam, "The Effect of α-Particles on Structural, optical and Morphological Properties for Cadmium Selenide Thin Film," J Phys Conf Ser, Vol. 1973, No. 1, (2021).

[101] B. Science and T. Mandi, "Handbook of Physics," Phys Today, Vol. 12, No. 12, pp. 52–54, (1959).

[102] S. S. K. Al-obaidi, "Effect of Annealing on the Structural and Optical Properties of Nanostructured TiO_2 Films Prepared by PLD" (2012).

[103] D. Neamen, Semiconductors Physics and Devices (2003).

[104] K. S. Sharba, A. S. Alkelaby, M. D. Sakhil, K. H. Abass, N. F. Habubi, and S. S. Chiad, "Study of Optical and Structural Properties of (NiO)1-x(CuO)x Nanostructures Thin Films," NeuroQuantology, Vol. 18, No. 3, pp. 66–73, (2020).

[105] Z. T. Khodair, M. A. Al-Jubbori, A. M. Shano, and F. I. Sharrad, "Study of Optical and Structural Properties of (NiO)1-x(CuO)x Nanostructures Thin Films," Chemical Data Collections, Vol. 28, p. 100414, (2020).

[106] M. F. Al-mudhaffer, M. a Nattiq, M. Ali, A. Appl, and S. Res, "Linear optical properties and energy loss function of Novolac : Epoxy blend film," Arch Appl Sci Res, Vol. 4, No. 4, pp. 1731–1740, (2012).

[107] M. V. V. Prasad, K. Thyagarajan, and B. R. Kumar,"Effect of Rotational Speed on Linear and Non-Linear Optical Properties of Sol-Gel Spin Coated Nanostructured CdS Thin Films," Journal of Nanoscience and Technology, Vol. 5, No. 2, pp. 688–693, May (2019).

[108] N. F. Habubi, K. H. Abass, S. Chiad, D. M. A. Latif, J. N. Nidhal, and A. I. Al Baidhany, "Dispersion Parameters of Polyvinyl Alcohol Films doped with Fe," J Phys Conf Ser, Vol. 1003, No. 1, (2018).

[109] A. S. Hassanien, "Studies on dielectric properties, opto-electrical parameters and electronic polarizability of thermally evaporated amorphous Cd50S50-xSex thin films," J Alloys Compd, Vol. 671, pp. 566–578, (2016).

[110] A. A. Attia, M. S. El-Bana, D. M. Habashy, S. S. Fouad, and M. Y. El-Bakry, "Optical constants characterization of As30Se70−xSnx thin films using neural networks," Journal of Applied Research and Technology, Vol. 15, No. 5, pp. 423–429, Oct. (2017).

[111] T. A. Hamdalla, T. A. Hanafy, and A. E. Bekheet, "Influence of Erbium Ions on the Optical and Structural Properties of Polyvinyl Alcohol," Journal of Spectroscopy, Vol. 2015, (2015).

[112] A. Abu El-Fadl and A. M. Abd-Elsalam, "Influence of nickel substitutions on the structural, optical and spectroscopic properties of potassium zinc chloride sulfate single crystals," Journal of Taibah University for Science, Vol. 12, No. 6, pp. 826–836, (2018).

[113] I. Solomon, M. P. Schmidt, C. Sénémaud, and M. Driss Khodja, "Band structure of carbonated amorphous silicon studied by optical, photoelectron, and x-ray spectroscopy," Phys Rev B, Vol. 38, No. 18, pp. 13263–13270, (1988).

[114] H. S. Shaaker, W. A. Hussain, and H. A. Badran, "Determination of the optical constants and optical limiting of doped malachite green thin films by the spray method," Adv. Appl. Sci. Res, Vol. 3, No. 5, pp. 2940–2946 (2012).

[115] A. El-Denglawey, M. M. Makhlouf, and M. Dongol, "The effect of thickness on the structural and optical properties of nano Ge-Te-Cu films," Results Phys, Vol. 3, No. 5, pp. 2940–2946 (2018).

[116] K. H. Abass , A. Adil , A. J. Alrubaie, H. R. .Bahaa, A. M. Kadim, S. H.

Talib, K. A. Mohammed and A. S. Jassim, "Fabrication and Characterization of p-SnS/n-Si Solar Cell by Thermal Evaporation Technique and the Effect of Ag-doped on Its Efficiency", International Journal of Nanoscience, Vol. 22, No. 01, P.2350003, (2023).

[117] M. A. Zahid, S. Q. Hussain, Y. H. Cho and J. Yi, J. , "Optical properties of CaF_2 thin film deposited on borosilicate glass and its electrical performance in PV module applications" Applied Sciences, 10(16), 5647. (2020).

[118] A. Jafari, K. Tahani, D. Dastan, S. Asgary, Z. Shi, X. T. Yin, S. Ţălu, "Ion implantation of copper oxide thin films; statistical and experimental results. Surfaces and Interfaces, Vol.18, p.100463, (2020).

[119] L. F. Nassir, " Optical Properties Study of II-VI Semiconductors NPs Prepared by Laser Ablation in Liquid Technique" Journal of Engineering and Applied Sciences 14 (Special Issue 7): 10067-10074, (2019).

[120] D. Sinkhonde, "Quantitative study on surface porosity and roughness parameters of mineral and organic admixtures based on multi-scale characterization techniques," Cleaner Materials, Vol. 7, Mar. (2023).

[121] S. Chander and M. S. Dhaka, "Influence of thickness on physical properties of vacuum evaporated polycrystalline CdTe thin films for solar cell applications," Physica E Low Dimens Syst Nanostruct, vol. 76, pp. 52–59, (2015).

[122] A. M. Shano, A. A. Habeeb, Z. T. Khodair, and S. K. Adnan, "Effects of Thickness on the Structural and Optical Properties of Mn3O4 Nanostructure Thin Films," J Phys Conf Ser, Vol. 1818, No. 1, pp. 0–10, (2021).

[123] R. G .Kadhim, “Study of Some Optical Properties of Polystyrene-Copper Nanocomposite Films”, World Scientific News, Vol. 30, p.14-25, (2016).

[124] E. R. Shaaban, N. Afify, and A. El-Taher, "Effect of film thickness on microstructure parameters and optical constants of CdTe thin films," J Alloys Compd, Vol. 1818, No. 1, pp. 0–10, (2009).

[125] H. Kafashan, R. Ebrahimi-Kahrizsangi, F. Jamali-Sheini, and R. Yousefi, "Effect of Al doping on the structural and optical properties of electrodeposited SnS thin films," Physica Status Solidi (A) Applications and Materials Science, Vol. 213, No. 5, pp. 1302–1308 (2016).

[126] C. R. Chiu, C. L. Fang, S. S. Tsang, and Y. F. Chen, "Performance evaluation of the semiconductor industry based on a metafrontier approach," Technological and Economic Development of Economy, Vol. 24, No. 3, pp. 825–843, Jan. 2018

[127] V. N. Babentsov, Lashkaryov Institute of Semiconductor Physics, National Academy of Sciences of Ukraine 94 PACS 71 (2006).

[128] Q. Chang, J. Sui, Z. Chai, and W. Wu, "Temperature-dependent excitonic photoluminescence and nonlinear absorption of cdte nanocrystal/polyvinyl alcohol films," Nanomaterials, Vol. 11, No. 7, Jul. (2021).

[129] B. A. Hasan and I. H. Shallal, " Structural and Optical Properties of SnS Thin Films," Journal of Nanotechnology & Advanced Materials, Vol. 2, No. 43, (2014).

[130] O. K. Echendu and I. M. Dharmadasa, "Graded-bandgap solar cells using all-electrodeposited ZnS, CdS and CdTe thin-films," Energies (Basel), Vol. 8, No. 5, pp. 4416–4435, (2015).

[131] H. Hakim, N. Al- Garah and A . Hashim, “The effect of aluminum oxide nanoparticles on optical properties of (polyvinyl alcohol-polyethylene glycol) blend”, Journal of Industrial Engineering Research, Vol. 1, pp.94-98, (2015).

[132] H. Guo, Q. Li, Y. Xu, Y. Huang, and S. Du, "Line of sight correction of high-speed liquid crystal using overdriving technology," Electronics (Switzerland), vol.1 , (2020).

[133] L. G. Daza, R. Castro-Rodríguez, M. Cirerol-Carrillo, E. A. Martín-Tovar, J. Méndez-Gamboa, R. Medina-Esquivel, I. Pérez-Quintana, and A. Iribarren, "Nanocolumnar CdS thin films grown by glancing angle

deposition from a sublimate vapor effusion source," Journal of Applied Research and Technology, vol.15, p. 271, (2017).

[134] Z. Ghorannevis, E. Akbarnejad, and M. Ghoranneviss, "Effects of various deposition times and RF powers on CdTe thin film growth using magnetron sputtering," Journal of Theoretical and Applied Physics, Vol. 10, No. 3, pp. 225–231, Sep. (2016).

[135] E. E. Assem, A. Ashour, E. R. Shaaban, and A. Qasem, "Implications changing of the CdS window layer thickness on photovoltaic characteristics of n-CdS/i-AgSe/p-CdTe solar cells," Chalcogenide Letters, Vol. 19, No. 11, pp. 825–839, Nov. (2022).

[136] A.I. Ali, J.Y. Son, A.H. Ammar, A. Abdel Moez and Y.S. Kim, "Optical and dielectric results of Y0.225Sr0.775CoO3±δ thin films studied by spectroscopic ellipsometry technique", Results Phys. 3 (2013) 167–172.

الخلاصة

هناك العديد من الاستخدامات الكهروضوئية للأغشية الرقيقة من أشباه الموصلات II-VI. إحدى هذه المواد التي أثبتت فعاليتها في إنشاء الخلايا الشمسية وأجهزة الكشف الضوئية وتطبيقات الأجهزة الضوئية الأخرى هي تيلوريد الكادميوم (CdTe).

في الدراسة الحالية ، تم تحضير أغشية تيلوريد الكادميوم الرقيقة عن طريق التبخير الحراري للمادة تحت فراغ عالي وإيداعها على ركائز زجاجية تم الحصول على سماكات مختلفة (٦٥ ,٧٢ , ٨٠ ,88, 100 , ١١٠ ,124 , ١٤٠) نانومتر.

تم دراسة تأثير سماكة الفيلم على الخصائص التركيبية والمورفولوجية والبصرية. تم العثور على أغشية تيلورد الكادميوم المبخرة حراريًا ذات هيكل مكعب من اختبار الاشعة السينية . لوحظ تحسن كبير في التبلور مع زيادة السماكة.

يتم فحص مورفولوجيا الفيلم بواسطة مجهر القوة الذرية (AFM) للتأكد من أن الأفلام المزروعة لها سطح متجانس جيد. زادت الخشونة وجذر متوسط القيمة التربيعية ومتوسط القطر مع زيادة السماكة من السماكة (100-140) نانومتر ، من السماكة (65 - 88 نانومتر) كان شكل الغشاء غير مستقر.

تمت دراسة الخواص البصرية للأغشية بواسطة مقياس طيف ضوئي مرئي للأشعة فوق البنفسجية في نطاق الطول الموجي (٢٠٠-١١٠٠) نانومتر ، عندما يزداد السماكة ،تزداد الامتصاصية بينما تنخفض النفاذية. انخفضت فجوة الطاقة المباشرة من 3.60 إلى 3.42 الكترون فولت مع زيادة السماكة ووجد أن النفاذية (T) والامتصاصية (A) وفجوة النطاق البصري تعتمد بشكل ملحوظ على سمك الفيلم ، معامل الانكسار ، معامل الانقراض ، الحقيقي وأظهرت النتائج التي تم الحصول عليها من الثوابت العازلة الحقيقي والخيالي أن سمك الفيلم يؤثر بشدة على المعلمات البصرية. تم دراسة دالة فقدان الطاقة السطحية (SELF) ودالة فقدان الطاقة الحجمية (VELF) وجد أنها تزداد مع زيادة السماكة.

كما تم تقييم معاملات التشتت للأغشية باستخدام نموذج Wemple-DiDomenico (WDD) تم تقييم طاقة التشتت (E_d) وطاقة المذبذب (E_o) للأغشية وتنوعت في نطاق (10.20-2.18) eV و(7.65-5.02) eV على التوالي. كما تم حساب معلمات التشتت البصري (M_{-1} و M_{-3}) والتي تراوحت من (1.333-0.43) ومن (0.0227-0.0171) على التوالي.

وزارة التعليم العالي والبحث العلمي

جامعة بابل

كلية التربية للعلوم الصرفة

قسم التربية فيزياء

تصنيع وتوصيف اغشية CdTe النانوية المحضرة بتقنية التبخير الحراري

رسالة مقدمة الى كلية التربية للعلوم الصرفة / جامعة بابل

وهي جزء من متطلبات نيل درجة الماجستير في تربية الفيزياء

أعداد

حنان سالم هادي صالح الحسون

بكالوريوس علوم في الفيزياء

جامعة بابل (٢٠١٦)

بأشراف

أ.د. خالد حنين عباس

١٤٤٥ هـ

٢٠٢٣ م